STARS AND CIRCUMSTELLAR MATTER

ISO SPECTROSCOPY OF STARS: THE POTENTIAL OF THE ARCHIVE

Laurens B.F.M. Waters[1,2]

[1]Astronomical Institute, University of Amsterdam, Kruislaan 403, NL-1098 SJ Amsterdam, The Netherlands
[2]Instituut voor Sterrenkunde, Katholieke Universiteit Leuven, Celestijnenlaan 200B B-3001 Heverlee, Belgium

ABSTRACT

The ISO archive allows systematic studies of the infrared properties of stars with a wide range of properties, ranging from pre–main-sequence stars to red giants at the end of their life. We illustrate the potential of the ISO archive using hot stars and evolved stars as examples.

Key words: ISO – Stars – Circumstellar Matter

1. INTRODUCTION

The infrared spectral region contains a large number of diagnostics that can be used to study the nature of stars and their immediate surroundings. Both ionized gas, molecular gas as well as dust have prominent spectral features that prove a wide variety of physical and chemical conditions relevant for stellar studies. The Infrared Space Observatory (Kessler et al. 1996), during its 2.5 year active phase, has provided a unique data set of 2-200 μm spectra and images of stars and circumstellar matter. It is now possible, thanks to the easy access that the ISO archive provides, to conduct systematic studies using large samples obtained with all four instruments. These data sets have a homogeneous quality. This paper focuses on the spectrographs SWS (De Graauw et al. 1996) and LWS (Clegg et al. 1996). We discuss some recent results obtained for hot, massive stars and evolved low- and intermediate mass red giants, focusing on studies of large samples (see also García-Lario & Perea Calderón 2002). This paper does not intend cover the complete literature on ISO results on stars. For a comprehensive review of ISO results on circumstellar dust, we refer to Molster & Waters (in press).

2. HOT STARS

Hot, massive stars are characterized by strong stellar winds that are driven by UV radiation pressure on numerous ionic lines. These winds are important both for the evolution of the star itself (mass loss strips the outer layers, eventually exposing the core of the star), and of the galaxy in which it lives: large amounts of momentum and energy are added to the interstellar medium (ISM) by the most massive stars in galaxies. The mass loss as well as matter ejected during supernova explosions enriches the ISM with products of nuclear burning.

While most of the energy of hot stars is emitted in the UV, the infrared spectral region still is important: often, hot stars are obscured by large amounts of foreground extinction, especially when they are still young. This implies that we can only find and study young massive stars by the infrared light they emit. At long infrared wavelengths, thermal dust emission from the surrounding molecular cloud often hinders studies of massive hot stars. Typically, the 1-5 μm spectral region can be used to determine the nature of hot, obscured stars. This region contains several important transitions from HI, HeI, HeII, C, N, O, and Fe which are sensitive to temperature, gravity and stellar wind properties. In Fig. 1 we show a series of spectra of hot stars (Lenorzer et al. 2002a) taken in the nominal mission as well as in the post-helium phase (see Vandenbussche, 2002). Using the near-IR only as a diagnostic, it is possible to determine the equivalent MK classification of B stars in spectral type to within two subtypes, and in luminosity class to within two subclasses. In addition, the mass loss rates of OB supergiants can be estimated with an accuracy of 0.25 dex.

The wide spectral coverage of the ISO data allows studies of many transitions of HI. In stars with a large amount of circumstellar matter, such as rapidly rotating Be stars and Luminous Blue Variables (LBVs), the HI recombination lines are in emission. The observations allow us to study the *Pfund and Humphreys series decrement*: the dependence of line flux on intrinsic line strength (Einstein A coefficient). The Be stars, whose line emission is from a high density, compact circumstellar disk, show only a modest decrement: the weaker lines are still surprisingly strong. The LBVs, whose line emission is dominated by a more or less spherical wind, show a steep decrement and only weak emission from high-level transitions.

In Fig. 2 we show a line flux ratio diagram illustrating the widely different behaviour of both groups of stars. The trend in Fig. 2 (Lenorzer et al. 2002b) can easily be understood as an optical depth effect: in Be stars the lines are mostly optically thick and so line flux ratios do not reflect intrinsic line strength ratios. In stellar winds however, the average gas density is much lower than in Be stars, and their line flux ratios behave as expected for case B recombination line theory. The group of B[e] stars is intermediate between the LBVs and the Be stars: B[e] stars have a disk, but the forbidden line emission that characterizes them indicates that a lower density region must also exist. This results in an intermediate position in Fig. 2.

Proceedings of the Symposium *"Exploiting the ISO Data Archive - Infrared Astronomy in the Internet Age"*,
24–27 June 2002, Sigüenza, Spain (C. Gry, S. B. Peschke, J. Matagne et al. eds., ESA SP-511)

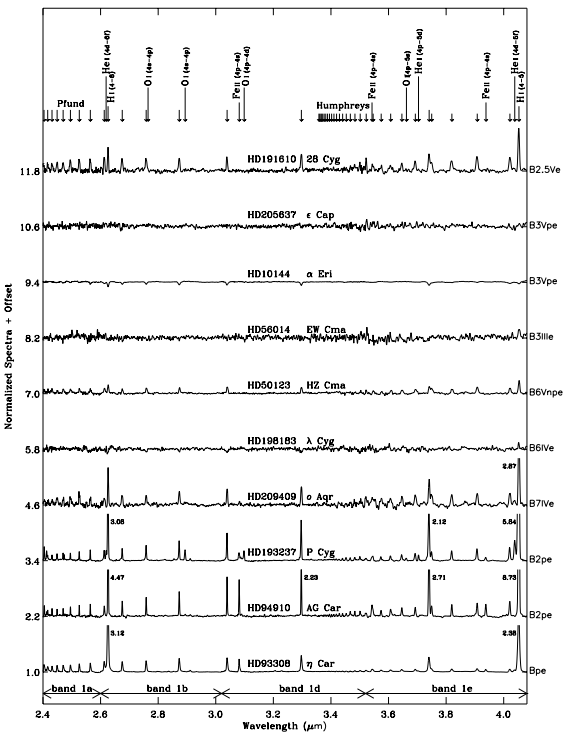

Figure 1. ISO-SWS spectra of hot stars with circumstellar gas. The spectra were normalized to the continuum. A large number of lines can be found, sometimes in emission. Stars with strong emission lines have dense winds or a dense gaseous disk. Taken from Lenorzer et al. (2002a).

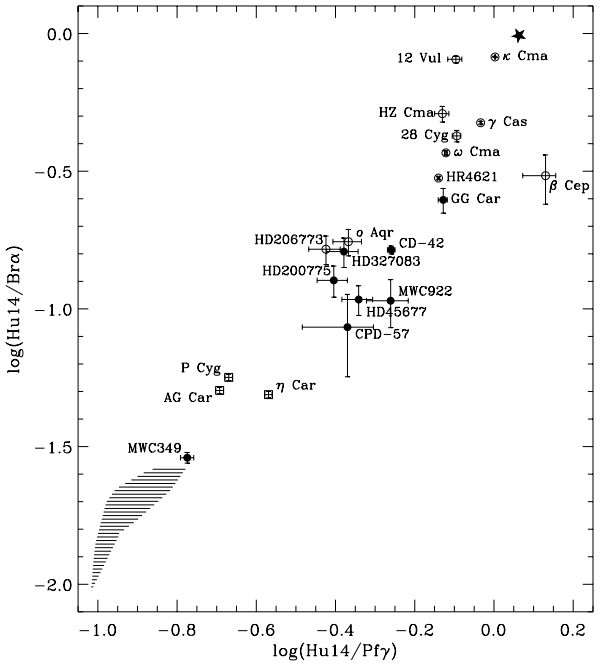

Figure 2. Line flux ratio diagram, comparing the line strengths of the HI 14-6, Pfund γ and Brα line of a large number of stars observed with ISO-SWS. Notice that the Be stars (whose lines are very optically thick) are concentrated in the upper right part of the diagram, close to the point where opaque lines are expected. The LBVs however (whose lines are from a large volume with on average low densities) occupy a region near the lower left part of the diagram, close to the locus for optically thin case B recombination (shaded region). The B[e] stars, that have disks but also regions of lower gas densities, are in between the Be stars and the LBVs. Figure taken from Lenorzer et al. (2002b).

3. EVOLVED STARS

All low and intermediate mass stars develop a dense stellar wind during the last phases of their life, when they have evolved to the red giant or asymptotic giant branch (AGB). This wind is characterized by a low expansion velocity (typically 5-30 km/s), and low temperatures. Densities and temperatures are favorable for the formation of dust particles. In stars with high mass loss rates, the dust can completely obscure the central star.

The ISO archive contains many spectra of cool giants, AGB stars and Red Supergiants. This reflects the fact that the ISO spectrographs were ideal instruments to study their photosphere and surroundings: the bulk of the energy of AGB stars is emitted in the ISO wavelength region, and, as mentioned above, contains many diagnostic bands of both gas and dust. The internal evolution of AGB stars causes them to come in two chemical 'flavors': oxygen-rich, i.e. with a C/O ratio less than unity, and carbon-rich, with C/O exceeding one. Below, we discuss recent results for both types of AGB stars.

3.1. OXYGEN-RICH STARS

The ISO 2-20 μm spectra of oxygen-rich AGB stars are dominated by gas-phase absorption and/or emission bands from simple and abundant molecules: H_2O, CO, CO_2, OH, SiO, SO_2. The bands not only originate from the 'photosphere' of the star, but also from the warm molecular layer which surrounds all mass-losing AGB stars. In fact, the distinction between photosphere and envelope is difficult to make observationally, and may be rather meaningless given the very extended atmosphere these stars possess.

A systematic archival study of ISO spectra of oxygen-rich stars with low or intermediate mass loss rates (restricting the study to stars with 10 μm silicate emission) was carried out by Cami (2002). He divided stars into two categories, based on the appearance of the 15 μm bending mode band of CO_2 (emission or absorption). This resulted in two distinct groups of stars, that also share properties at other wavelengths (see Fig. 3). The absorption sample on average shows stronger molecular absorption bands at short wavelengths. Contrary, the emission sample shows on average weaker absorption or a mix of absorption and emission bands. In addition, the absorption sample shows more dust emission: more molecular circumstellar gas correlates with more dust.

Modeling of the molecular bands proves difficult, but some important trends can be quantified (Cami, 2002): there is clear evidence for the presence of an optically thick H_2O layer in

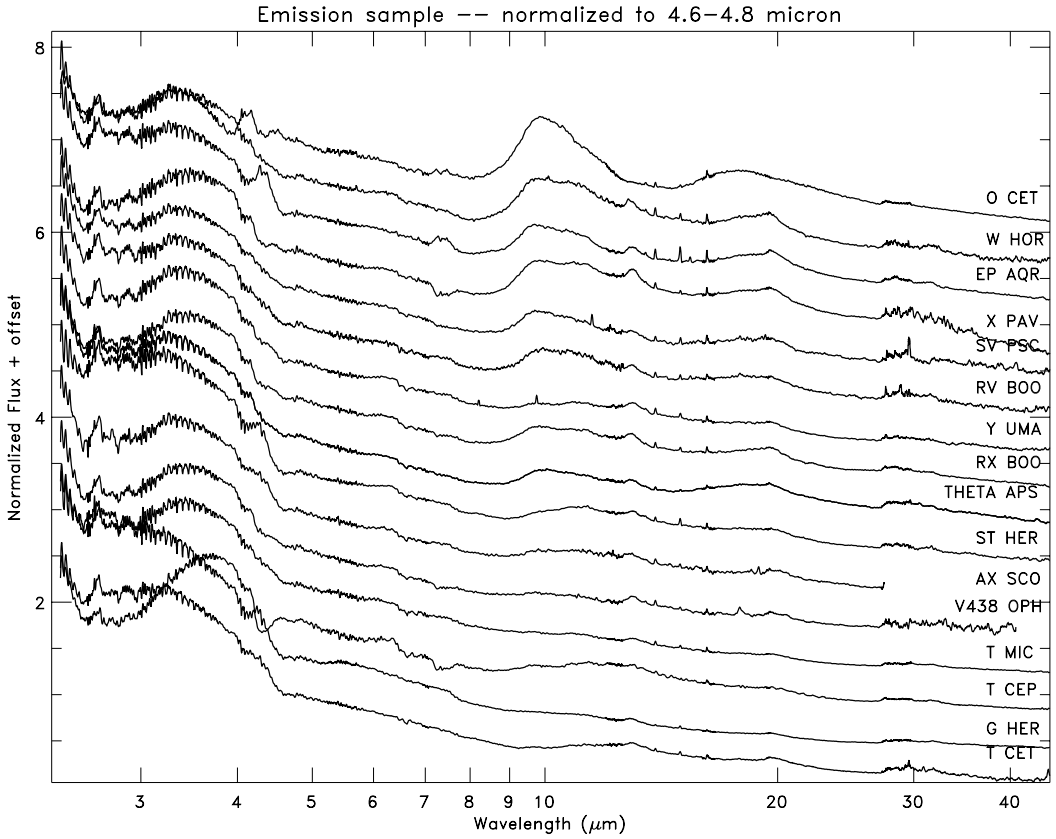

Figure 3. Oxygen-rich AGB stars observed with ISO-SWS and showing the 15 μm CO_2 band in emission. The spectra are normalized to the mean 4.6-4.8 μm flux and ordered in sequence of increasing 10 μm flux. Notice that sometimes molecular bands at short wavelength are in emission; the nature of the dust emission also varies widely. Figure taken from Cami (2002).

some stars, causing a pseudo-continuum with a color temperature that can be significantly lower than the effective temperature. This optically thick water layer is most often found in Mira variables, while it is not prominent in semi-regular variables. Apparently the more regular pulsations of mira stars cause a more extended and/or denser molecular gas layer around the star. Surprisingly, the mass loss rates of the stars with and without optically thick water layer are not very different.

Apart form the molecular gas, the ISO spectra also allow detailed studies of the composition of the dust. It is immediately clear from inspecting Fig. 3 that there is a wide variation in the nature of the dust which condenses in oxygen-rich AGB stars with low mass loss rates. While the traditional amorphous silicate band peaks at 9.7 μm and is seen in stars with high mass loss rate (roughly 10^{-6} $M_\odot$/yr or higher) , the peak is often found near 11 μm for lower mass loss rates. Clearly, these stars do not produce amorphous silicates but rather simple oxides (Cami 2002; Fig. 4): a rather narrow band near 13 μm, first identified in IRAS-LRS spectra of AGB stars by Vardya et al. (1986) is identified with spinel ($MgAl_2O_4$; Posch et al 1999). A peak near 19.5 μm is also evident, which is attributed to $Mg_{0.1}Fe_{0.9}O$ (Cami 2002; Posch et al. 2002).

The picture that emerges is that objects with low gas densities begin nucleation of dust by production of simple oxides, but do no succeed in forming amorphous silicates. Only above a certain threshold density, amorphous silicates become the dominant dust species. Dust nucleation in higher density winds may also start with simple oxides, who then serve as condensation seeds for amorphous silicates. These then dominate the emission, swamping any simple oxide emission. Whether crystalline silicates, seen in stars with very high mass loss rates, are also produced in lower mass loss stars remains to be seen. Kemper et al. (2001) show that crystalline silicates may go undetected in stars with intermediate mass loss rates due to a contrast effect: the crystalline silicates are cooler than their amorphous counterparts.

3.2. CARBON-RICH STARS

Carbon-rich stars show a conspicuous evolution of the energy distribution and of their dust composition as their mass loss rate increases, and even more strongly when they leave the AGB to become planetary nebulae (PNe) (Kwok et al. 1999). In Fig. 5 we show this strong evolution from AGB to PN (see Hony et al. 2002a). These spectra show that even cool post-AGB stars develop emission in the famous infrared emission bands, that can be identified with Polycyclic Aromatic Hydrocarbons (PAHs). In addition, "plateau" emission is evident in the 10 μm re-

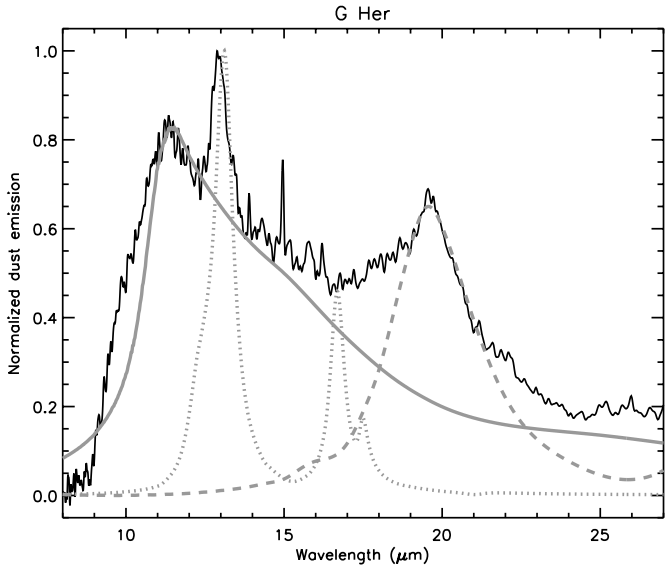

Figure 4. The normalized dust emission spectrum of the AGB star G Her. The different spectral structures can be identified with natural spinel ($MgAl_2O_4$; Posch et al. 1999, dotted line), compact amorphous Al_2O_3 grains (full grey line) and $Mg_{0.1}Fe_{0.9}O$ (dashed line). Figure taken from Cami (2002); See also Posch et al. (2002).

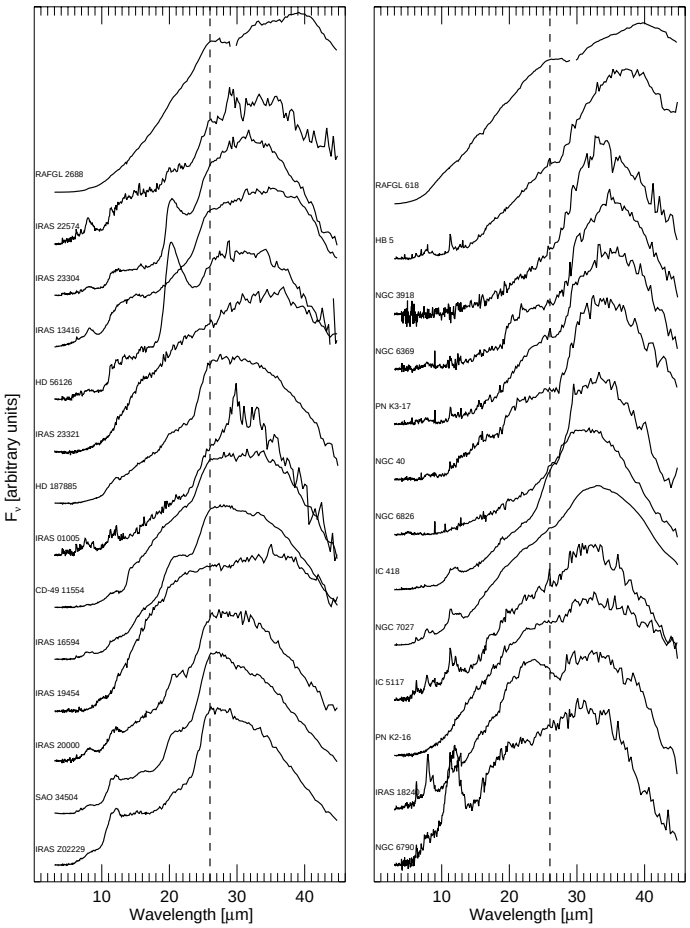

Figure 5. Overview of ISO-SWS and LWS spectra of carbon-rich post-AGB stars and PNe. The dashed line indicates the position of the 30 μm band in AGB stars (peaking at 26 μm). The band shifts to 35 μm in PNe. Figure taken from Hony et al. (2002a).

gion which may be due to Hydrogenated Amorphous Carbon (HAC). PAHs and HAC are not known to be present in AGB stars, which may imply that these materials are produced by e.g. destruction of carbonaceous dust which formed when the star was still on the AGB.

Almost all carbon-rich AGB stars show evidence for an emission band near 30 μm, first noted in KAO spectra of (among others) IRC+10 216 by Forrest et al. (1981). Goebel & Moseley (1985) suggested that solid MgS is the carrier of the band. However, subsequent studies, especially after the first ISO data of carbon-rich AGB stars became available, showed that there is considerable variation in the wavelength and width of the band. This led Waters et al. (2000) and Volk et al. (2002) to suggest that it may be a blend of two carriers, and shed some doubt on the MgS identification.

A systematic study of the behaviour of the 30 μm band became possible when the ISO archive became available. Hony et al. (2002a) studied the ISO-SWS and ISO-LWS spectra of 75 carbon-rich objects, ranging from low mass loss AGB stars to evolved PNe. Most of these objects indeed show the 30 μm band. Hony et al. (2002a) noted a correlation between the peak wavelength and the colour temperature of the underlying continuum. There is a systematic shift of the band from about 26 to 35 μm going from AGB to PN (Fig. 5). It is important to realize that the 30 μm band is very wide. This large width of the band can be fitted when MgS particles with a continuous distribution of ellipsoids (CDE) for the shape of the particles is assumed. A change in temperature of the MgS then easily results in a shift of the peak position of the band by several microns.

A simple model for MgS, assuming a CDE distribution and adjusting the temperature to the observed peak position of the band, gives very good results for the bulk of the ISO spectra (Fig. 6; Hony et al. 2002a). This simple model shows that MgS is most likely the carrier of the 30 μm band; there is no need for a second component. While both the width and the peak position can be well fitted in the case of AGB and post-AGB stars, the model fails to reproduce the width of the band in PNe. In these objects the band is narrower than expected on the basis of the trends seen in AGB and post-AGB stars. This may be due to the fact that in PNe the MgS is altered, and has different optical properties. In addition, some sources show an additional, rather narrow emission band, peaking at about 26 μm. This band can be well fitted by a small amount of *spherical* MgS grains. Hony et al. (2002a) were able to show that the temperature of the MgS grains is different (usually lower) than that of the underlying continuum. This shows that the MgS grains are not in thermal contact with the grains responsible for the continuum, presumably amorphous carbon. Surprisingly, the warmest carbon stars have rather cool MgS, contrary to the trend seen in the bulk of the sample. Also, post-AGB stars have rather warm MgS. This may indicate the MgS is most efficiently heated by mid-IR photons.

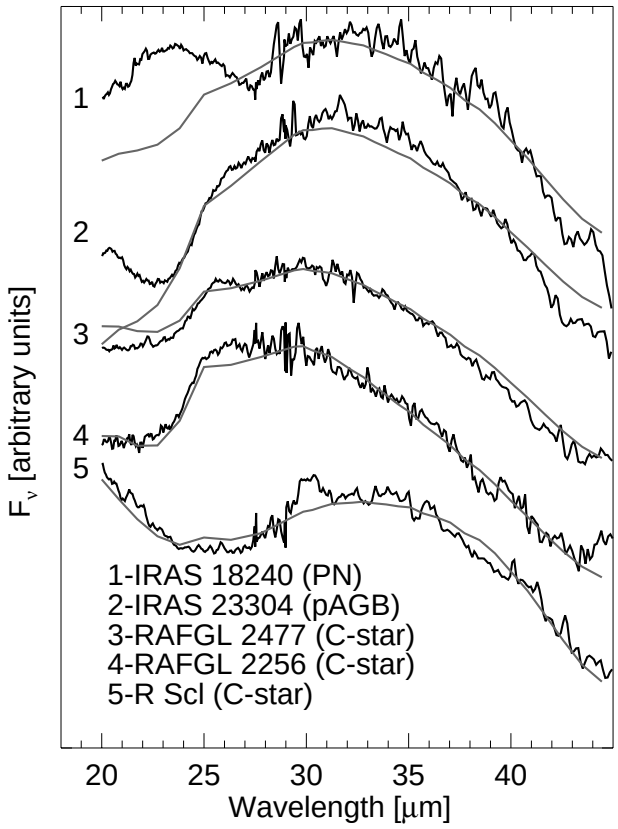

Figure 6. Single temperature fits to the 30 μm band of selected stars using a CDE shape distribution of MgS grains. Notice the shift in wavelength of the band. Figure taken from Hony et al. (2002a).

Two carbon-rich planetary nebulae, K3-17 and M2-43, show an emission band at 23 μm (Hony et al. 2002b). These two objects show no evidence for a mixed chemistry, making an identification with an oxygen-rich component unlikely. In addition, weak bands near 34, 38 and 44 μm are present as well. The 23 μm band as well as the weak ones in the 30-40 μm range can be fitted using the FeS Troilite. FeS has been predicted to condense in carbon-rich environments (Lodders & Fegley 1999), but has so far not been identified. Since the 23 μm band is rarely seen, small FeS particles are not often formed in carbon-rich outflows. This may be an observational selection effect: large, $\approx 1\mu$m sized FeS grains are opaque and would not show a strong resonance. Alternatively, the formation of solid FeS in AGB winds may be inhibited because S is effectively locked up in MgS, which is believed to form before FeS can.

ACKNOWLEDGEMENTS

It is a great pleasure to thank Jan Cami, Sacha Hony, Ciska Kemper, Annique Lenorzer, Bart Vandenbussche, Xander Tielens, Alex de Koter, Pat Morris, Frank Molster, Jeroen Bouwman, Teije de Jong, Conny Jäger, Thomas Henning, Mike Barlow, and Lindsay Keller for their contributions to the research described in this report. Many thanks also to the ISO instrument teams that made all of this possible.

REFERENCES

Cami J.: 2002, Molecular gas and dust around evolved stars. Ph.D. thesis, University of Amsterdam, The Netherlands
Clegg P.E., Ade P.A.R., Armand C., et al.: 1996, A&A 315, L38
de Graauw T., Haser L.N., Beintema D.A., et al.: 1996, A&A, 315, L49
Forrest W.J., Houck J.R., McCarthy J.F.: 1981, ApJ,248, 195
García-Lario P., Perea Calderón J.V., 2002, this volume
Goebel J.H., Moseley S.H.: 1985, ApJ, 290, L35
Hony S., Bouwman J., Keller L.P., Waters L.B.F.M.: 2002a, A&A, 393, L103
Hony S., Waters L.B.F.M., Tielens A.G.G.M.: 2002b, A&A, 390, 533
Kemper F., Waters L.B.F.M., de Koter A., Tielens A.G.G.M.: 2001, A&A, 369, 132
Kessler M.F., Steinz J.A., Anderegg M.E., et al.: 1996, A&A, 315, L27
Kwok S., Volk K., Hrivnak B.J.: 1999, A&A, 350, L35
Lenorzer A., de Koter A., Waters L. B. F. M.: 2002a, A&A, 386L, 5L
Lenorzer A., Vandenbussche B., Morris P., de Koter A., Geballe T.R., Waters L.B.F.M., Hony S., Kaper L.: 2000b, A&A, 384, 473L
Lodders K., Fegley B.: 1999, In: IAU Symp. 191: Asymptotic Giant Branch Stars, vol. 191, pp. 279–+
Posch T., Kerschbaum F., Mutschke H., Dorschner J., Jäger C.: 2002, A&A, 393, L7
Posch T., Kerschbaum F., Mutschke H., et al.: 1999, A&A, 352, 609
Vardya M.S., de Jong T., Willems F.J.: 1986, A&A, 304, L29
Volk K., Kwok S., Hrivnak B.J., Szczerba R.: 2002, ApJ, 567, 412
Vandenbussche B., 2002, this volume
Waters L.B.F.M., Molster F.J., Hony S., et al.: 2000, ASP Conf. Ser. 196: Thermal Emission Spectroscopy and Analysis of Dust, Disks, and Regoliths, pp. 3–14

STATUS AND POTENTIAL OF THE ISOGAL SURVEY

Joris Blommaert

Instituut voor Sterrenkunde, K.U. Leuven, Celestijnenlaan 200B, 3001 Leuven, Belgium

for the ISOGAL collaboration [1]

ABSTRACT

ISOGAL was one of the largest programmes observed with ISO and combines mid-infrared ISOCAM data with near-infrared DENIS data of the inner Galaxy. It provides information on galactic structure, stellar populations, diffuse emission, stellar mass-loss and the (recent) star formation history of the inner disk and bulge of the Galaxy. In this review, the status of the data-analysis is discussed together with the products provided by the ISOGAL project: a five-bands Point Source Catalogue, containing over 100,000 sources, and the set of reduced and calibrated images. I also discuss the status of two stellar studies. One is on YSO's and how to select these from the ISOGAL PSC. The other one concerns the AGB stars in the central bulge and the presence of circumstellar dust and mass loss.

Key words: ISO – AGB stars – AGB: mass loss – YSO – Galactic Centre

1. INTRODUCTION

ISOGAL is a 7 and 15 μm survey of the inner Galaxy, covering the inner galactic bulge and sampling the obscured disk within the solar circle. The main scientific goals were to study the galactic structure and stellar populations of the galactic bar, inner disk, molecular ring and spiral arms, the central stellar cluster and inner bulge. Further fields of study include the old stellar population (RGB and AGB (with mass loss)), interstellar extinction, diffuse emission and the detection of young stars.

About 16 degree^2 were observed in ISOCAM (Cesarsky et al. 1996) raster mode using $6''$ or (less frequently) $3''$ Pixel Field Of View. In comparison with IRAS our survey provides data that are 2 orders of magnitude more sensitive and have one order of magnitude higher spatial resolution. It is also more sensitive, by one to four magnitudes and has a higher spatial resolution than the recent infrared survey of the galactic disk, MSX (e.g. Price et al. 2001).

[1] ISOGAL Co-Investigators include: C. Alard, J. Blommaert, C. Cesarsky, N. Epchtein, M. Felli, P. Fouqué, R. Genzel, G. Gilmore, H. Habing, A. Omont (PI), M. Pérault, S. Price, A. Robin and G. Simon. A number of associate members of the ISOGAL Collaboration have contributed to the results presented here: S. Ganesh, I. Glass, M. Messineo, D. Ojha, M.-A. Miville-Dêschenes, F. Schuller, M. Schultheis.

A systematic cross-identification with near-infrared (I, J, K_s) DENIS (Epchtein et al. 1997) sources is performed for the ISOGAL detected sources. This has lead to a five-wavelengths ISOGAL catalogue (see Section 3 and Schuller et al. 2002) The combination of near- with mid-infrared allows a reliable determination of the nature of the sources and of their interstellar reddening. About 80% of the ISOCAM sources are matched with sources from the DENIS survey. The ISOGAL data offer thus a powerful tool for the analysis of stellar populations in the heavily obscured regions of the inner Galaxy.

The ISOGAL Point Source Catalogue (version 1.0) and the set of reduced images is now ready and is about to be made available through the Vizier Service at the Centre de Données Astronomique de Strasbourg (CDS, http://vizier.u-strasbg.fr/viz-bin/VizieR) and also via the server at the Institut d'Astrophysique de Paris (http://www-isogal.iap.fr). Two papers accompany the public release of the catalogue. One is the Explanatory Supplement of the ISOGAL-DENIS Point Source Catalogue (Schuller et al. 2002) and an overview paper (Omont et al. 2002) which describes results obtained with ISOGAL in many different fields and which are described in 25 refereed journal papers.

In the sections below I will give an overview of results obtained on galactic bulge AGB stars and YSO's. Other results of ISOGAL include the identification and properties of interstellar dark clouds (Pérault et al. 1996, Hennebelle et al. 2001), quantification of the infrared extinction law and source de-reddening (Jiang et al. 2002 and these proceedings) and a study of infrared stellar populations in the central parts of our Galaxy (van Loon et al. 2002). A more comprehensive overview of ISOGAL results can be found in Omont et al. (2002).

2. OBSERVATIONS AND DATA REDUCTION

ISOGAL observations were performed throughout the whole ISO satellite lifetime (November 1995 - April 1998). Unfortunately a large fraction of the fields were not observed simultaneously at 7 and 15 μm, which hampers the study of variable AGB stars (Section 5). The observed regions of in total $\approx$ 16 degree^2 were distributed along the inner galactic disk (mostly within $\mid l \mid < 30^o, \mid b \mid < 1^o$). The central region ($\mid l \mid < 1.5^o, \mid b \mid < 0.5^o$) was almost entirely observed, except very close to the centre itself and a few other fields as they would saturate the detector. For comparison and to extend our study, some fields at larger longitude and at higher

Proceedings of the Symposium *"Exploiting the ISO Data Archive - Infrared Astronomy in the Internet Age"*, 24–27 June 2002, Sigüenza, Spain (C. Gry, S. B. Peschke, J. Matagne et al. eds., ESA SP-511)

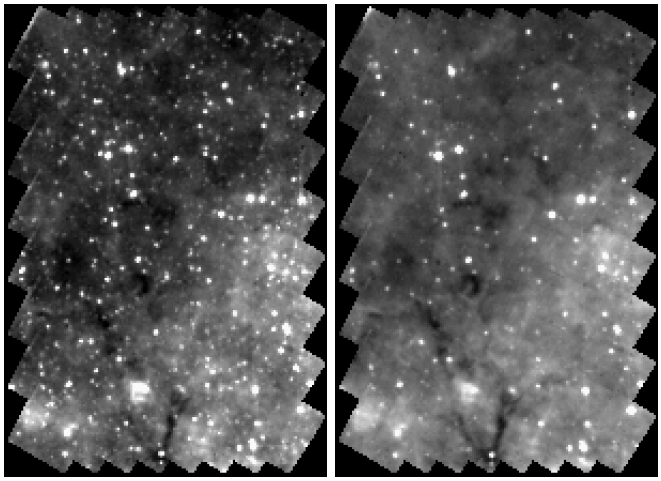

Figure 1. Typical images of ISOGAL rasters (left: 7 μm, right: 15 μm). This field is centred at l=7.33^o, b=0.15^o (0.1^o $\times$ 0.16^o). Patchy or filamentary infrared dark clouds are visible and are a common feature in ISOGAL images.

latitude (in the Bulge) were observed. Major difficulty for the measurements in the galactic plane was to avoid bright ($\approx$ 6 Jy at 12μm) sources which would saturate the detector. For this reason, the observations were performed in small rasters (≈ 0.1 deg^2). The pixel field of view selected was 6$''$ (resulting in a total field of view of $3' \times 3'$ per raster position). The raster step size was 1.5$'$. Generally, broadband filters were used: LW3 (12-18μm) and LW2 (5-8.5μm) and only short integration times (40×0.28 seconds). In special cases, like near the galactic centre or on active star formation regions, narrow band filters at the same central wavelengths and a smaller pfov (3$''$) were used to allow higher fluxes. The overall sensitivity is better than 10 mJy (corresponding to 10 mag for LW2 and 8.5 mag for LW3). Additionally, 18 ($3' \times 3'$) fields were selected for ISOCAM CVF (5-17μm) measurements. One example of this spectroscopic mode will be discussed in Section 5.

The data reduction consists of several "standard" steps like the removal of cosmic ray impacts, dark current subtraction and flat fielding, which are performed within the Cam Interactive Analysis package. Special care is taken for the time-dependent behaviour of the detector, but the applied corrections are still not perfect for point sources. Improved corrections have become available and will be used in a future release of new ISOGAL products (see Section 6). In the often crowded fields we use sophisticated source extraction methods. The photometry is done by psf-fitting. For the ISO results we are presenting here, we generally have a photometric accuracy better than 0.2 mag (RMS). The final astrometry accuracy is improved for almost all fields to about 1$''$, through the connection to the DENIS astrometry. A detailed description of the present data reduction techniques and the quality of the obtained products is given in the Explanatory Supplement of the ISOGAL PSC (Schuller et al. 2002).

3. ISOGAL PRODUCTS

At this stage, two main products are made available by the ISOGAL consortium. One is the set of ISOGAL images, which are mosaic images produced from the raster measurements and the other is the multi-wavelength point source catalogue (Schuller et al. 2002). The images are produced within the CIA package and use the so-called "inversion" method for the time dependent behaviour of the observed signal. This means that the images still contains defects (like remnants of observed point sources) as the correction of especially point sources is insufficient. Better correction methods are now available and will be used in a future release of the ISOGAL data (Miville-Deschênes et al., in preparation). An important improvement over the normal ISO products available through the ISO Data Archive (http://www.iso.vilspa.esa.es) is the astrometry which has been improved to an accuracy of about 1$''$, using the available DENIS astrometry. The set of 384 images is available through the web (http://www-isogal.iap.fr/Fields/). For fields which contain both 7 and 15 μm data, two-colour images are available. The ISOGAL PSC offers magnitudes for five bands: I, J, K_s, [7], [15], where the near-infrared bands are taken from DENIS where available. The PSC contains about 105,000 sources of which about half have 7-15 μm associations and 78% have DENIS associations. A full description of the catalogue entries is given in Explanatory Supplement (Schuller et al. 2002). All the data will be made available through VizieR and the ISOGAL web page (see the Introduction) when the Explanatory Supplement is published.

4. YOUNG STELLAR OBJECTS

Young stars, still enshrouded with dusty disks or cocoons are excellent targets to be picked up by infrared surveys. IRAS suffered too much of source confusion to detect these sources near the galactic plane. With the higher spatial resolution of ISOGAL it is possible to search for them in the galactic plane and centre. A limitation in the ISOGAL survey comes from the restriction that areas with bright sources, like often the case for star formation regions, had to be avoided in order not to saturate the ISOCAM detector. This was somewhat circumvented by using smaller pixel sizes (3$''$ pfov) and narrower filters. The main criterion with near- and mid-infrared colours is a very large excess in the colours [7]-[15] or K_S-[7]. However, there still exists a strong confusion with post-MS stars like is discussed in Felli et al. (2000) and (2002). In their most recent paper they look for ISOGAL counterparts of the Becker et al. (1994) (VLA, 6cm) radio-identified UC HII regions (see Figure 2). Because of the confusion in colours with red AGB stars like OH/IR stars, an additional criterion of selecting only the brightest objects was added. This leads of course to the limitation of selecting only very luminous and thus massive YSOs (For $F_{15} > 0.3$ Jy, L> 2500 $L_\odot$ at 5 kpc, implying M > 10 $M_\odot$).

Using these criteria, Felli et al. (2002) selected 715 sources from the ISOGAL PSC (2% of the total number of sources with good detections at both 7 and 15 μm). An additional evidence

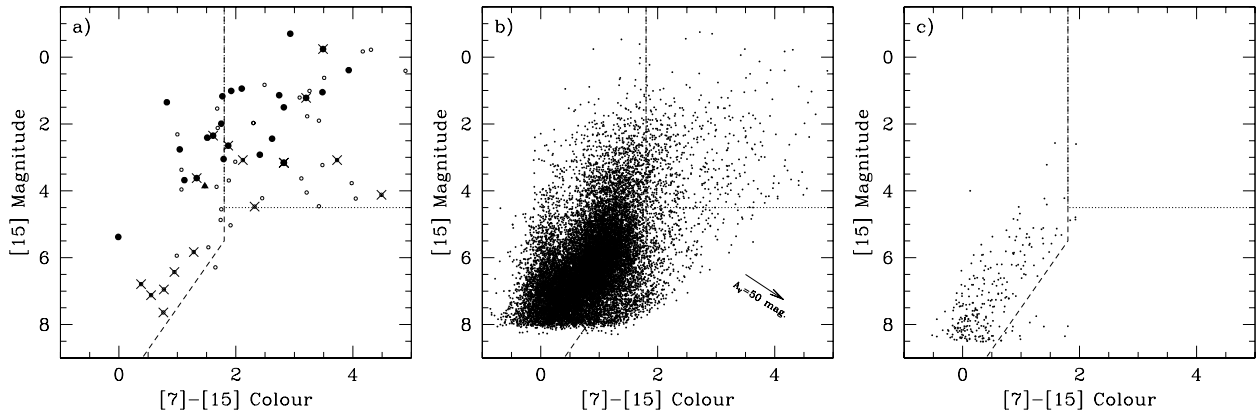

Figure 2. ISOGAL [15] vs [7]-[15] diagrams from Felli et al. (2002). Diagram a) shows the Becker et al. (1994) radio sources which have good 7 and 15 μm detections. Small open circles refer to unclassified radio sources, either not associated with IRAS sources, with low association probability or with ambiguous IRAS colours/fluxes; filled circles represent UC HII or candidate UC HII; the triangle marks the only PN in the sample. The middle diagram shows the same colour magnitude diagram for all ISOGAL sources within the Becker et al. (1994) survey region. Diagram c) contains sources taken from ISOGAL fields at high latitudes ($|b| > 3°$). In all diagrams the dashed line shows the criteria used to derive YSO candidates in Felli et al. (2000), the dotted horizontal line shows the more conservative limit on [15] adopted in the Felli et al. (2002) paper.

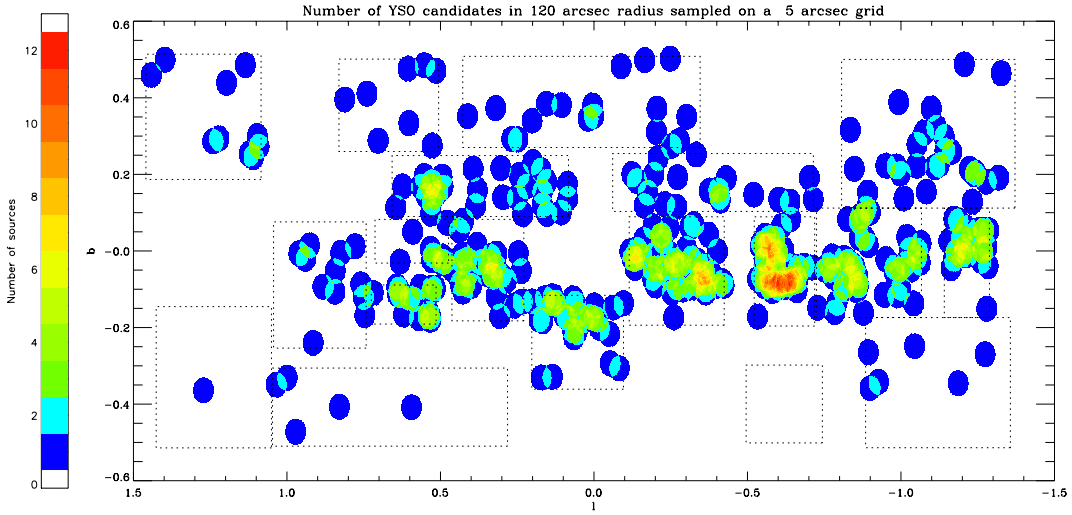

Figure 3. Number densities of candidate YSO's in the Galactic Centre area (Schuller 2002). These were selected using the criteria from Felli et al (2002). The dashed lines indicate the borders of the ISOGAL observed fields.

for the fact that these sources are indeed predominantly YSOs is the fact that most of the sources turn out to be extended in the ISOGAL images.

The majority of the young ISOGAL stars selected by Felli et al. (2002) are located in the molecular ring or in the central bulge. An interesting example is the galactic centre region itself where little is known about the starformation history. Figure 3 shows the distribution of candidate YSOs near the galactic centre. A strong concentration can be seen towards the star forming region Sgr C. Preliminary results also show that there is a clear overlap of their distribution with the mid-IR dark condensations, which were suggested to be pre- and proto-stellar cloud cores (Pérault et al. 1996, Teyssier et al. 2002).

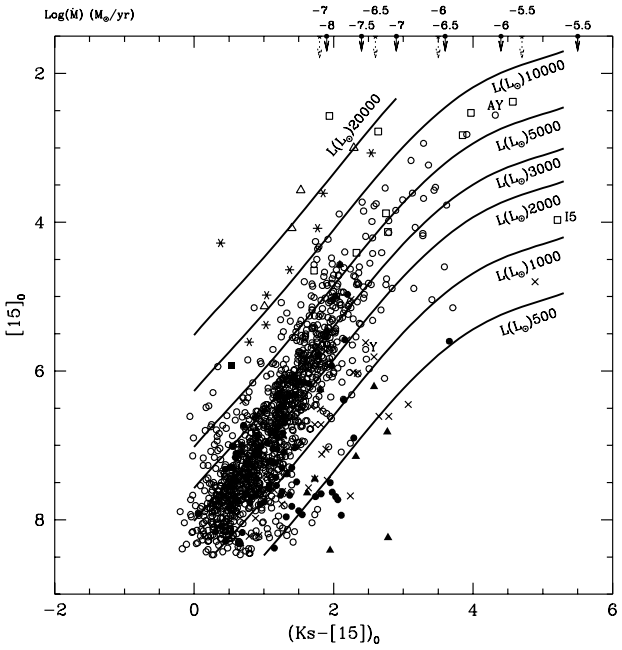

Figure 4. ISOGAL [15] versus $(K_s\text{-}[15])_o$ diagram of galactic bulge sources, taken from Ojha et al (2002). The different symbols are used to indicate sources for which different sorts of associations or data exist. The curves represent sequences of luminosities ranging from 500 to 20,000 $L_\odot$, with increasing mass-loss rates. The approximate scales of mass-loss rates are displayed at the top. For further details on how these were derived see Ojha et al. (2002)

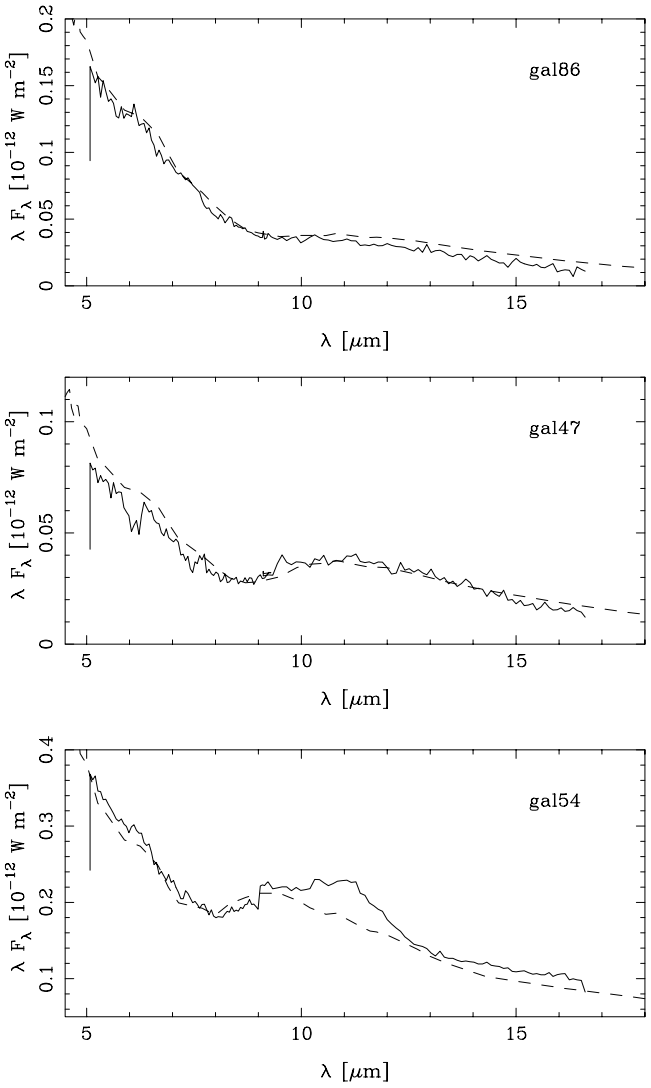

Figure 5. The CVF spectra of Bulge AGB stars shown together with fits from radiative transfer modelling (Groenewegen, 1993). The type of dust used is a combination of silicate dust and Aluminium Oxide. The mass loss rates range from 10^{-9} to a few 10^{-7} $M_\odot$/yr.

The ISOGAL catalogue also contains less massive young stars, mainly in nearby spiral arms at 1 or 2 kpc. Their colours are similar to the young stars in well studied star forming regions (Nordh et al. 1996 and Bontemps et al. 2001). The ISOGAL colours alone are not sufficient to be certain about their nature. For this reason follow up studies, especially with near-infrared spectroscopy is being performed. Further progress in this field can be expected from the new reduction method of the ISOGAL data (Section 6) which gives better quality maps, especially in regions with extended emission.

5. AGB STARS AND MASS LOSS

A [15] vs $(K_s\text{-}[15])_o$ diagram of sources selected in the direction of the bulge, taken from Ojha et al. (2002), is shown in Figure 4. A clear linear sequence of increasing $(K_s\text{-}[15])_o$ colour for brighter 15μm fluxes can be seen, as was also originally presented in the earlier Omont et al. (1999) paper for the [15] vs [7]-[15] diagram. Such red colours cannot be explained by very cold photospheres, but are influenced by dust emission.

On basis of near-infrared DENIS magnitudes and colours of Bulge fields with low and homogeneous extinction, it was demonstrated that the observed sources are red giants (Omont et al. 1999, Glass et al. 1999). Most of the ISOGAL 15μm sources have $(K_s)_o < 8.2$ mag and are thus above the RGB limit (Tiede et al. 1995). A comparison by Glass et al (1999) of ISOGAL data with a spectroscopic survey of Baade's window NGC 6522 (Blanco 1986), shows that M giants as early as M2 are detected by ISOGAL but that it is complete from M5 onwards. The increasing red colour of $(K_s\text{-}[15])_o$ as function of [15], can be explained by an increasing mass-loss rate. The exact amount of the mass loss rate is model-dependent, but is in the order of 10^{-9} to a few 10^{-7} $M_\odot$/yr.

Figure 6 shows a $(I\text{-}J)_o$ vs [7]-[15] diagram. The near-infrared colour is related to spectral type (caused by the increasing depths of the TiO and VO bands which influence the I-band magnitude) whereas the mid-infrared colours indicate the amount of circumstellar dust. The diagram gives a nice illustration of the expectation that mass loss increases for later spectral types. An important point to mention is that the relatively low mass-loss rates ($< 10^{-7}$ $M_\odot$ / yr) observed by the 15 μm excess cannot be observed through the near-infrared colours. *It is*

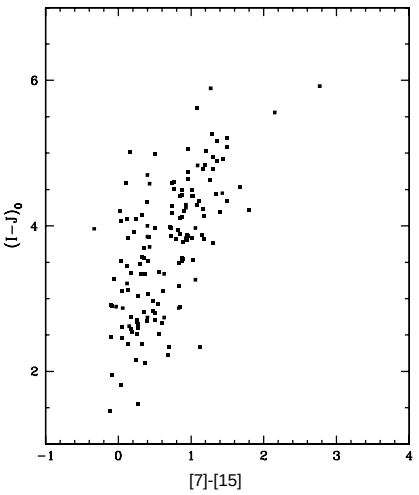

Figure 6. (I-J)$_o$ vs [7]-[15] diagram of a low extinction field in the galactic bulge.

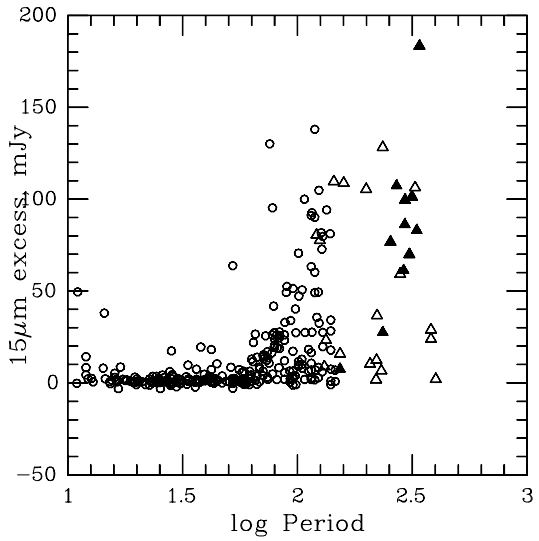

Figure 7. 15 μm excess (indicative of mass loss) vs logP, taken from Alard et al. (2001).

only by combining the deep DENIS and ISOGAL surveys that we are able to investigate the first systematic evidence of dust emission at this early stage, before the onset of the large mass loss ($> 10^{-7}$ $M_\odot$ / yr) like is seen in Miras and OH/IR stars.

A further investigation of the circumstellar dust of the mass losing AGB stars comes from ISOCAM Circular Variable Filters measurements. Eighteen 2-dimensional integral field spectroscopy measurements (6″ pixels, 5-17 μm, $\lambda/\delta\lambda > 35$) were performed of which 3 on bulge fields of low and homogeneous extinction. In total about 60 sources were detected. As was expected from the colours, several showed clear evidence of a mid-IR excess related to the circumstellar dust. In Figure 5 examples are shown for stars with mid-infrared excess ranging from small to intermediate. Important to notice is that most sources do not show the silicate 9.7 μm feature, but rather a broad feature with a maximum peaking at longer ($\sim 12\mu$m) wavelengths. Such features are known from previous work on IRAS data (Sloan & Price 1995 and references therein). They have been associated with amorphous aluminium oxide grains (Onaka et al. 1989, Speck et al. 2000). Such features are mostly seen in low mass-loss rate sources, confirming the interpretation that ISOGAL is mainly detecting the onset of mass-loss on the AGB.

Another important characteristic of AGB stars is their variability. Typical examples are Mira and Semi-Regular variables, with periods in the range of hundred to a few hundred days. Mass loss and variability are related in the sense that the longer period, and larger amplitude variable stars also show higher mass loss rates with the extreme examples being the OH/IR stars which have the longest periods (up to a thousand days) and the highest mass loss rates ($\sim 10^{-5}$ $M_\odot$/yr). Alard et al. (2001) combined the ISOGAL data with data coming from the gravitational lensing experiment MACHO for the Baade windows. In comparison to earlier searches for variable stars (e.g. Lloyd Evans 1976), the new surveys find variability down to much smaller amplitudes (0.5 mag compared to better than 0.1 mag). Alard et al. 2001 conclude that almost all sources detected at 7 and 15 μm and thus above the RGB-limit are variable. A period of 70 days or longer is a necessary but not a sufficient condition for mass loss to occur (Figure 7).

6. ISOGAL IN THE FUTURE

New treatment of the data has already started and will lead to a new set of images and a new version of the PSC. The new data-analysis uses an optimized method for ISOCAM raster measurements and is described in Miville-Deschênes et al. (2001). This method uses spatial redundancy and new transient correction method and reduces the noise in the map. It leads to a better reconstruction of extended emission and twice as many point sources are detected. An example of an image treated this way is given in Figure 8.

Several observational projects using the ISOGAL catalogue are on-going. Some examples are: near-infrared spectroscopy of galactic centre sources, a SiO maser radio survey of AGB stars near the galactic centre to study their kinematics, Timmi2 observations of YSO's. Further stellar work includes for instance the analysis of star forming regions like M16 and W51 which were observed within the ISOGAL project and an extension of the AGB studies to the galactic disk.

REFERENCES

Alard, C., Blommaert, J.A.D.L., Cesarsky, C., et al. (ISOGAL and MACHO Collaborations), 2001, ApJ 552, 289
Becker, R.H., White, R.L., McLean, B.J., Helfand, D.J., Zoonematkermani, S. 1994, ApJS 91, 347
Blanco, V.M., 1986, AJ 91, 290
Bontemps, S., André, P., Kaas, A.A., et al. 2001, A&A 372, 173
Cesarsky, C., Abergel, A., Agnèse, P., et al, 1996, A&A 315, L32
Epchtein, N., et al 1997, Messenger 87, 27

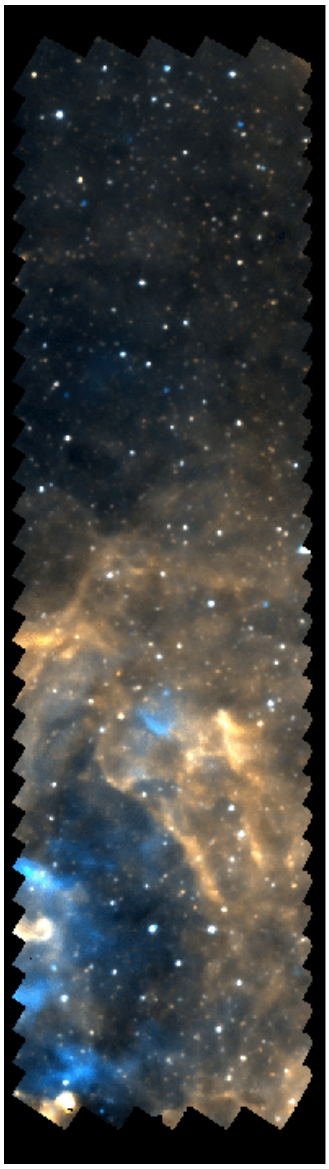

Figure 8. An example of an ISOGAL raster image produced with the improved data analysis method (Miville-Deschênes et al. 2001). It shows a composite image of 7 (blue) and 15 μm (red).

Felli, M., Comoretto, G., Testi, L., Omont, A., Schuller, F., 2000, A&A 362, 199

Felli, M., Testi, L., Schuller, F., Omont, A., 2002, A&A 392, 971

Glass, I.S., Ganesh, S., Alard, Blommaert, J.A.D.L., Gilmore, G., et al, 1999, MNRAS 308 127

Groenewegen, M.A.T., 1993, Ph D Thesis, Univ. of Amsterdam

Hennebelle, P., Pérault, M., Teyssier, D., Ganesh, S. 2001, A&A 365, 598

Jiang, B., Omont, A., Ganesh, S., Simon, G. Schuller, F., 2002, submitted to A&A

Lloyd Evans, T., 1976, MNRAS, 174, 169

Miville-Deschênes, M.-A., Boulanger, F., Abergel, A., Bernard, J.-P., A&AS 146, 519

Nordh, L., Olofsson, G., Bontemps, S., et al. 1996, A&A 315, L185

Ojha, D.K., et al, 2002, submitted to A&A

Omont A., Ganesh, S., Alard, C., Blommaert, J.A.D.L., Caillaud, B., et al, 1999, A&A 348 755

Omont A., et al, 2002, submitted to A&A

Onaka, T., de Jong, T., Willems, F.J., 1989, A&A 218 169

Ott S., et al, 1997, "Design and Implementation of CIA, the ISOCAM Interactive Analysis System", in ASP Conf. Ser. Vol. 125, Astronomical Data Analysis Software and Systems (ADASS) VI, ed. G. Hunt & H.E.Payne, (San Francisco: ASP), 34

Pérault, M., Omont, A., Simon, G., et al. 1996, A&A 315, L165

Price, S.D., Egan, M.P., Carey, S.J., et al. 2001, AJ 121, 2819

Schuller, F., 2002, PhD thesis, Paris VI, Pierre et Marie Curie University

Schuller, F., Ganesh, S., Messineo, M., Moneti, A., Blommaert, J.A.D.L., et al., 2002, submitted to A&A

Sloan, G.C., Price, S.D., 1995, ApJ 451 758

Speck, A., Barlow, M.J., Sylvester, R.J., Hofmeister, A.M., 2000, A&AS 146, 437

Teyssier, D., Hennebelle, P., Pérault, M., 2002, A&A 382, 624

Tiede, G.P., Frogel, J.A., Terndrup, D.M., 1995, AJ 110, 2788

van Loon, J.Th., Gilmore, G.F., Omont, A., Blommaert, J.A.D.L., Glass, I.S., et al. 2002, MNRAS in press

ACKNOWLEDGEMENTS

The ISOCAM data presented in this paper were analysed using 'CIA', a joint development by the ESA Astrophysics Division and the ISOCAM Consortium. The ISOCAM Consortium is led by the ISOCAM PI, C. Cesarsky.

THE SCIENTIFIC POTENTIAL OF THE POST-HELIUM DATABASE

Bart Vandenbussche

Institute of Astronomy K.U.Leuven, Celestijnenlaan 200B, 3001 Leuven, Belgium

ABSTRACT

After the depletion of the liquid Helium used for the cooling of the telescope and the focal plane instruments of ISO, the temperature of the focal plane remained sufficiently low to operate the InSb band 1 detectors of the SWS. Observing time was granted to a programme aimed at extending the MK-classification to the near-infrared. Good quality spectra (2.36μm – 4.1μm) of 238 stars at moderate resolution ($\lambda/\delta\ \lambda \approx$ 1500 – 2000) were obtained in the time slots available during the satellite engineering test programme.

Low scheduling priority was given to the programme stars that were already observed at a similar resolution during the nominal part of the mission in the framework of various other programmes. The dataset has been completed with these 55 nominal-phase spectra. The resulting data-set, the ISO-SWS post-helium atlas of near-infrared stellar spectra, contains 293 spectra covering a large range of spectral types and luminosity classes. The calibrated and reduced data is now available electronically.

We illustrate the potential of this database for near-infrared classification of stars, stellar population synthesis and the reduction of ground-based L-band spectra. We also show the first results of our application of Autoclass, an unsupervised Bayesian classification, on the Post-He data and suggest other AUTOCLASS applications on the ISO archive.

1. INTRODUCTION

Since the publication of the optical spectral atlas by Morgan et al. (1943), several authors have published spectral atlases of stars covering a broad range in spectral types and luminosity classes. With the development of spectrometers more sensitive towards the near-infrared and infrared, spectral atlases in these wavelength regions have become available. The IRAS LRS atlas (Olnon et al. 1986) contains more than 5000 low-resolution ($\lambda/\delta\ \lambda \approx$ 20–60) spectra between 7.7 and 22.6 μm. Recent work includes atlases of Fourier Transform Spectrograph spectra of MK-standards in the H, J, and K-band by Meyer et al. (1998), Wallace et al. (2000) and Wallace & Hinkle (1996). Förster-Schreiber (2000) published a library of near-infrared K-band spectra of 31 late-type giants and supergiants and two carbon stars at a spectral resolution of 830 and 2000. The spectral library by Lançon (2000) includes about 200 spectra between 0.5 and 2.5 μm of cool, mostly variable, giants and supergiants. Heras et al. (in preparation) describe the mid-infrared spectral characterisation of stars without dust excess using full ISO-SWS spectra at low resolution ($\lambda/\delta\ \lambda \approx 300$), most of which were obtained in the 'STARTYPE' ISO observing programme. An extension of the 'STARTYPE' project with the classification of all SWS full spectra contained in the ISO archive is in preparation (Kraemer, this volume).

A moderate resolution spectral atlas of stars between 2.3 and 4 μm, covering a broad range in spectral type and luminosity classes is not available. This wavelength range is accessible from the ground, but it is seriously contaminated by strong telluric lines, e.g. of H_2O. Providing such an atlas was the prime scientific driver of the ISO-SWS post-helium programme.

2. SOURCE SELECTION

The sources in the Post-Helium observation program were selected on the basis of three criteria :

1. The ISO visibility around the expected Helium boil-off date. The predictions of this date had an estimated accuracy of $\pm$ two weeks.
2. The brightness of the source. Since the integration time of the Post-He observation template is fixed, the signal-to-noise ratio is determined by the brightness of the source. Therefore only sufficiently bright stars are in the sample ($>$ 1Jy across the entire wavelength range covered).
3. Covering a large range of spectral types and luminosity classes.

The programme stars were selected primarily from The Bright Star Catalogue (Hoffleit & Warren 1991) according to these criteria. The Wolf-Rayet stars were selected from van der Hucht et al. (1997). Many of the selected stars had been observed already during the nominal operations phase of the ISO satellite at a comparable resolution and wavelength coverage during the nominal operations of the ISO satellite. The observation modes meeting those criteria are the SWS AOT1 speed 4 observation mode and some AOT6 observations (de Graauw et al. 1996). We avoided the duplication of these observations during the post-helium phase. Instead, the spectra of 55 programme stars obtained during the nominal phase were added to the final dataset.

The complete dataset contains 293 measurements. Those are the selected measurements of which the signal to noise ratio is better than 10, allowing the identification of the molecular and atomic spectral features. Fig. 1 shows a HR-diagram for

Proceedings of the Symposium *"Exploiting the ISO Data Archive - Infrared Astronomy in the Internet Age"*, 24–27 June 2002, Sigüenza, Spain (C. Gry, S. B. Peschke, J. Matagne et al. eds., ESA SP-511)

the programme stars. The sample covers spectral types between O4 and M9, carbon stars and luminosity classes from the main-sequence to supergiants.

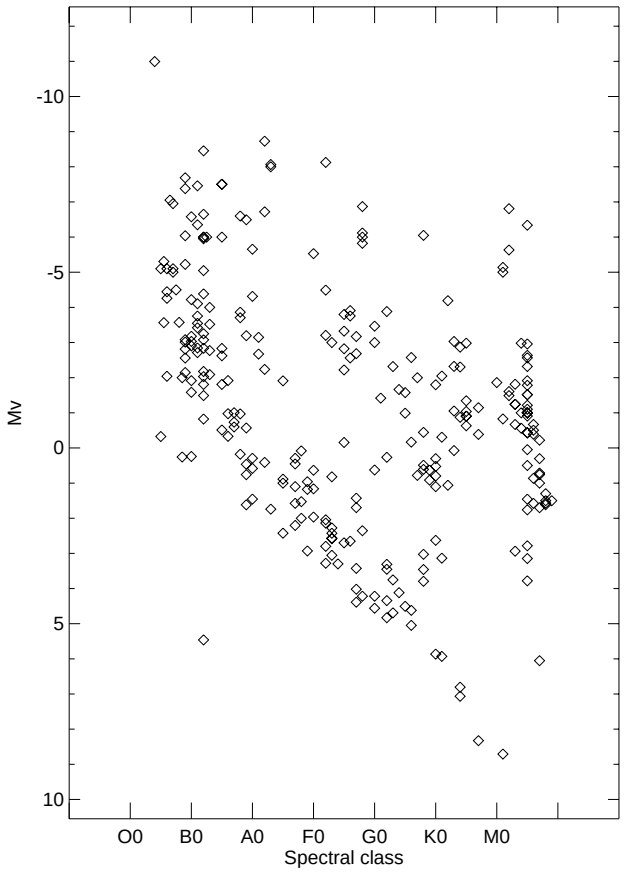

Figure 1. Hertzsprung-Russell diagram of the programme stars. Spectral classes are taken from the literature; absolute V magnitudes are calculated from Hipparcos parallaxes and photometry. No bolometric correction was applied. For WR-stars, carbon stars and other stars without reliable photometry or distance the approximate location is indicated.

3. POST-HE CALIBRATION

During the test programme following the liquid Helium depletion of ISO, the temperature of the focal plane remained sufficiently low to operate the InSb band 1 photodiodes of the SWS. As the temperature of the focal plane increased, changes in the measured positions of the grating scanner mirror and changes in the response of the instrument could be seen. We have shown that the drifts in the instrument characteristics are smooth and have been calibrated accurately with the calibration observations performed in the course of the programme (Vandenbussche et al. 2002a). Table 1 gives the flux calibration budget of the ISO-SWS post-He observations and compares them to the nominal ISO-SWS observations.

Table 1. The flux calibration error budget of the ISO-SWS post-helium observations and the nominal ISO-SWS observations

Error source	Post-He	Nominal
Absolute error on the average flux		
Absolute flux conversion	5 %	2 %
Absolute Pointing error	8 %	4 %
Relative errors – broadband		
RSRF	5 %	3 %
Relative errors – small scale		
Dark noise	1 Jy	1 Jy
RSRF	1 %	1 %
Pointing jitter	0-2.5 %	–
Line intensity of unresolved lines		
Unresolved fringes	20 %	20 %
Linewidth jitter	5 %	5 %

4. DATA REDUCTION

We have reduced the data within the SWS Interactive Analysis package (SIA) [1].

The nominal SWS observations were processed with the algorithms and calibration parameters of the Off-Line-Processing pipeline OLP 10.

As described in the previous section, the changing characteristics of the SWS instrument during the Post-Helium phase required a different calibration.

All calibrated spectra have been reduced further in a consistent way. First a noise filter was applied. Data points that were more than 3 times the standard deviation away from the mean in a resolution bin were discarded. This process was repeated five times. The resolution bins were defined according to the average resolution per AOT-band.

Per AOT-band the data points were rebinned to the average resolution in the band. In order to meet the Nyquist criterion for complete sampling of the measurement, we have oversampled four times when applying the noise filter and the rebinning.

Finally, small corrections to the absolute flux level of the four AOT-bands were applied to align them to each other. The data in the small overlap regions between the spectral bands was used to determine the scaling factors. The strategy we followed was to keep fixed as many bands as possible. The correction factors applied are small (mostly of the order of a few percent) and are listed in Vandenbussche et al.(2002b)

The data reduction applied was optimised to present a continuous spectrum at the highest defensible resolution. If accurate line intensities are needed, users of the Post-Helium data should revert to line-fitting procedures on unbinned spectra which we have made available in the ISO Data Archive.

5. NEAR-INFRARED STELLAR SPECTRA

The 2.36 μm - 4.05 μm region is a valuable spectral probe for both hot and cool stars. HI lines (Bracket, Pfund and Humphreys series), HeI and HeII lines, atomic lines and molecu-

[1] SIA is a joint development of the SWS consortium. Contributing institutes are SRON, MPE, KUL and the ESA Astrophysics Division.

lar lines (CO, H_2O, NH, OH, SiO, HCN, C_2H_2, ...) are sensitive to temperature, gravity and/or the nature of the outer layers of the stellar atmosphere (outflows, etc.). In this section we give a qualitative discussion of the spectral features seen in the different spectral classes covered in our sample. For the spectral classes where several post-Helium spectra are available we have selected the spectra with the best signal-to-noise.

5.1. OB STARS

The spectra in the observed wavelength region of the normal OB-type giants and dwarfs show Hydrogen lines in absorption of the Bracket (Brα [4.0523 μm], Brβ [2.6259 μm]), Pfund (Pfγ [3.7406 μm] – Pf22 [2.4036 μm]) and Humphreys series (Hu14 [4.0209 μm] and higher). Some O supergiants show these Hydrogen lines in emission and also show Helium ionic lines (HeII(7–6) [3.0917 μm]). The Be stars in the sample exhibit their Hydrogen lines in emission. These lines originate from the gas in the circumstellar disk.

A detailed quantitative discussion of the post-He spectra of OB-stars can be found in Lenorzer et al. (2002a).

The spectra of Wolf-Rayet stars are characterised by various broad emission lines originating in the hot dense stellar winds that drive the extremely high mass loss of these stars. We see emission lines of HeI, HeII, CIII, CIV and the forbidden [CaIV] line at 3.21 μm (See also van der Hucht et al. 1996, Willis et al. 1997 and Morris et al. 1999). A discussion of all ISO-SWS observations of WR stars is in preparation by Morris et al.

5.2. AF STARS

The near-infrared spectrum of A through F-type stars is dominated by the HI lines of the Bracket (n=4), Pfund (n=5) and Humphreys (n=6) series. We normally see those lines in absorption, except in some stars with a shell (e.g. Herbig Ae/Be stars) where the hydrogen emission originating in the shell can fill in some of the photospheric absorption (e.g HD 190073).

5.3. G STARS

In the spectra of G-type stars we see important contributions from various atomic lines. Towards later type G-stars the strength of the Hydrogen absorption lines weakens and we start to see molecular species. The CO first overtone band appears between 2.36–2.45 μm.

5.4. KM STARS

In cool stars (K,M) the spectrum shows atomic lines, but is dominated by molecular bands. We see the CO first overtone (2.36–2.45 μm), the OH band (3.02–3.4 μm), the H_2O band (2.36–3.8 μm) and the onset of the SiO first overtone (beyond 4.00 μm). The strength of the bands as we see them does not only depend on the fundamental stellar parameters. The emission from the circumstellar dust can fill in and weaken the photospheric absorption bands considerably. Fig. 2 depicts a number of cool giants ranging from K0 to M8 in spectral type.

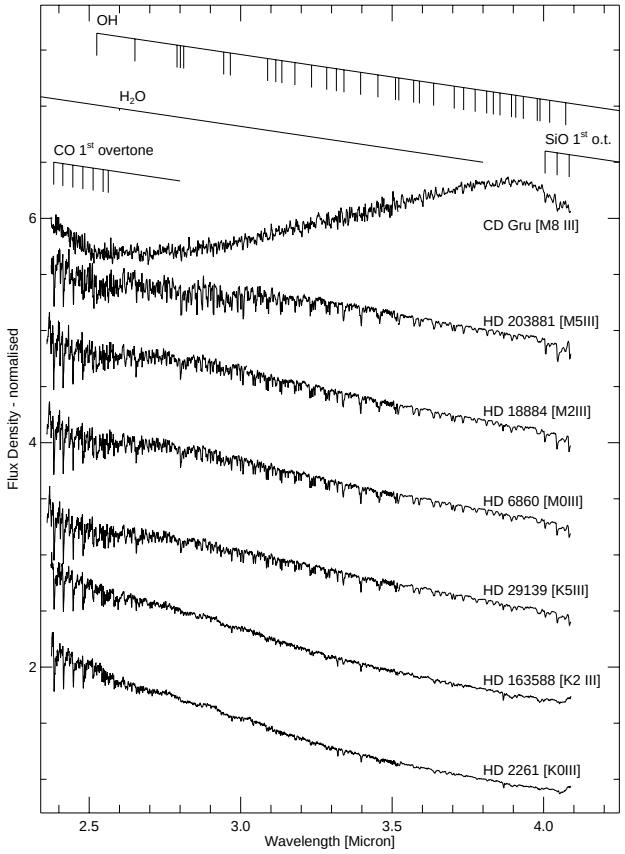

Figure 2. Spectral features in the spectra of K and M stars. Only the strongest lines of the OH, CO and SiO molecular bands are indicated. A multitude of fainter lines in these bands and in the H_2O band are not resolved and contribute to a substantial depression of the continuum.

It should be noted that the strength of the molecular bands in M giants can be strongly variable. Aringer et al. (2002) show important variations in time resolved SWS spectra of M-type Miras.

5.5. CARBON STARS

Secchi (1868) was the first to identify the class of carbon stars among red giants based on the presence of C_2 lines in the optical spectrum. Wallerstein & Knapp (1998) review what we have learned about carbon stars since then. The optical spectra also show lines of CH, CN, heavy elements like Tc, ^{12}C and ^{13}C. Various theories exist on the mixing mechanisms that bring those elements to the surface. Many carbon giants on the Asymptotic Giant Branch (AGB) are variable and show a high mass loss. The circumstellar dust shell obscures their photospheres at visible wavelengths and causes an excess at mid-infrared and far-infrared wavelengths.

At near-infrared wavelengths the circumstellar dust is optically thin and we see a broad absorption feature centred around

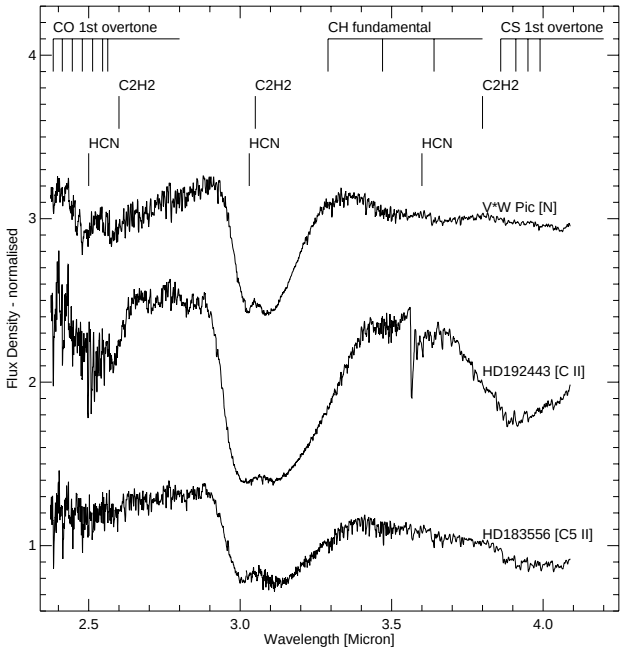

Figure 3. Spectral features in the spectra of Carbon stars: The flux scale is in Jy, normalised to 1 at 3.8 μm and offset for the different spectra. Only the strongest lines of the CO, CS and CH molecular bands have been indicated.

3.05 μm. This band is due to the stretching modes of C_2H_2 and HCN. The strength and shape of the bands associated with several vibrational transitions of HCN (2.5μm, 3.6μm, 3.85 μm) and C_2H_2 (2.6μm, 3.8μm) varies from source to source. We also recognise the CO first overtone band around 2.5 μm, the CH fundamental band (3-4 μm) and the CS first overtone band around 4 μm (Aoki et al 1998). Fig. 3 shows three carbon-rich objects with the important molecular bands indicated.

6. ELECTRONIC AVAILABILITY OF THE DATA

The reduced data can be retrieved from the data archive at the ISO Data Centre[2]. The complete atlas is available online on the web[3].

The atlas can be also be downloaded in PDF format. In the atlas we have ordered the spectra of our sample according to spectral type as found in the literature. For each star we have listed some relevant literature values at the bottom of the page. We list the source's HD number if available, together with other names of the source. The spectral type is listed if available. For some stellar sources such as novae or planetary nebulae we have not specified the MK-classification here, but rather a description of the nature of the source.

For every source the V magnitude and B-V color is given. If available, we have listed the Hipparcos magnitudes and colors here. If not, other values from the literature are taken. The IRAS number of the source in the Point Source Catalog is listed together with the in-band fluxes at 12, 25, 60 and 100 μm. Unfortunately, the 1986 edition of the PSC does not indicate if the flux densities are flux densities or upper limits for the faintest sources. Care should be taken when interpreting low flux values. We also list the ISO observation identification (TDT) which identifies the plotted observation uniquely in the ISO Data Archive.

Furthermore, we indicate relevant positional properties: Right Ascension [RA], Declination [Dec], Proper Motion in Right Ascension [pm(RA)], Proper Motion in declination [PM(dec)] and parallax. From these values and the spacecraft attitude control system data we have calculated the offset between the source position and the center of the SWS slit. The values are calculated in the coordinate frame of the spacecraft y- and z-axis. These correspond to the cross-dispersion and the dispersion direction of the SWS instrument.

7. EARLY-TYPE SPECTRAL DIAGNOSTICS

One of the primary goals of the Post-He programme was to establish near-infrared spectral diagnostics for spectral type, luminosity class, mass loss and CSM geometry. This enables the interpretation of observations of obscured stars where the near-infrared is the only available window.

Lenorzer et al (2002a) have used the Post-He data to derive that the strength of the Pfund lines constrains the spectral class of B main-sequence stars and giants to within 2 subtypes. The width of the Bracket-β line determines the luminosity class. The same paper shows a relationship between the width of the Bracket-α line and the mass loss of normal O and B supergiants with an accuracy of 0.25 dex.

The Post-He data have also led to a method to determine the geometry of the circumstellar material of early-type stars base on Hydrogen line ratios. Lenorzer et al. (2002b) found that the Hu14/Pf7 and the Hu14/Brα line ratios allow to distinguish between LBVs, B[e] and Be stars.

8. LATE-TYPE SPECTRAL DIAGNOSTICS

Similar to the work already done on hot stars, we plan to analyse the Post-He spectra of later types to establish near-infrared spectral diagnostics for those stars. The strength and the width of the Hydrogen lines in A, F and G stars will be correlated with Effective Temperature, Gravity, etc. . . .

For KM-giants and carbon stars, the near-infrared spectrum is dominated by blended molecular bands. Here a process is needed where the different molecular bands are subsequently subtracted from the spectrum according to consistent synthetic spectra, e.g. the Joint Characteristics method discussed by Cami (2002).

9. UNBIASED CLASSIFICATION

We have initiated work on an unbiased classification of the Post-He spectra. Goal is to get unbiased evidence for morphological differences in groups of Post-He spectra, and to corre-

[2] http://www.iso.vilspa.esa.es
[3] http://www.ster.kuleuven.ac.be/pub/isoph

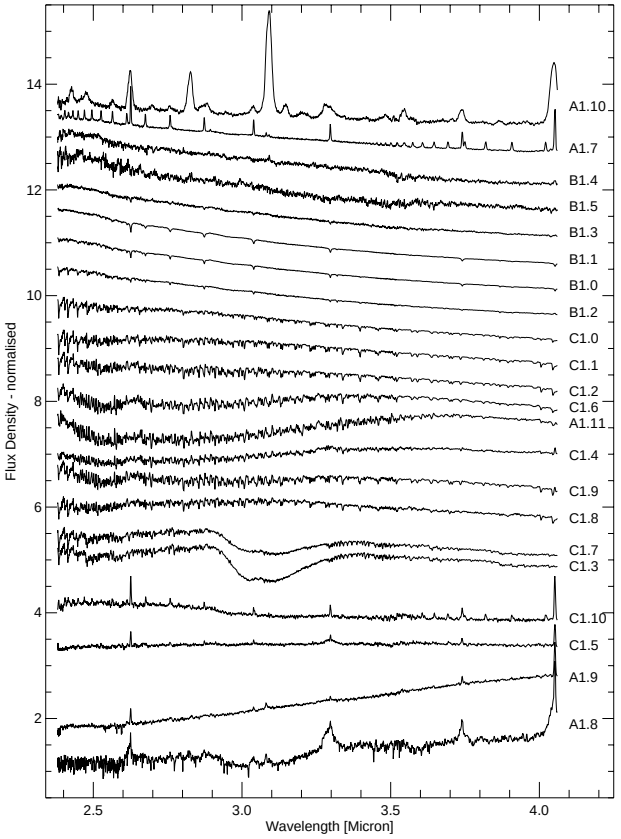

Figure 4. The mean of the spectra in each of the 22 classes in the A1 B1 and C1 classification. The average spectrum of Class A1.12 has been discarded since the low S/N does not allow any comparison to the other average spectra.

late those groups with stellar properties like temperature, gravity, mass loss, pulsation period, . . .

We have applied an unsupervised Bayesian classification on the set of spectra using the *Autoclass* software (Cheeseman & Stutz 1996, Hanson et al. 1991). The classification criteria offered to the algorithm are the flux densities at 2539 wavelengths. The *Autoclass* run converges in the sense that the classifications with the highest likelihood found are very similar. In a next iteration two sets of similar classes have been offered again to the classification algorithm to further refine the classification. The result is a set of 23 classes of spectra for which we have unbiased evidence that they are distinguishable in the dataset. Fig. 4 shows the average spectrum of these classes.

When comparing Autoclass class membership and MK classification according to the literature, we see that the sequence of Autoclass classes B1.0 – B1.2 – C1.0 – C1.1 – C1.2 – C1.6 follows the MK classification. Especially towards late-type stars the Autoclass classes correlate with the MK classification on subclass level.

In the case of classes C1.3 and C1.7, containing 7 and 4 carbon stars respectively, we see that both classes contain stars with an MK classification as C5II and C6II. Fig. 5 shows a color diagram with V-K against B-V colors for the stars in both

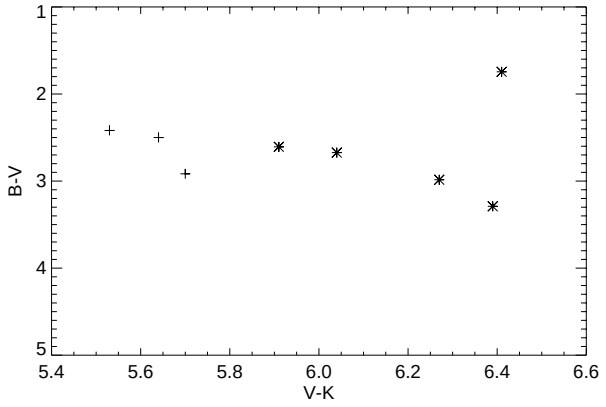

Figure 5. V-K against B-V colors for the stars in classes C1.3 (+) and C1.7 (*).

classes. We see that there is no significant difference in the B-V color between the two classes. The V-K colors of stars in both classes, however, are significantly different.

We conclude that our Autoclass classification is sensitive to properties of carbon stars the MK classification is not sensitive to. To elaborate on this preliminary result we have initiated a more detailed study to correlate the Autoclass classes with fundamental stellar parameters of the member stars, their mass loss rates and pulsation. We will report on these correlations in the near future.

10. POPULATION SYNTHESIS

The post-helium atlas is a valuable dataset for the interpretation of near-IR spectra of external galaxies in population synthesis projects. In the NIR the integrated galaxy's spectrum is the sum of the spectra of the individual stars in the system.

11. L-BAND TELLURIC STANDARDS

Lenorzer et al. (2002, private communication) have successfully used post-helium atlas spectra as reference spectra for telluric standards in the reduction of ground-based L-band spectra obtained at UKIRT and VLT-ISAAC. The main problem in the calibration of ground-based near-infrared spectra is that the most prominent features in ground-based IR spectra are the telluric features of the Earth's Atmosphere. Some of the telluric lines do not scale linearly with airmass and therefore it is necessary to observe a standard star of which the spectrum is known, at the same airmass and with the same instrument setup as those of the science target. We plan to select the spectra of suitable telluric standards in the post-helium atlas and present this to the community as a library of stellar spectra for L-band spectrophotometric calibration.

12. AUTOCLASS BEYOND THE POST-HE DATA

The autoclass classification of the ISO-SWS Post-He spectra has been a first step towards an autoclass classification on all

the spectra in the ISO legacy archive. We plan to apply Autoclass on the dataset of all full ISO-SWS spectra (2.36-45 μm) first. In a later stage we might also consider adding all spectral data to the classification since Autoclass III is in principle robust against missing values for some attributes. The average spectrum of classes found in such a large classification could reveal subtle features present in different sources that stay hidden in the noise of the individual observations.

13. CONCLUSION

The post-Helium atlas, containing 296 ISO-SWS band 1 spectra of stars of different spectral types, has been made available to the community and offers plenty of potential for further scientific exploitation. We have illustrated how the atlas can be used to establish near-infrared diagnostics of stellar properties and circumstellar material. We also indicated other applications in synthetic population studies and the use of these spectra as references for telluric standards for ground-based L-band observations. The unsupervised Autoclass classification of the post-Helium spectra suggests that the technique can be applied to discover subtle features in larger spectral datasets in the ISO data-archive.

REFERENCES

Aoki, W., Tsuji, T., & Ohnaka, K. 1998, A&A 340, 222

Aringer, B., J⊘rgensen, U. G., Kerschbaum, F. et al., 2002, in ASP Conf. Ser. 259: Radial and Nonradial Pulsationsn as Probes of Stellar Physics, 538

Cami, J. 2002, PhD thesis, Universiteit van Amsterdam

Cheeseman, P. & Stutz, J. 1996, in Advances in Knowledge Discovery and Data Mining, 153–180

de Graauw, T., Haser, L. N., Beintema, D. A., et al. 1996, A&A 315, L49

Förster Schreiber, N. M. 2000, AJ 120, 2089

Hanson, R., Stutz, J., & Cheeseman, P. 1991, Bayesian classification theory, NASA Tech. rep.

Hoffleit, D. & Warren, J. W. H. 1991, The Bright Star Catalogue 5th Revised Ed.

Lançon, A. & Wood, P. R. 2000, A&AS 146, 217

Lenorzer, A., de Koter, A., & Waters, L. B. F. M. 2002a, A&A 386, L5

Lenorzer, A., Vandenbussche, B., Morris, P., et al. 2002b, A&A 384, 473

Meyer, M. R., Edwards, S., Hinkle, K. H., & Strom, S. E. 1998, ApJ 508, 397

Morgan, W. W., Keenan, P. C., & Kellman, E. 1943, in Astrophysics monographs University of Chicago Press

Morris, P. W., Bouwman, J., Crowther, P. A., et al. 1999, in ESA SP-427: The Universe as Seen by ISO, Vol. 427, 247+

Olnon, F. M., Raimond, E., Neugebauer, G., et al. 1986, A&AS 65, 607

Secchi, A. 1868, MNRAS 28, 196+

van der Hucht, K. A., Conti, P. S., Lundstrom, I., & Stenholm, B. 1997, VizieR Online Data Catalog, 3085, 0+

van der Hucht, K. A., Morris, P. W., Williams, P. M., et al. 1996, A&A 315, L193

Vandenbussche, B., Beintema, D., de Graauw, T., et al. 2002a, A&A, 390, 1033

Vandenbussche, B., Beintema, D., de Graauw, T., et al. 2002b, VizieR Online Data Catalog

Wallace, L. & Hinkle, K. 1996, ApJS 107, 312+

Wallace, L., Meyer, M. R., Hinkle, K., & Edwards, S. 2000, ApJ, 535, 325

Wallerstein, G. & Knapp, G. R. 1998, ARA&A 36, 369

Willis, A. J., Dessart, L., Crowther, P. A., et al. 1997, MNRAS 290, 371

WATER OBSERVED IN RED GIANTS AND SUPERGIANT STARS – MANIFESTATION OF A NOVEL PICTURE OF THE STELLAR ATMOSPHERE OR ELSE EVIDENCE AGAINST THE CLASSICAL MODEL STELLAR PHOTOSPHERE

Takashi Tsuji

Institute of Astronomy, School of Science, The University of Tokyo, Mitaka, Tokyo, 181-0015 Japan

ABSTRACT

We detected the H_2O 6.3 μm bands in more than 30 red giants stars from K5III to M8III as well as in some early M supergiants on the SWS spectra retrieved from the ISO Data Archive. This result, however, shows serious inconsistency with the present model photospheres which predict H_2O only in the latest M (super)giant stars. Also H_2O was once discovered in the early M (super)giant stars nearly 40 years ago with the balloon-borne telescope named Stratoscope II. This discovery was so unexpected at that time that it was not understood correctly and overlooked for a long time. Now, we reflect on our ignorance of this important discovery during the 40 years and should consider more seriously the meaning of the rediscovery of water in so many red (super)giant stars with ISO.

Key words: ISOSWS – MOLsphere – Photosphere – Water

1. INTRODUCTION

At this monumental epoch to celebrate the opening of the ISO active archive phase, it may be instructive to recall a short history of stellar spectroscopy in space. At the infancy of the infrared astronomy in the 1960's, an ambitious attempt to observe stellar spectra with a balloon-born telescope was undertaken and this mission named Stratoscope II, launched on March 1963, successfully observed infrared spectra (0.8 – 3.1 μm) of several red giant and supergiant stars (and invaluable spectra of Jupiter). The results showed beautiful spectra of water in Mira variables *o* Cet and R Leo (Woolf et al. 1964). This result was well in accord with the theoretical prediction (Russell 1934) and thus was well appreciated at that time.

However, the Stratoscope observers reported a more surprising result that water was detected in the earlier M giants μ Gem (M3III) and ρ Per (M4II) as well as in the early M supergiants α Ori (M2Iab) (Woolf et al. 1964) and μ Cep (M2Ia) (Danielson et al. 1965). However, this discovery was not in accord with the understanding of cool stellar atmosphere at that time and it was finally reinterpreted that the absorption bands at 0.9, 1.1, 1.4, & 1.9 μm identified with H_2O by the Stratoscope observers should instead be due to the CN Red System which also has band heads at about the same positions (Wing & Spinrad 1970). This proposition was more easily accepted by the astronomical community since then, since CN had been observed in a wide range of oxygen-rich stars from the Sun to red supergiants, not to speak of carbon stars.

Meanwhile, the discovery of water, at least in the coolest Miras, confirmed the importance of water as a source of opacity in cool stars, and actual computation of the non-grey model photospheres revealed that this is true in red giant stars with $T_{\rm eff}$ cooler than about 3200 K (Tsuji 1978), which roughly corresponds to M6III (Ridgway et al. 1980). This result was well consistent with the detection of the strong H_2O bands in the Miras but was contradicting with the identification of H_2O in the M2 - M4 (super)giants by the Stratoscope II observers. Thus, this result lent further support to the Wing-Spinrad proposition. A blind spot in this apparently reasonable conclusion, however, was that we were not aware at that time that the model photosphere, often referred to inadvertently as model atmosphere, is simply a model of the *photosphere* ($0 \lesssim \tau < \infty$) and not of the *atmosphere* ($-\infty < \tau < \infty$), which may still involve unknown problems.

Since then, important infrared missions such as IRAS and COBE have been successfully undertaken, but few observations of the near infrared stellar spectra were done in space, except for continued efforts with KAO which provided fine low resolution stellar spectra (e.g. Strecker et al. 1979). Finally, ISO launched on November 1995 (Kessler et al. 1996) provided the means by which to observe astronomical spectra at higher resolutions for a wider spectral coverage at last. One of the unexpected results in the initial ISO observations with SWS (de Graauw et al. 1996) was a detection of water in the M2 giant β Peg (Tsuji et al. 1997) and in several early M supergiants in $h + \chi$ Per clusters (Tsuji et al. 1998). It took sometime before we recognized that the Stratoscope II observers correctly identified water in the M2 – M4 (super)giant stars and that the Wing-Spinrad proposition was not correct (Tsuji 2000a). Further, IRTS launched by ISAS on March 1995 detected H_2O bands at 1.9 μm in several M (super)giants earlier than M6 (Matsuura et al. 1999). Also, ground-based mid-infrared spectroscopy revealed H_2O pure-rotation lines in α Ori and α Sco (Jennings & Sada 1998).

All these results that H_2O exists in red (super)giants earlier than about M6, however, could not be understood with the present model photospheres. We now encounter a serious problem: are we confronting with a fall of the classical model stellar photosphere or else with a rise of a novel picture of the stellar atmosphere (including the photosphere as a part)? A rather intriguing story of water in red (super)giant stars still remains

Proceedings of the Symposium *"Exploiting the ISO Data Archive - Infrared Astronomy in the Internet Age"*, 24–27 June 2002, Sigüenza, Spain (C. Gry, S. B. Peschke, J. Matagne et al. eds., ESA SP-511)

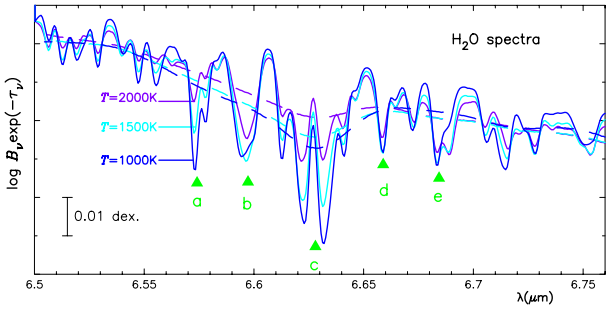

Figure 1. Spectra of water for $N_{\rm col} = 10^{18}$ cm^{-2} and $T_{\rm ex} = 1000, 1500,$ and 2000 K are shown for high ($R \approx 1600$; solid lines) and low ($R \approx 200$; dashed lines) resolutions of SWS.

open, and we hope to utilize the extensive ISO Data Archive to extend and finalize this fascinating story.

2. A RED GIANT SAMPLE

Our initial detection of water was done with the H_2O 2.7 μm bands which, however, are contaminated by OH, CO, and other molecular bands. Then, we analyzed the H_2O 6.3 μm bands which are little disturbed by other molecular bands. The expected spectra of the H_2O ν_2 bands computed with the use of HITEMP (Rothman 1997) based on a single absorption slab model are shown in Fig.1.

We first examined a dozen of high resolution spectra of red giants in the ISO Data Archive. The H_2O 6.3 μm bands are detected in the K5 giant Aldebaran (but not in other two K giants) as well as in all the M giants between M0III and M3.5III (Tsuji 2001), and also in the later M giants (M6-7III), as shown in Fig. 2. We found $T_{\rm ex} \approx 1500$K (and $\log N_{\rm col}$ noted on Fig. 2) by referring to the spectra such as shown in Fig.1. It is remarkable that SWS detected such faint water bands in the K giant star α Tau. This result is quite unexpected but confirmed recently in another K giant Arcturus (α Boo) with the high resolution ground-based spectroscopy in the 12 μm region (Ryde et al. 2002).

Next, we extend our survey to a larger sample of the low resolution SWS spectra. We found dozens of spectra in this category from the ISO Data Archive. At the lower resolution, some details of the band structure seen at the higher resolution are smeared out (Fig.1). Nevertheless we can detect the dip at 6.63 μm due to the H_2O ν_2 bands in 25 M giants from M0III to M8III. Some examples are shown in Fig.3 and we estimated $N_{\rm col}$ values for these M giants, again with the single slab model of Fig.1.

The resulting values of $N_{\rm col}$ from the high and low resolution samples are plotted against spectral types in Fig.4. For comparison, the predicted values of $N_{\rm col}$ from the spherically extended non-grey model photospheres are shown by the dashed line. It is clear that the observed $N_{\rm col}$ values cannot be explained at all by the predicted ones. Thus, H_2O detected in M giants should be non-photospheric in origin, but where does it come from?

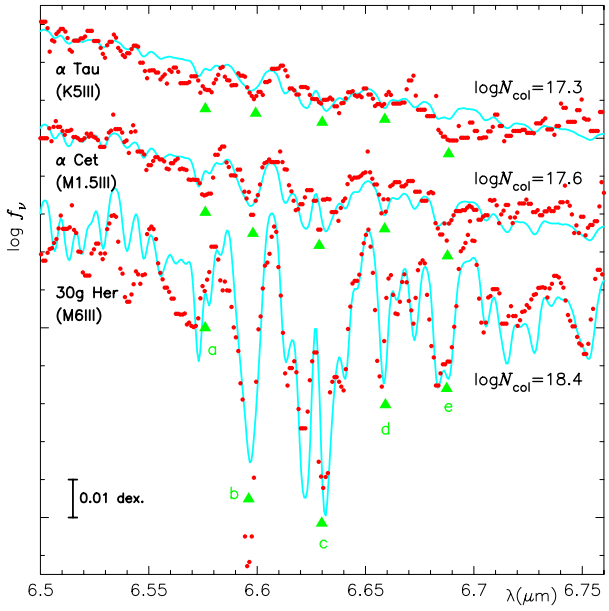

Figure 2. Observed high resolution SWS spectra (filled circles) are compared with the water spectra of Fig.1 (solid lines).

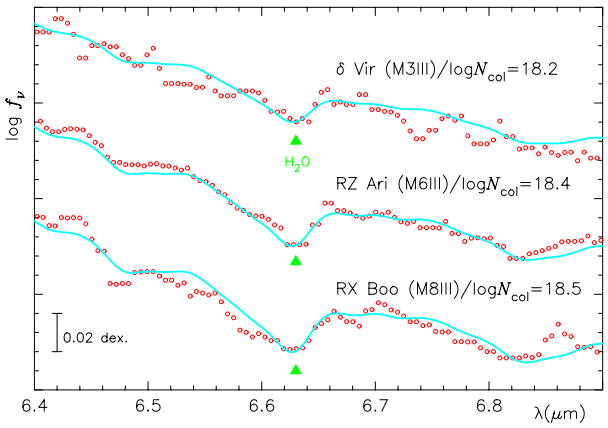

Figure 3. Observed low resolution SWS spectra (open circles) are compared with the water spectra of Fig.1 (solid lines).

3. A RED SUPERGIANT SAMPLE

In red supergiant stars, the H_2O 6.3 μm bands are found as absorption in α Ori (M2Iab) and α Sco (M2Ib), as in K - M giants. Further, water appears in absorption at $\lambda < 5$ μm but in emission at $\lambda \gtrsim 5$ μm throughout in μ Cep (M2Ia) (Tsuji 2000b). This detection of water in distinct emission should be an important clue to the origin of H_2O, since such emission should most probably originate in the outer atmosphere and not, for example, in the "starspots".

To account for the emission, we upgrade our single slab model to a spherically extended molecular sphere (MOLsphere for simplicity). Since we already know that $T_{\rm ex} \approx 1500$ K and $N_{\rm col} \approx 3 \times 10^{20}$ cm^{-2} from the Stratoscope II data (Tsuji 2000a), an additional free parameter is the inner radius of the MOLsphere r_i. For simplicity, we consider only H_2O whose

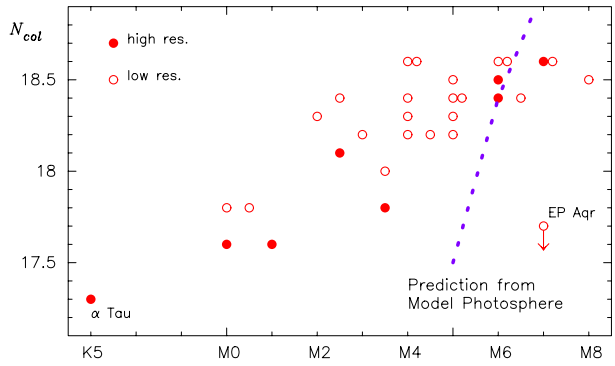

Figure 4. The observed $N_{\rm col}$ values from the high and low resolution SWS spectra (filled and open circles, respectively) plotted against spectral types are compared with the predicted $N_{\rm col}$ values based on the model photospheres (dashed line).

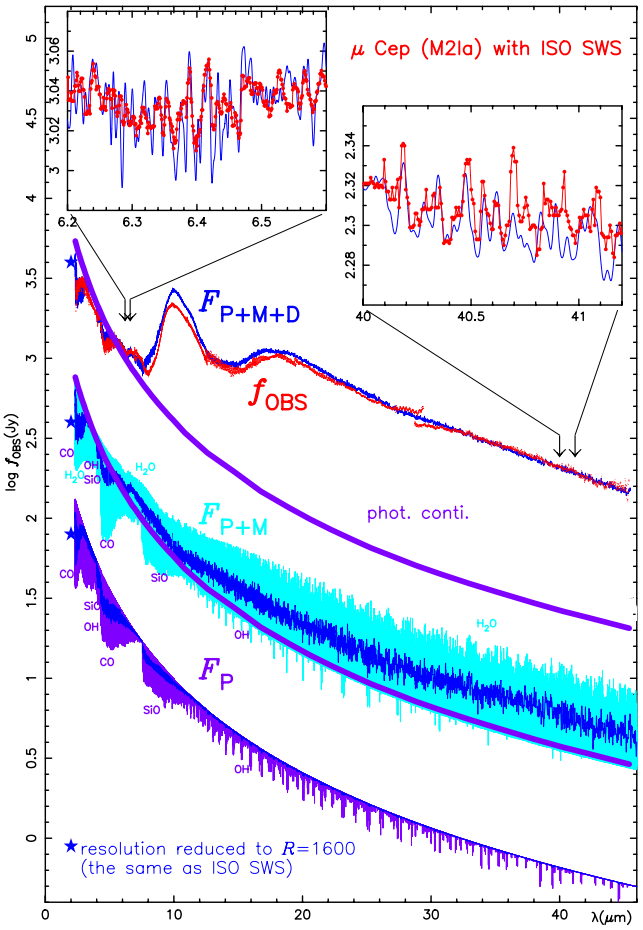

Figure 5. Photospheric spectrum $F_{\rm P}$ (bottom) based on the spherically symmetric non-grey model photosphere ($T_{\rm eff}$ = 3600 K, M_* = 15 $M_\odot$, R_* = 650 $R_\odot$) is used as the boundary condition for solving radiative transfer in the MOLsphere. The resulting emergent spectrum from the MOLsphere $F_{\rm P+M}$ (middle) is further diluted by the emission due to the optically thin dust envelope and $F_{\rm P+M+D}$ (top) is the final spectrum to be compared with the ISO spectrum f_{obs}. The computations of $F_{\rm P}$ and $F_{\rm P+M}$ are done with a resolution of $R \approx 10^5$ and the results are convolved with the slit function of SWS (R = 1600).

absorption cross-section is as large as 10^{-18} cm^2 and thus the H_2O gas is optically thick. Then we solve the transfer equation with the photospheric radiation, resulting in $F_{\rm P}$, as a boundary condition, which shows absorption bands due to CO, CN, OH, SiO etc (Fig.5). We found that the resulting emergent flux from the MOLsphere $F_{\rm P+M}$ with $r_{\rm i} \approx 2R_*$ (R_* is the stellar radius) accounts for the prominent emission lines due to H_2O at $\lambda \gtrsim 5$ μm as well as the absorption bands at $\lambda < 5$ μm (Tsuji 2000b).

Further, we found that the huge infrared excess can be explained by an optically thin dust envelope with $\tau^{\rm d}_{10\mu m} \approx 0.1$ and $r^{\rm d}_i \approx 13.5R_*$. Then the dust emission is simply added to $F_{\rm P+M}$. The entire spectra of μ Cep observed with the ISO SWS (corrected for $A_{\rm V} = 1.5$ mag.) can reasonably be explained by our final spectrum resulting from Photosphere+ MOLsphere + Dust Envelope, $F_{\rm P+M+D}$. Some details of the water emission in the 6 μm and 40 μm regions can be well reproduced by our model as shown in the inserted boxes of the left and right, respectively, in Fig.5. So far, the huge IR excess of μ Cep was thought to be due to dust alone, but now it is clear that it includes water emission originating in the MOLsphere.

4. DISCUSSION AND CONCLUDING REMARKS

Although we have assumed MOLsphere for μ Cep, this is not a theoretical model of the usual meaning but simply a kind of working hypothesis or an empirical model at best. We know nothing about the origin of the MOLsphere and it is a major challenge how to resolve this issue. Such a difficulty, however, may be shared with the origin of the chromosphere as well as of the mass-loss outflow (at least in non-pulsating stars). With this reservation, our empirical model for μ Cep is reasonably successful, and a problem is if such a model can be extended to other cases. Although we see no emission in the 6 μm region in our large sample of red giant stars, it is interesting to notice that the H_2O column densities tend to lever-off at about M5 and then to be smaller than the predicted photospheric values (Fig.4). Moreover, water bands almost disappear in M7 giant EP Aqr. These results suggest that the photospheric H_2O bands may be filled in by the emission due to H_2O itself in the late M giants. Also, in the late M giants, H_2O appears as emission in the 40 μm region (Tsuji et al. 1999), CO_2 shows prominent emission in the 15 μm region (Jasttanont et al. 1998), and SO_2 shows emission as well as absorption in the 7 μm region (Yamamura et al. 1999). Based on these observations, it should be reasonable to assume the presence of MOLsphere in late M giants.

However, a possibility that there are some serious flaws in the present model photospheres cannot be excluded, especially for K (see Ryde et al. 2002) and early M giants for which there is no direct evidence for MOLsphere. This case offers a more serious problem, since our present stellar spectroscopy (e.g. abundance analysis) loses its basis. Also, if this is the case, we must give up to have a unified picture for cool luminous stars including K and early M giants. We are yet tempted to

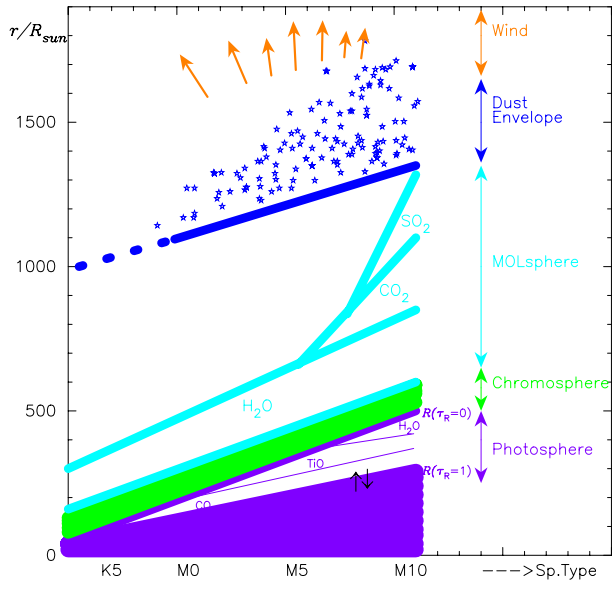

Figure 6. A working hypothesis on the evolution of the atmospheric structure of red giants with Sp. Type. Stellar radius R_* is defined by $\tau_{\rm Ross} \approx 1$ but photosphere extends to where $\tau_{\rm Ross} \approx 0$. Presently, self-consistent modelings are possible for the photosphere and interior ($0 < \tau < \infty$), but not at all for other components in the outer atmosphere ($-\infty < \tau < 0$).

have a unified picture, ISO's innovation of which may be illustrated as in Fig.6. The presence of the high excited molecular gas has been known for late (super)giants from the H_2O and SiO masers for a long time, but ISO revealed that the presence of such a warm molecular gas, including not only H_2O and SiO but also CO_2 and SO_2, may be a general phenomenon in red giant and supergiant stars.

In concluding, we summarize our present viewpoint:

1. Water was discovered in several early M (super)giants nearly 40 years ago with Stratoscope II, but this discovery has been mis-interpreted and overlooked until recently. We regret that this important discovery did not provide major impact on the theory of cool stellar atmosphere during these 40 years. We certainly hope that such an unfortunate history should not be repeated with the ISO data.

2. After 40 years, we confirmed H_2O absorption bands in more than 30 red giant stars from K5III to M8III with the use of the ISO Data Archive. Thus ISO finally established that the presence of water is a general phenomenon in red giant stars including K and early M types.

3. With ISO SWS, we detected water in emission in the M2 supergiant μ Cep. This fact suggests that water should be in the outer atmosphere rather than in the photosphere. Also, emission not only of H_2O but also of CO_2 and SO_2 are detected in late M giants with ISO and, by implication, water in all the red giant stars may also be originating in the outer atmosphere.

4. We conclude that the presence of a rather warm molecular sphere – MOLsphere – may be a general feature in red giant and supergiant stars. Thus ISO revealed a novel picture of the atmosphere consisting not only of the photosphere, chromosphere, and wind so far known but also of a new component – MOLsphere. Certainly, the ISO Data Archive should be an invaluable tool by which to explore the fundamental problem on the atmospheric structure of red giant and supergiant stars.

ACKNOWLEDGEMENTS

I thank I. Yamamura and T. Tanabé for helpful discussion on the ISO data analysis. This work, supported by JSPS grant No. 11640227, was carried out with the facilities at NAO ADAC.

REFERENCES

Danielson, R. E., Woolf, N. J., Gaustad, J. E. 1965, ApJ 141, 116
de Graauw, Th., Haser, L. N., Beintema, D. A., et al. 1996, A&A 315, L49
Jasttanont, K., Feuchtgruber, H., de Jong, T., et al. 1998, A&A 330, L17
Jennings, D. E., Sada, P. V. 1998, Science 279, 844
Kessler, M. F., Steinz, J. A., Anderegg, M. E., et al. 1996, A&A 315, L27
Matsuura, M., Yamamura, I., Murakami, H., et al. 1999, A&A 348, 579
Ridgway, S. T., Joyce, R. R., White, N. M., Wing, R. F. 1980, ApJ 235, 126
Rothman, L. S. 1997, High-temperature molecular spectroscopic database (CD-ROM) (Andover: ONTAR Co.)
Russell, H. N. 1934, ApJ 79, 317
Ryde, N., Lambert, D., Richter, M. J., Lacy, H. 2002, preprint (astro-ph 0207368)
Strecker, D. W., Erickson, E. F., Witteborn, F. C. 1979, ApJS 41, 501
Tsuji, T. 1978, A&A 62, 29
Tsuji, T. 2000a, ApJ 538, 801
Tsuji, T. 2000b, ApJ 540, L99
Tsuji, T. 2001, A&A 376, L1
Tsuji, T., Ohnaka, K., Aoki, W., Yamamura, I. 1997, A&A 320, L1
Tsuji, T., Ohnaka, K., Aoki, W., Yamamura, I. 1998, Ap&SS 255, 293
Tsuji, T., Aoki, W., Ohnaka, K. 1999, ESA SP-427 229
Wing, R. F., Spinrad, H. 1970, ApJ 159, 973
Woolf, N. J., Schwarzschild, M., Rose, W. K. 1964, ApJ 140, 833
Yamamura, I., de Jong, T., Onaka, T., et al. 1999, A&A 341, L9

THE TRANSITION FROM AGB STARS TO PLANETARY NEBULAE AS SEEN BY ISO

Pedro García-Lario[1] **and José V. Perea Calderón**[2]

[1] ISO Data Centre, European Space Agency, Villafranca del Castillo, Ap. Correos 50727, 28080 Madrid, Spain
[2] INSA S.A., Villafranca del Castillo, Ap. Correos 50727, 28080 Madrid, Spain

ABSTRACT

We present a classification scheme for stars evolving in the transition phase between the Asymptotic Giant Branch (AGB) and the Planetary Nebula (PN) stage based on the detailed analysis of low resolution infrared SWS spectra from 2 to 45 μm of a large sample of stars available in the Infrared Space Observatory (ISO) Data Archive. The classification is made on the basis of the detection and analysis of: i) gas phase features in the extended atmospheres of the AGB stars; ii) solid state features in the neutral circumstellar shells surrounding the transition objects; and iii) nebular emission lines in the ionized PNe. This information, combined with the observed overall infrared energy distribution, is used to determine the evolutionary stage of each of the sources in the sample. The results here presented provide a complete view of the spectroscopic evolution expected in this short transition phase as a function of the mass of the progenitor star as the starting point for future spectroscopic research on this field in the infrared range.

Key words: ISO – AGB stars – Planetary Nebulae

1. INTRODUCTION

The short transition phase between the end of the AGB and the formation of a new PN is still poorly understood. The main reason for this is twofold. First, only a small number of objects are known in this phase, as this is a short-lived evolutionary stage. Second, in many cases, stars evolve through this phase heavily obscured by the strong circumstellar envelopes formed during the previous AGB phase, thus making observations difficult in the optical range (Kwok 1993).

However, these stars are among the brightest sources in the sky at infrared wavelengths and, thus, they were the target of many of the observations included in the Infrared Space Observatory (ISO) Data Archive, especially in the spectral range from 2 to 45 μm, covered by the Short Wavelength Spectrograph (SWS), where the most important gas phase and solid state features under analysis are found.

2. SELECTION OF THE SAMPLE

The ISO Data Archive was systematically searched for spectra taken with the SWS in the low resolution mode (AOT 01) corresponding to stars classified in the literature as AGB, post-AGB stars or PNe. This resulted in the identification of 330 sources with a reasonable signal-to-noise SWS01 spectrum corresponding to 77 original ISO proposals.

For all these sources the automated off-line processing pipeline data products (AAR files - OLP Version 10) were retrieved and used for our classification exercise.

3. CLASSIFICATION STRATEGY

Our classification strategy is based on the simultaneous analysis of several spectroscopic indicators like:

- **gas features**, corresponding to molecules formed in the outer layers of the stellar atmosphere and in the circumstellar shell
- **solid state features**, from the dust grains formed in the shell at distances from the central star where the temperature is low enough to allow condensation of the refractory elements contained in the gas
- **nebular emission lines**, if the temperature of the central star is high enough to ionize the gas ejected during the previous AGB phase
- **underlying infrared continuum**, mainly thermal emission from the dust in the envelope heated by the radiation coming from the central star

They provide us information about:

- **the dominant chemistry in the circumstellar gas**: through the detection of atomic or molecular lines corresponding to O-rich (SiO, SO_2, H_2O, CO_2) or C-rich (C_3, HCN, C_2H_2, CS) species, mainly in the near- and mid-infrared range
- **the dominant chemistry in the circumstellar dust**: through the detection of bands identified with O-rich (titanium and aluminum oxides, silicates, water ice) or C-rich (titanium and silicon carbide, PAHs) carriers, the expected main constituents of the dust grains
- **general properties of the gas**: temperature, density, ionisation state, chemical abundances, especially in the case of PNe
- **general properties of the dust grains**: size, composition, nucleation, growth, internal organisation (amorphous *vs.* crystalline in the case of the O-rich silicates; aliphatic *vs.* aromatic for the carbonaceous compounds)
- **evolutionary stage and mass loss history experienced by the central star**: through the detailed analysis of the overall spectral energy distribution from 2 to 45 μm combined with

Proceedings of the Symposium *"Exploiting the ISO Data Archive - Infrared Astronomy in the Internet Age"*, 24–27 June 2002, Sigüenza, Spain (C. Gry, S. B. Peschke, J. Matagne et al. eds., ESA SP-511)

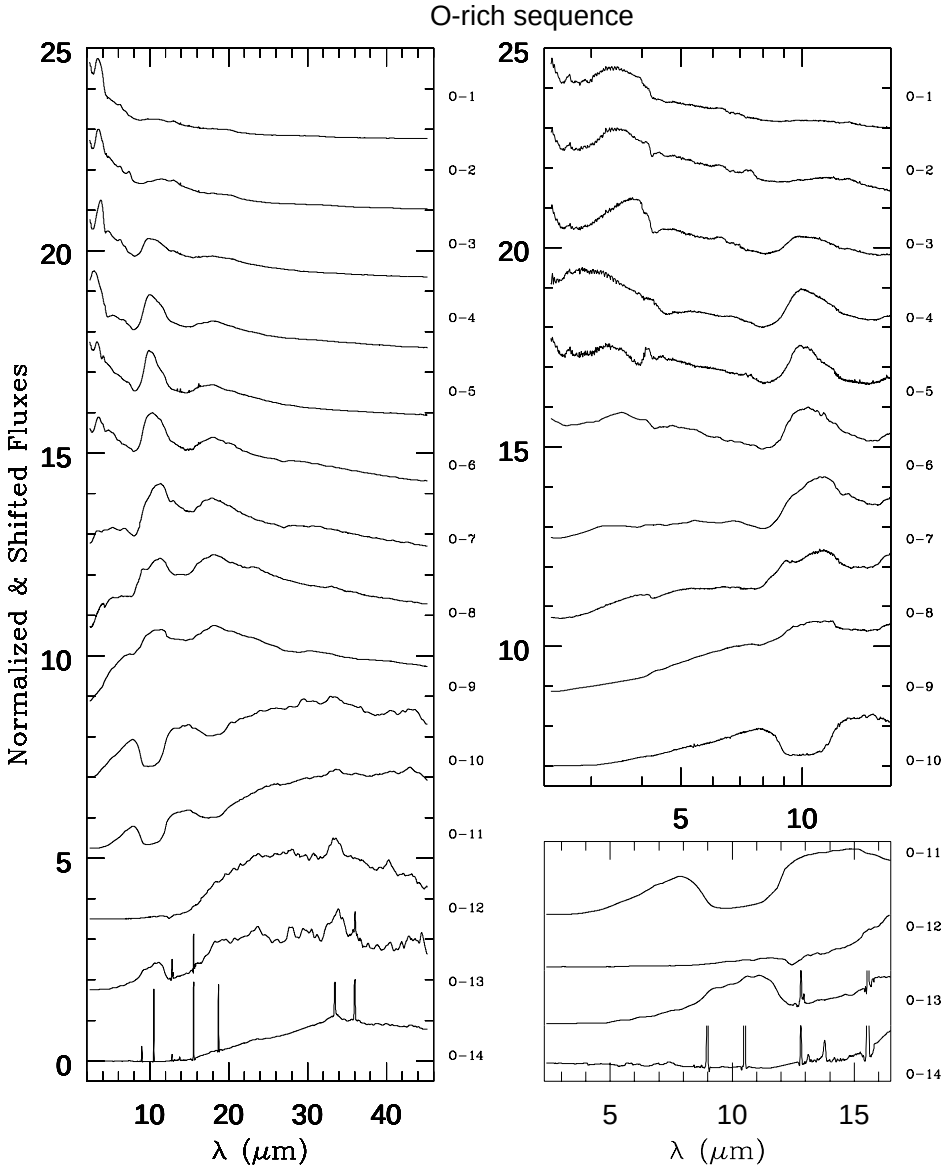

Figure 1. The proposed evolutionary sequence for O-rich AGB stars in their way to become PNe. In the left panel the whole spectral range covered by SWS is shown from 2 to 45 μm, while in the right panel we present just the short wavelength region expanded in order to show in detail the most important features used in our analysis in this spectral range.

the relative strength of the dust features present in the same spectral range

According to the above considerations we propose an evolutionary scheme for O-rich and C-rich AGB stars, shown in Figs. 1 and 2 respectively, which nicely reproduce the changes predicted to occur in these stars in their way to become PNe.

They represent essentially two sequences of:

– **increasing mass loss rate** while stars are still evolving along the AGB, reflected by the increasing strength of the solid dust features visible in the ISO spectra (silicate emission bands at 10 and 18 μm in O-rich AGB stars; silicon carbide emission at 11.3 μm in C-rich AGB stars)

– **increasing thickness** of the circumstellar shell, especially at the end of the AGB phase, when the above mentioned bands can turn into absorption as the envelope becomes optically thick to the radiation at mid-IR wavelengths and no emission from the heavily obscured central star is detected at the short wavelength range of the ISO spectrum, which at this stage is completely dominated by the thermal emission from the cool dust in the envelope

– **gradual cooling of the circumstellar envelope** when the star enters the post-AGB phase, as can be derived from the evolution of the overall energy distribution. At this moment the strong mass loss suddenly stops and the peak of the in-

frared emission starts shifting towards longer wavelengths, reflecting the lower temperature of the dust in the envelope. This is accompanied by a rapid increase of the effective temperature of the central star, which eventually produces the ionisation of the gas in the circumstellar envelope, leading to the formation of a new PN and the detection of nebular emission lines over-imposed on the cool thermal dust continuum

– **changing properties in the dust grains**, which turn from amorphous to crystalline (aliphatic to aromatic in the case of a C-rich chemistry) suddenly after the end of the AGB phase when the mass loss reaches its maximum rate, in a process which is yet unexplained, but may have to do with grain destruction in the so-called 'superwind' phase, leading to the formation of strong crystalline silicate features in the case of O-rich envelopes, and PAHs and other aromatic C-rich compounds in those which are C-rich

4. TWO DIFFERENT CHEMICAL PATHS

From the analysis of the spectroscopic indicators above mentioned and if the proposed evolutionary scheme shown in Figs. 1 and 2 is correct we can conclude that all sources in the transition phase from the AGB to the PN stage experience very similar changes in their observational properties, in spite of displaying a totally different chemical composition.

Currently accepted nucleosynthesis models (Groenewegen & de Jong 1993; Busso, Gallino & Wasserburg 1999; Lattanzio & Forestini 1999) predict a strong difference in the chemical composition of the stellar atmospheres of AGB stars as a consequence of the different initial masses of their progenitor stars (they are in a range between 0.8 and 8 $M_{\odot}$).

Initially all stars in the Universe are born O-rich (C/O $<$1), and thus, they are expected to reflect this O-rich chemical composition in their atmospheres. However, during the thermal pulses that take place at the end of the AGB phase, important amounts of carbon can be formed as a consequence of the incomplete burning of helium in the triple-α process. This carbon can be dredged-up to the surface of the star by convection and increase the C/O ratio to a value larger than the unity, leading to the formation of C-rich molecules in the outer atmosphere of the star. Eventually, this change of chemistry will also be reflected in the composition of the dust grains formed in the circumstellar envelope.

According to theory, this transformation of O-rich stars into C-rich stars is expected to occur only in intermediate-mass AGB stars (between 2 to 4 $M_{\odot}$). The reason is that, on one side, high-mass AGB stars ($M \geq 4-5\ M_{\odot}$) experience the so-called 'hot bottom burning'. This is a process which occurs at the bottom of the convective envelope only when the temperature is so high ($T \geq 2 \times 10^7$ K) that ^{12}C is transformed into ^{14}N via the CNO-cycle. This slows down or even prevent the formation of high-luminosity carbon stars and, thus, high-mass AGB stars, which evolve very fast, remain O-rich all the way along the AGB until they reach the PN stage. Instead, they may become N-rich, which is exactly what we observe in the most massive PNe known in our Galaxy (the so-called 'type I' PNe). On the other side, low-mass stars (below $\sim$2 $M_{\odot}$) evolve very slowly and are expected to remain also O-rich along their whole life as AGB stars because they experience too few thermal pulses to modify the original C/O $<$ 1 ratio.

Actually, the sequence of O-rich spectra shown in Fig. 1 is only representative of the evolution expected for high-mass O-rich AGB stars. A third sequence would be needed to represent the evolution of low-mass O-rich AGB stars. Because of their slow evolution and lower mass loss rates they are not expected to develop an optically thick envelope and, thus, the silicate bands would never be visible in absorption. In addition, in the most extreme cases they would not be able to develop an observable PN, since by the time when the central star could reach a temperature high enough to produce the ionisation of the gas in the circumstellar envelope this would be too far away, almost completely diluted in the interstellar medium.

5. OPEN QUESTIONS

Although we can see that the available ISO spectra in the Data Archive can be used to reproduce qualitatively well the evolutionary sequence predicted by the existing models, the situation is far from being simple.

For instance, our sample contains both O-rich stars ($\sim$70%) and C-rich stars ($\sim$23%) but also contains a few cases ($\sim$7%) in which a mixed chemistry is found whose origin is not yet well understood.

In addition, some broad bands visible in the ISO spectra of C-rich post-AGB stars centered at 26 and 30 μm are still not identified and more laboratory data is needed to determine unambiguously the nature of their carrier(s).

Our proposed evolutionary scheme suggests that crystallisation of the dust grains (both C-rich and O-rich) is taking place in the circumstellar envelopes of AGB stars at the end of the AGB phase for still unknown reasons.

As we can see, and as it usually happens in science, the results obtained raise more questions than they answer. In order to address these questions properly in the future we will certainly need additional spectroscopic data in the infrared range taken from other space observatories, combined with observations taken at other wavelengths and with laboratory data. The goal should be to quantitatively determine the effective contribution of low-mass and intermediate-mass stars to the chemical enrichment of our Galaxy and ultimately extended this analysis to other galaxies to understand the chemical evolution of our entire Universe.

REFERENCES

Busso M., Gallino R., Wasserburg G.J., 1999, ARA&A 37, 239
Groenewegen M.A.T., de Jong T., 1993, A&A 267, 410
Kwok S., 1993, ARA&A 31, 63
Lattanzio J., Forestini M., 1999, in: IAU Symp. 191 on *Asymptotic Giant Branch Stars*. Eds. T. Le Bertre, A. Lebre, and C. Waelkens, p. 31

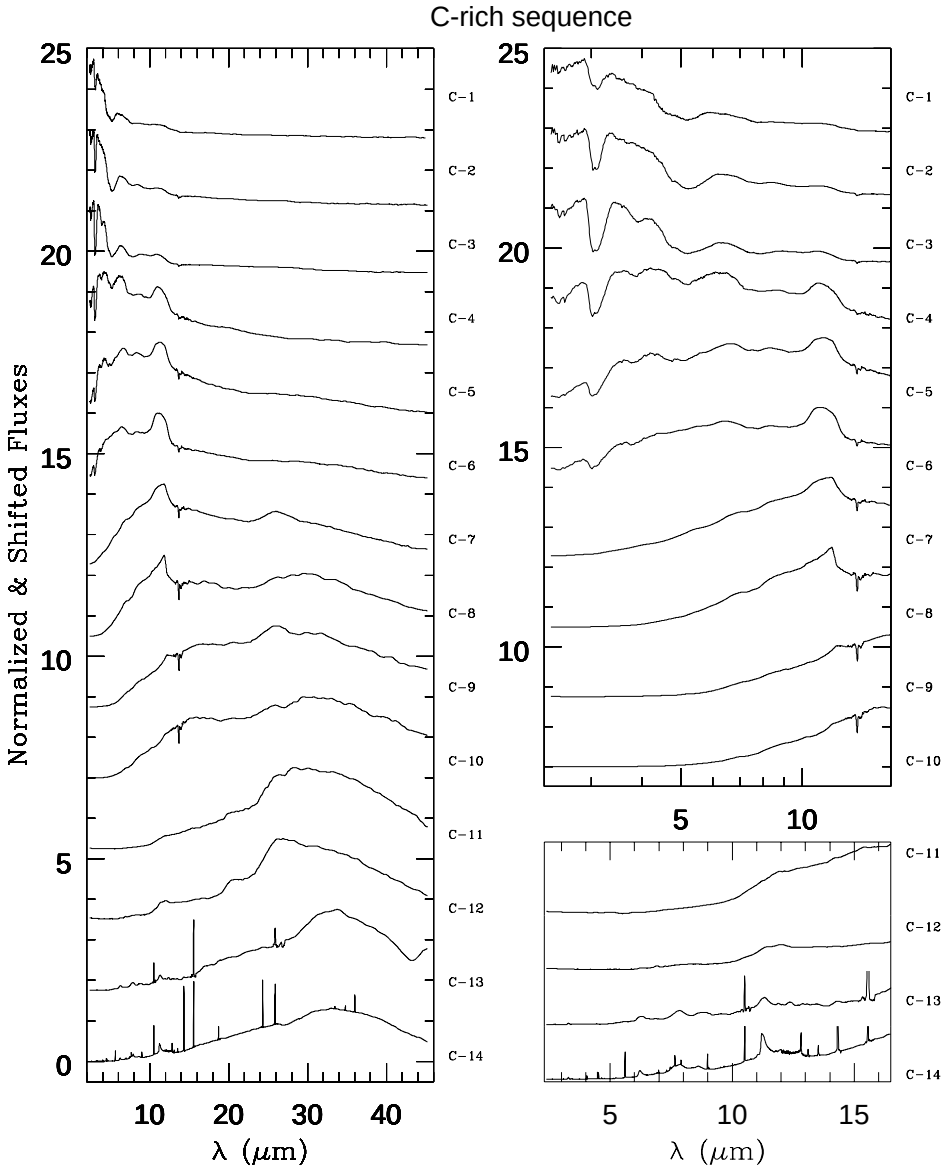

Figure 2. The proposed evolutionary sequence for C-rich AGB stars in their way to become PNe. In the left panel the whole spectral range covered by SWS is shown from 2 to 45 μm, while in the right panel we present just the short wavelength region expanded in order to show in detail the most important features used in our analysis in this spectral range.

RADIATIVE PUMPING OF 1612 MHZ OH MASERS: OH/IR SOURCES WITH IRAS LRS SPECTRA AND 34.6 MICROMETER ABSORPTION FEATURE

Ryszard Szczerba[1], **Jin Hua He**[2], **and Pei Sheng Chen**[2]

[1]N. Copernicus Astronomical Center, Rabiańska 8, 87-100 Toruń, Poland
[2]Yunnan Astronomical Observatory, National Astronomical Observatories, CAS, Kunming 650011, P.R. China

ABSTRACT

The population inversion which leads to the 1612 MHz OH maser emission has long been thought to be radiatively pumped. Since OH rotational lines involved in this pumping scheme lie in the far–infrared they became observable only after the launch of the ISO satellite. With the aim to investigate the pumping conditions of the 1612 MHz OH maser emission in more detail we have searched the ISO Archive for SWS observations around 34.6 μm of 1024 OH/IR sources with IRAS LRS spectra from compilation of Chen et al. (2001). Surprisingly, among 81 OH/IR sources which have appropriate SWS data only already reported objects: VY CMa, IRC+10420 and the Galactic center, show clear 34.6 μm absorption line. We discuss possible reasons for non–detection of this pumping line.

Key words: ISO – radiative pumping of the 1612 MHz OH maser.

1. INTRODUCTION

The first detection of intense radio emission from OH molecules was reported by Weaver et al. (1965) and soon an explanation based on maser amplification through induced processes was invoked (Litvak et al. 1966, Perkins et al. 1966). Shklovsky (1966) was first who proposed a radiative pumping mechanism for OH masers and his idea was elaborated in detail by Elitzur et al. (1976) for infrared (IR) stars which exhibit the 1612 MHz OH satellite line (hereafter OH/IR stars). In this scheme the required inversion of F=1 and F=2 sub-levels (even and odd parity, respectively) in the lowest rotational level is achieved by absorption of infrared photons (predominantly at 34.6 μm) from the ground state of OH molecule ($^2\Pi_{3/2}$ J=3/2) and consequent radiative decays to lower levels via other far-infrared (FIR) transitions.

Due to atmospheric absorption in the FIR region, OH rotational lines are inaccessible from the ground and only indirect checks of the pumping scheme was possible using infrared flux extrapolated to about 35 μm. For example, it was shown that there are enough FIR photons (about 4 FIR photons for one OH photon - Elitzur 1992) to pump the 1612 MHz OH maser (Evans & Beckwith 1977, Nguyen-Q-Rieu et al. 1979, Epchtein et al. 1980). Direct confirmation of this theory become possible only with the launch of the Infrared Space Observatory (ISO, Kessler et al. 1996) which allows observation of the pumping transition(s) and other FIR OH lines from OH maser sources. First clear absorption at 34.6 μm in the Short Wavelength Spectrometer (SWS, de Graauw et al. 1996) spectrum of supergiant NML Cyg was reported by Justtanont et al. (1996) and in case of the Galactic center by Lutz et al. (1996). A detailed analysis supporting the radiative pumping cycle for circumstellar masers have been presented by Sylvester et al. (1997) in the case of another supergiant IRC+10420. They detected not only the pumping line at 34.6 μm in the SWS 02 spectrum of IRC+10420 (now resolved into Λ-doublet components), but also rotational cascade lines at 98.7, 163.1 and 79.2 μm. Thai-Q-Tung et al. (1998) performed modeling of pumping conditions and maser radiative transfer calculations for this supergiant. Their results are in agreement with the observed FIR OH lines, confirming the theoretical pump scheme. There are three more sources for which published SWS observations show absorption of the 1612 MHz pumping line at 34.6 μm. Namely, Neufeld et al. (1999) showed that this line is seen in the supergiant star VY CMa, Skinner et al. (1997) have reported its detection towards the ultra-luminous infrared galaxy Arp 220 and Bradford et al. (1999) have observed it in the starburst galaxy NGC 253. Summarizing, up to now there are 6 published detections of 34.6 μm absorption line from OH maser sources (from 3 supergiants: NML Cyg, IRC+10420, VY CMa, from 2 galaxies: Arp 220, NGC 253 and from the Galactic center).

In this paper we report on a search of the ISO Data Archive (IDA) for further evidence of absorption at 34.6 μm among OH/IR sources which were observed with the ISO SWS. In Section 2 we describe our working sample, present the 1612 MHz OH/IR sources which have available SWS observations around 34.6 μm, discuss briefly the SWS data reduction process and present examples of the SWS spectra for OH/IR sources with detected absorption line at 34.6 μm. Finally, in Section 3 we discuss briefly the results obtained.

2. OBSERVATIONS

Chen et al. (2001) discussed properties of the 1612 MHz OH sources associated with the InfraRed Astronomical Satellite (IRAS) counterparts which have Low Resolution Spectra (LRS) available. Altogether this sample consists of 1024 OH/IR sources for which the difference between OH maser and IRAS position is smaller than 1′. These sources were classified according to the Volk & Cohen (1989) classification scheme and it was found that sources with silicate emission (class E) form

Proceedings of the Symposium *"Exploiting the ISO Data Archive - Infrared Astronomy in the Internet Age"*, 24–27 June 2002, Sigüenza, Spain (C. Gry, S. B. Peschke, J. Matagne et al. eds., ESA SP-511)

Table 1. Results of the IDA search for SWS data covering 34.6 μm region within 1 arcmin around IRAS position of OH/IR sources from list of Chen et al. (2001).

IRAS name	LRS class	IDA name	SWS AOT 01	02	06	07
01037+1219	E	WX Psc	+	+	+	+
01304+6211	A	OH 127.8+0.0	+	–	–	–
02192+5821	E	S Per	+	–	+	–
03507+1115	E	IK Tau	–	–	+	+
05073+5248	E	IRC+50137	+	–	–	–
05373−0810	C		+	–	–	–
05380−0728	U		+	–	–	–
05506+2414	H		+	–	–	–
06053−0622	H	MON R2 IRS3	+	–	+	–
06238+0904	C		+	–	–	–
07027−7934	H		+	–	–	–
07209−2540	E	VY CMa	+	–	+	+
10197−5750	H	Roberts 22	+	–	–	–
10580−1803	E	R Crt	–	+	–	–
13517−6515	E		+	–	–	–
15452−5459	U		+	–	–	–
15559−5546	P		+	–	–	–
16235+1900	E	BS 6119	+	–	–	–
16279−4757	H		+	–	–	–
16280−4008	H	NGC 6153	+	+	–	–
16342−3814	H		+	–	–	–
17004−4119	A		+	–	–	–
17010−3840	A		+	–	–	–
17103−3702	L	NGC 6302	+	+	+	–
17150−3224	H		+	–	–	–
17319−6234	E		+	–	–	–
17347−3139	H		+	–	–	–
17360−3012	E		+	–	–	–
17393−3004	U	1742−3005	+	–	–	–
17411−3154	A	AFGL 5379	+	–	–	–
17418−2713	A		+	–	–	–
17424−2859	H	GC Sgr A*	+	+	+	+
17430−2848	H	GCS 3 I	+	–	–	–
17431−2846	H	G0.18−0.04	+	–	–	–
17443−2949	A		+	–	–	–
17463−3700	F	H1−36	+	–	–	–
17501−2656	E	AFGL 2019	+	–	–	–
17516−2526	U		+	–	–	–
17554+2946	E	AU Her	+	–	–	–
17574−2403	H	W 28A2	+	–	–	–
18050−2213	E	VX Sgr	+	–	–	–
18095+2704	H		+	–	–	–
18123+0511	F		+	–	–	–
18139−1816	I	OH 12.8−0.9	+	–	–	–
18196−1331	A	GL 2136	+	–	+	–
18257−1000	A	OH 21.5+0.5	+	–	–	–
18276−1431	H	OH 17.7−2.0	+	–	–	–
18348−0526	A	OH 26.5+0.6	+	+	–	–
18349+1023	E	V1111 Oph	–	+	+	–
18385−0617	A	OH 26.2−0.6	+	–	–	–
18460−0254	A	OH 30.1−0.7	+	–	–	–
18488−0107	A	OH 32.0−0.5	+	–	–	–
18498−0017	H	OH 32.8−0.3	+	–	–	–
18549+0208	A	OH 35.6−0.3	+	–	–	–
18551+0323	C		+	–	–	–
18556+0811	E	EIC 722	+	–	–	–
18560+0638	A	OH 39.7+1.5	+	–	–	–
19039+0809	E	R−Aql	+	–	+	–
19114+0002	H	HD 179821	+	+	–	–
19192+0922	A	OH 44.8−2.3	+	–	–	–
19219+0947	H	VY 2−2	+	+	–	–
19244+1115	E	IRC+10420	+	+	+	+
19255+2123	H	PK 056+2.1	+	–	–	–
19283+1944	A		+	–	–	–
19327+3024	P	BD +30 3639	+	+	–	–
19343+2926	H	M1−92	+	+	–	–
19550−0201	E	RR Aql	+	–	–	–
20000+4954	E	Z Cyg	+	–	–	–
20043+2653	A		+	–	–	–
20077−0625	E	IRC−10529	+	–	–	–
20255+3712	H	S 106	+	+	–	–
20272+3535	A		+	–	–	–
20406+2953	H		+	–	–	–
20529+3013	E	UX Cyg	+	–	–	–
21554+6204	A		+	–	–	–
22036+5306	U	HD 235718	+	–	–	–
22176+6303	H	S 140	+	+	–	+
22177+5936	A	OH 104.9+2.4	+	–	–	–
22556+5833	E	AFGL 2999	+	–	–	–
23412−1533	E	R Aqr	+	–	–	–
23416+6130	E	PZ Cas	+	–	–	–

Table 1. contd..

the largest group (about 57%) followed by the group with silicate absorption (class A: about 16%) and by group of sources with red-continuum (class H: about 6%). Information about LRS classification (i.e. about optical depth at least in the case of E and A sources) was intended to be used for interpretation of the 34.6 μm absorption line detection frequency in our sample of OH/IR sources.

We have searched the IDA for SWS data within 1 arcmin around IRAS position of 1024 galactic OH/IR sources from Chen et al. (2001) list (NML Cyg is not included in our sample as there is no IRAS observations for this supergiant, while Arp 220 and NGC 253 are extragalactic mega-maser sources). The results of our search for SWS data around 34.6 μm are given in Table 1. The associated IRAS name is given in column 1, IRAS LRS spectrum classification in column 2 and most frequently used source name from the original ISO proposals (if different from the IRAS one) in column 3. Sign + in columns 4, 5, 6 and 7 means that at least one SWS spectrum, covering wavelengths range around 34.6 μm, taken with Astronomical Observation Template (AOT) 01, 02, 06 and 07, respectively, is available. In some cases (e.g. GC Sgr A*) there are many SWS spectra available inside a 1′ circle around IRAS position. All of them were carefully checked but a complete analysis will be published elsewhere.

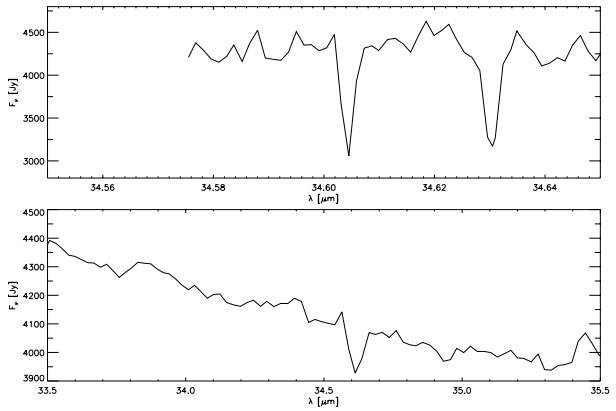

Figure 1. SWS 07 (upper panel) and SWS 06 (bottom panel) spectrum of supergiant VY CMa (IRAS 07209−2540) around 34.6 μm.

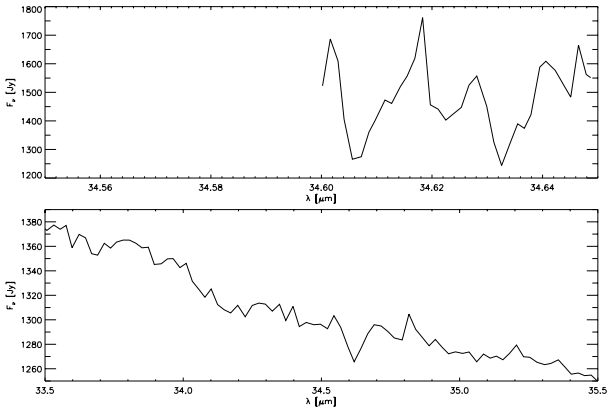

Figure 2. SWS 07 (upper panel) and SWS 06 (bottom panel) spectrum of supergiant IRC+10420 (IRAS 19244+1115) around 34.6 μm.

The ISO SWS 01, 02, 06 and 07 data (offline processing – OLP version 9.5) analyzed in this work were all processed using ISAP (ISO Spectroscopic Analysis Package) version 2.1. Recently, new versions of OLP (10.0, 10.1) have been released, but these newer data should not change our conclusions as far as the detection/non-detection frequency of the 34.6 μm absorption line is concerned. Data analysis consisted of extensive bad data removal primarily to minimize the effects of cosmic rays. First, all detectors were compared to identify possibly narrow features and then the best detector was chosen to compare one by one with others during the process of bad data removal. However, there are usually fewer scans in SWS 07 data than in other AOT's, so all scans were processed simultaneously in these cases. In the next step the spectra were scaled to the same flux level to correct for different responsivities of the detectors and any remaining outliers removed. When scaling, spectra were shifted by the *offset* mode if their overall flux density was lower than about 100 Jy, while by the *gain* mode when they had flux density higher than this limit. For SWS 06 spectra, the two scan directions correspond to two different lines and it is not possible to shift them simultaneously within ISAP. Therefore, scaling was done for the two directions separately. In addition, whenever memory effects or irregularities were present in the two scans of SWS 01 or 02 data, we averaged them separately and the resulting two sub–spectra were used to check reality of possible features. Finally, spectra were averaged across detectors, scans and lines (if applicable), using median clipping to discard points that lay more than 2.5σ from the median flux. Spectra were averaged typically to resolution of 400, 500, 800 and 1500 for SWS 01 data taken with speed 01, 02, 03 and 04, respectively, and to resolution of 3000 (SWS 02), 1500 (SWS 06) and 30000 (SWS 07) for the other observation modes. Finally, when the 34.6 μm absorption line was detected we used ISAP to determine continuum level and fit a single Gaussian profile to estimate line parameters. Only in case of the 34.6 μm line which was resolved into Λ–doublet components we fit Gaussian profile to each of them.

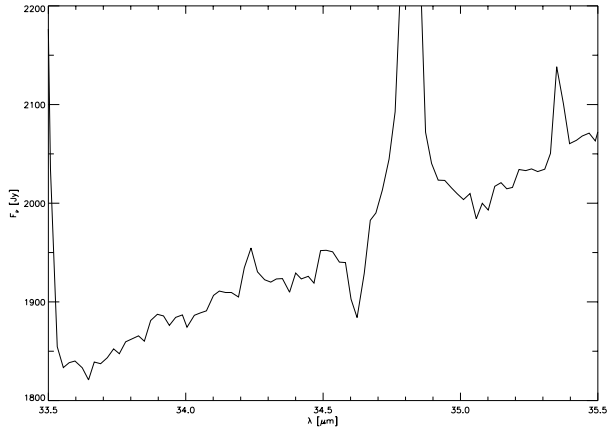

Figure 3. SWS 01 spectrum of Sgr A* (IRAS 17424−2859) around 34.6 μm.

Altogether, we have processed 159 SWS spectra (114 for AOT 01; 21 for 02; 16 for 06 and 8 for 07) around 34.6 μm for 81 OH/IR sources which have IRAS LRS spectra. The 34.6 μm absorption feature was undoubtedly detected in the SWS spectra taken toward *only* 3 OH/IR sources from our sample: supergiant VY CMa (IRAS 07209 −2540); supergiant IRC+10420 (IRAS 19244+1115) and the Galactic center (IRAS 17424−2859). In Figs.1–3 we present examples of unpublished spectra for these 3 sources. A detailed discussion of all detections (including tentative ones) for the more complete sample of OH/IR sources will appear elsewhere. Information about presented spectra, the obtained number of 34.6 μm photons ($n_{34.6}$) and number of the OH photons (n_{OH}) are given in Table 2.

3. DISCUSSION

As we discussed in Sect. 1 the theory of radiative pumping of the 1612 MHz OH maser emission seems to be well established. In addition, pump rates ($n_{OH}/n_{34.6}$) determined from the ISO SWS spectra analyzed here (5% – TDT 73601963 and

Table 2. Observational details for sources with detected 34.6 μm absorption line.

source name	Obs. mode	TDT	$n_{34.6}\,10^5$ $[m^{-2}s^{-1}]$	$n_{OH}\,10^2$ $[m^{-2}s^{-1}]$
VY CMa	07	73601963	14.1+17.9	1597[1]
	06	73402218	45.8	
IRC+10420	07	36401613	10.4+9.9	620[2]
	06	31600936	7.3	
GC Sgr A*	01(04)	09500203	18.4	41.1[3]

[1]Neufeld et al. (1999); [2]Sylvester et al. (1997); [3]Derived from 17 maser sources (Sjouwerman et al. 1998) which are located within 1′around IRAS 17424−2859 position. For SWS 07 observations $n_{34.6}$ is given as a sum of two numbers which correspond to each Λ–doublet component. Number in parenthesis denote speed of SWS 01 observations.

3.5% – TDT 73402218 for VY CMa; 3.1% – TDT 36401613 and 8.5% – TDT 31600936 for IRC+10420 but only 0.2% – TDT 09500203 for the Galactic center) do not contradict the proposed pumping scheme which requires about 4 FIR photons for one OH photon. Therefore, it is surprising that there are *only* 3 cases among 81 OH/IR sources with appropriate ISO SWS data which show a clear absorption at 34.6 μm.

Certainly, the detection rate of the 34.6 μm pumping line depends on the signal to noise ratio of the SWS spectra. Sources with tentative detection of this absorption line (not discussed here) have rather noisy spectra and it is difficult to prove the reality of the line. In any case, the number of sources with tentative detections is rather small and low signal to noise ratio does not probably solve the problem of the 34.6 μm line non–detection in other sources with good signal-to-noise SWS spectra around 35 μm. Another factor which could influence the detection of this absorption feature is the spectral resolution. However, among analyzed data there are spectra with high resolution (SWS 01 speed 4, SWS 02, SWS 06 and, especially, SWS 07) which do not show absorption at 34.6 μm. The detection rate also does not depend on the source flux. In our sample we have sources with flux at 34.6 μm well in excess of 1000 Jy and still there is no signature of *any* absorption at 34.6 μm. Therefore, we believe that explanation of this puzzling result is related to the geometry (relative location and size) of masering and dusty regions and/or to differences in physical conditions inside circumstellar (or interstellar) shells (clouds). Possibly, regions containing masering OH molecules (OH spots) are much smaller than regions emitting IR photons and absorption at 34.6 μm is filled by more spatially extended IR emission. However, the fact that the 34.6 μm absorption line is seen *only* in supergiants and in the extragalactic sources (Galactic center is very likely to be similar to the later cases) is probably not a coincidence and requires more careful analysis of physical conditions around sources with detected and non–detected 34.6 μm pumping line. More detailed discussion based on sample of all known galactic OH/IR sources with IRAS identification will appear elsewhere.

ACKNOWLEDGEMENTS

This work has been partly supported by grant 2.P03D.024.18p01 of the Polish State Committee for Scientific Research and by the Chinese Academy of Sciences and the NNSF of China.

REFERENCES

Bradford C.M., Stacey G.J, Fischer J.A., et al. 1999, The Universe as seen by ISO, eds P. Cox and M.F. Kessler, ESA SP–427, 861
Chen P.S., Szczerba R., Kwok S., Volk K., 2001, A&A 368, 1006
de Graauw Th., Haser L.N., Beintema D.A., et al., 1996, A&A 315, L49
Elitzur M., 1992, Astronomical Masers, Kluwer, Dordrecht
Elitzur M., Goldreich P., Scoville N., 1976, ApJ 205, 384
Epchtein N., Guibert J., Nguyen-Q-Rieu et al., 1980 A&A 85, L1
Evans N.J., Beckwith S., 1977, ApJ 217, 729
Justtanont K., de Jong Th., Helmich F.P., et al., 1996, A&A 315, L217
Kessler M.F., Steinz J.A., Anderegg M.E., et al., 1996, A&A 315, L27
Litvak M.M, Mc Whorter A.L., Meeks M.L., Zeiger H.J., 1966, Phys. Rev. Lett. 17, 821
Lutz D., Feuchtgruber H., Genzel, R, et al., 1996, A&A 315, L269
Neufeld A.A., Feuchtgruber H., Harwit M., Melnick G.J., 1999, ApJ 517, L147
Ngueyen-Q-Rieu, M., Laury-Micoulaut C., Winnberg A., Schultz G.V., 1979, A&A 75, 351
Perkins F., Gold T., Salpeter E.E., 1966, ApJ 145, 361
Shklovsky I.S., 1966, Astron. Tsirk., No. 372
Sjouwerman L.O., van Langevelde H.J., Winnberg A., Habing H.J, 1998, A&AS 128, 35
Skinner, C.J., Smith, H.A., Sturm, E., et al., 1997, Nature 386, 472
Sylvester R.J., Barlow M.J., Nguyen-Q-Rieu et. al., 1997, MNRAS 291, L42
Thai-Q-Tung, Dinh-V-Trung, Nguyen-Q-Rieu, et al., 1998, A&A 331, 317
Volk K., Cohen M., 1989, AJ 98, 931
Weaver H., Williams D.R.W., Dieter N.,H., Lum W.T., 1965, Nature 208, 29

DEBRIS DISCS AROUND STARS: THE ISO LEGACY

Marie Jourdain de Muizon[1,2]

[1]Leiden Observatory, PO Box 9513, 2300 RA Leiden, The Netherlands,
[2]LESIA, Paris Observatory, 92190 Meudon, France

ABSTRACT

Debris discs around stars were first discovered by IRAS, the Infrared Astronomical Satellite in 1983. For the first time material orbiting another star than the Sun, but distinct from a circumstellar envelope, was observed through its far infrared emission. This major discovery motivated astronomers to investigate those discs by further analysing the IRAS data, using ground-based telescopes for the hunting of exoplanets, developing several projects using ISO, the Infrared Space Observatory, and now exploiting IDA, the ISO Data Archive. This review presents the main ISO results, statistical as well as individual, on debris discs in orbit around pre-main-sequence and main-sequence stars.

1. INTRODUCTION

Discs around stars appear during the early stages of stellar evolution. About 4.6 Gyr ago, the Sun - like any other star - formed in a local contraction of an interstellar cloud of molecular gas and dust. During its first few million years the Sun was surrounded by a warm rotating disc of gas and dust that on one hand fed material onto the forming star and on the other hand led to the formation of comets, planets and planetesimals, asteroids and other objects. This kind of warm disc is also found around other pre-main-sequence stars, such as T Tauri stars, Herbig Ae/Be stars and ZAMS stars (Robberto et al. 1999). They contain some original interstellar dust, are optically thick and extend to a few AU. After a few 10^7 years, the warm inner part of the solar disc was dissipated while a cooler debris disc remained in the outer part of the newly formed solar system. Such a disc contains mainly interplanetary dust resulting from collisions, is optically thin and extends up to a few hundred AU. It is such a debris disc that was first discovered by IRAS (Aumann et al. 1984) around Vega, α Lyr, one of the best calibrated and extensively used photometric standard in the visual range, then found to radiate more mid- and far-infrared emission than its photosphere can produce, and also around α PsA, ϵ Eri and β Pic. A systematic search for Vega-like discs in the IRAS survey led to several other identifications but was not very conclusive due to the limited sensitivity (Backman & Paresce 1993, Plets and Vynckier 1999). As follow-up of IRAS, several surveys were undertaken with ISO (Kessler et al. 1996). The most unbiased was obtained by Habing et al. (1999, 2001) but others concentrated on stars in open clusters (Spangler et al. 2001), G dwarfs (Decin et al 2000), or selected MS stars (Fajardo-Acosta et al 1999). Several case studies on the most ISO observed discs are also presented: Vega and β Pic (Heinrichsen et al. 1998, 1999), ρ^1 Cnc (Dominik et al. 1998), HD 207129 (Jourdain de Muizon et al. 1999), five Vega-like stars including α PsA (Fajardo-Acosta et al. 1997). Finally ISO spectroscopic observations evidenced the presence of amorphous and crystalline silicates, fosterite, PAHs (Meeus et al. 2001, Bouwman et al. 2001) and molecular hydrogen (Thi et al. 1999, 2001a, 2001b) in the discs of several pre-main-sequence stars. See also two more general reviews on the subject by Lagrange et al. (2000) and Zuckerman (2001).

2. ISO SURVEYS

2.1. GENERAL STATISTICS

Habing et al. (1999, 2001) proposed to determine the incidence of Vega-like debris discs in a distance limited sample of main-sequence stars. The stars were carefully selected from Johnson & Wright (1983) who computed far-infrared fluxes for 93% of the 2150 stars in the "Woolley catalog of stars within 25 pc from the Sun". After rejecting all stars either too faint for ISO at 60 μm or for which an infrared excess would be ambiguous to interpret as a disc, their final selection consisted of 84 main-sequence stars of spectral types from A to K. Within this range, no spectral type was privileged. The stars were measured with ISO at 25, 60, 90 and 170 μm in a total observing time of 65 hours.

Based on ISOPHOT (Lemke et al. 1996) C100 3×3 mini-maps at 60 μm, Habing et al. (1999, 2001) found that 17% of the stars in their sample do have a disc. Lachaume et al. (1999) determined the age of the 84 stars. It appeared that all stars younger than 300 Myr have a disc, 70% of the stars younger than 400 Myr still have a disc but this is the case for only 8% of the stars older than 1 Gyr. Thus it seems that most stars arrive on the main-sequence surrounded by a disc, and for the majority of them the disc is dissipated within a few hundred Myr (Fig. 1). The decay of the discs is attributed to the destruction and escape of planetesimals; indeed the collision of planetesimals is a good source of dust, necessary to replenish the disc because dust particles disappear on a much shorter timescale relative to the lifetime of the discs. The timescale of the dissipation of the disc corresponds to the end of the heavy bombardment phase in the Solar System, which is identified by dating the cratering on the Moon, Mercury, Ganymede and Callisto.

Proceedings of the Symposium *"Exploiting the ISO Data Archive - Infrared Astronomy in the Internet Age"*,
24–27 June 2002, Sigüenza, Spain (C. Gry, S. B. Peschke, J. Matagne et al. eds., ESA SP-511)

Craters are due to impacts from planetesimals and this bombardment appears to have stopped about 4 Gyr ago (Shoemaker & Shoemaker 1999, Morbidelli et al. 2001). Thus the timescale of 400 Myr would not trace, properly speaking, the disappearance of the dust discs, but the termination of the production of dust by collisions of planetesimals, hence the drastic reduction in the occurrence of these larger bodies (Jourdain de Muizon et al. 2001).

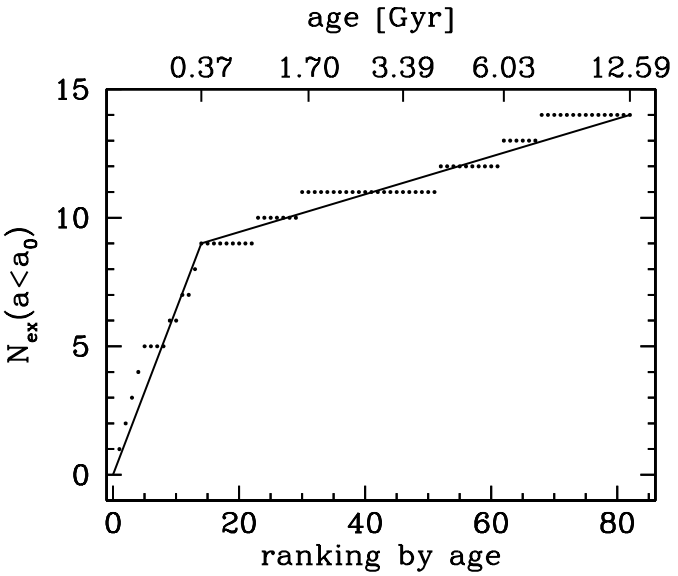

Figure 1. Cumulative distribution of stars with an infrared excess, as a function of the index, sorted by age. X-axis is rank at the bottom and age at the top of the figure. Y-axis is the number of stars up to that rank which have a disc. Each dot on the figure represents a star of the sample. For each star with an infrared excess, N_{ex} increments by one. The two segments of a continuous straight line correspond to the perfect situation in which most debris discs are no longer detectable after 400 Myr (from: Habing et. 2001).

Using 25 μm ISOPHOT data on 81 stars from the Habing et al. (2001) sample, Laureijs et al. (2002) found that 5 stars (6%) have an infrared excess that can be attributed to a disc of dust temperature between 50 and 120 K. The 5 stars are younger than 400 Myr, thus indicating that warm debris discs are relatively rare and concern the younger stars only. The survey confirms that there seems to be an absence of detectable amounts of dust close to the stars ($D \lessapprox 20$ AU). From a survey of 38 main-sequence stars using IRAS and ISOPHOT data, Fajardo-Acosta et al. (1999) found no star with a significant excess at 12 μm, and a fraction of $\sim$ 14% excess stars at 20 μm. However, this fraction is difficult to interpret since the ISOPHOT data in their study were inconclusive and the detections needed confirmation. The absence of 12 μm excess indicates that the discs are not warmer than 200 K.

2.2. G STARS

Decin et al. (2000) studied the incidence of the Vega phenomenon around G dwarfs. The stars were selected from the CORALIE sample (planet-search programme around stars closer than 50 pc and of spectral type from F8 to M1, excluding giants and faint cool dwarfs). Only southern stars were considered and the main selection criteria were observability and detectability by ISO at 60 μm. Confused systems such as multiple stars and those against a high cirrus background were rejected. Finally, this ISO programme consisted of 69 stars, 34 of which were effectively observed and results are given for 30 of them (ISOPHOT minimaps at 60 μm).

Of the 30 G dwarfs in Decin et al. (2000), 5 (17%) have a debris disc and 4 out of these 5 are older than 3 Gyr. This is in good agreement with Habing et al. (2001) who have 21 G dwarfs in their sample and find than 4 (19%) of them have a debris disc; 3 out of these 4 are older than 5 Gyr (they are part of their 8% stars older than 1 Gyr and which still have their disc, see Sect. 2.1). However, 2 of the excess stars in Decin et al. (2000) have fractional luminosities of their disc comparable to the disc of β Pic which was a unique case so far, whereas the others and all the discs around G stars in Habing et al. (2001) are between one and two orders of magnitude fainter. Also no correlation was found between the existence of a disc and a planet around the stars of the Decin et al. (2000) sample.

Thus for both groups of authors, about 18% of the G stars do have a disc and about 80% of these discs are around G stars older than 3 Gyr. Why do G stars appear to keep their discs longer than A, F or K stars is not yet understood. Around the Sun, the zodiacal light and the Kuiper Belt are probably some remnants of the earlier disc.

2.3. STARS IN OPEN CLUSTERS

Spangler et al. (2001) used ISOPHOT to observe a total of 148 stars, of which 87 young (50–700 Myr), nearby ($d < 120$ pc) main-sequence stars in open clusters (α Persei, Coma Berenice, Hyades, Pleiades, UMa) of spectral type A to K, 41 T Tauri stars in the clouds Chamaeleon I, Scorpius and Taurus ($d \approx 140 - 150$ pc), and a sample of 19 isolated young nearby field stars ($d < 60$ pc) and another field star. They obtained ISOPHOT chopped observations with C100 at 60 and 100 μm or raster at 60 and 90 μm. The goal was to determine an evolutionary sequence for circumstellar disc characteristics, hence their choice of well-studied clusters in which stellar ages are fairly well defined. Although spectral types span the range A to K the authors gave a preference to solar-type stars and privileged spectral types F and G in their star selection. They detected 36 stars, of which 33 show evidence for a far-infrared excess, i.e. 22% of their hole sample. More than one third were already thought to have an IR excess in their IRAS data, the rest are new ISO detections. These latter consist of 13 cluster stars, 5 young field stars and one other field star, with an ISO excess emission at 60, 90 or 100 μm. Among the main-sequence excess stars, spectral type F clearly dominates. Given

the sample size of the statistics, the 22% excess stars in Spangler et al. (2001) is not too far from the 17% in Habing et al. (2001) or in Decin et al. (2000). The difference is most likely due to the selection criteria, the sample of Habing et al. (2001) being the most unbiased and homogeneous. Discs around T Tauri stars are closer to accretion discs (optically thick) and are not properly so-called debris discs (optically thin) like those around main-sequence stars. We only include them in this ISO review because they are precursors of the debris discs but they cannot be treated equally when defining the incidence of debris discs.

A convenient parameter to describe systems exhibiting excess emission from circumstellar discs is the fractional excess luminosity, $f_d = L_{ex}/L_\star$, where L_{ex} is the luminosity of dust and $L_\star$ is the stellar bolometric luminosity. Although L_{ex} is not easy to estimate as it requires to know the complete infrared spectrum of the excess, it can be done approximately using both the IRAS and ISO data. A very interesting result of Spangler et al. (2001) is how the IR excess evolves with time. They established that the fractional excess luminosity f_d decreases with stellar age according to the power law $f_d \propto (\mathrm{age})^{-1.76}$. This is compatible with a collisionally replenished disc as suggested in Habing et al. (2001). Spangler et al. (2001) claim they don't see evidence for an abrupt cessation of the debris disc phenomenon as reported in Habing et al. (2001). It is indeed not obvious from their Fig. 1, but in fact 27 out of their 33 excess stars (82%) are younger than 400 Myr, and the other 6 are between 400 and 625 Myr. This is in perfect agreement with Habing et al. (2001). It is clear that debris discs are mostly found around young stars. Spangler et al.'s sample is biased towards young stars anyway. All excess stars in their sample are younger than the end of the late heavy bombardment on the Moon.

Robberto et al. (1999) present preliminary results on 97 very young stars in 5 open clusters, 3 of which are in common with those in Spangler et al. (2001), namely Chamaeleon, α Per and Pleiades, and they are all younger than 300 Myr. Using ISOPHOT with the C100 detector at 60 μm and P2 detector at 25 μm they detected only 4 stars, i.e 4.1% of their hole sample. The 4 stars detected are all T Tauri stars in the Chamaeleon I cluster; 3 of them are classical T Tauri stars which are still in the accretion phase (there are only 6 such stars known in this cluster) and the fourth one is probably in the transition phase. Their results show that the transition from an optically thick disc (or accretion disc) to an optically thin one (or debris disc) occurs on a timescale of ~ 10 Myr, with a transition phase lasting less than ~ 0.3 Myr.

3. CASE STUDIES

A few stars were observed rather extensively and with several ISO observing modes or instruments because they were particularly interesting cases. The best examples are α Lyr (Vega), β Pic, α PsA (Fomalhaut), ρ^1 CnC and HD 207129.

3.1. VEGA AND β PIC

The most detailed ISO studies of the discs around these two prototypes of debris discs are found in Heinrichsen et al. (1998, 1999). They are summarized in Table 1.

Table 1. ISOPHOT results on Vega and β Pic

ISOPHOT	Vega	β Pic
High resolution scans	60 μm (P32/C100)	25, 60 μm
Disc resolved	Yes: face-on	Yes: edge-on
Distance	7.8 pc	19.3 pc
Disc radius	86 AU at 60 μm 140 AU at 90 μm	84 AU at 25 μm 140 AU at 60 μm
Multifilter-Photometry	25, 60, 80, 100, 120, 150, 170 & 200 μm	4.85,7.3,11.3,12.8,16,25 60,80,120,150&170 μm
Adopted dust emissivity	$Q(\lambda) \propto 1/\lambda^{1.1}$	$Q(\lambda) \propto 1/\lambda$
Dust mass in disc	$1 - 5 \times 10^{-3} M_\oplus$	$1.0 - 3.3 \times 10^{-2} M_\oplus$
	Habing et al. 2001: $1.3 - 13 \times 10^{-4} M_\oplus$	Habing et al. 2001: $1.2 - 12 \times 10^{-2} M_\oplus$
Reference	Heinrichsen et al.1998 Proposal: Walker	Heinrichsen et al.1999 Proposal: Heinrichsen

Based on the 25 μm ISO data, the authors argue that the disc around β Pic is in fact much more massive than the cool dust derived from the ISO 60 μm emission. They suggest that there is some warm dust (300 to 500 K), extension of the inner disc seen in the optical, and a significant amount of cool dust in addition to that seen by ISO. The star could be surrounded by a large 'Oort' cloud of comets.

Walker & Heinrichsen (2000) present ISOPHOT-S spectra (from 6 to 12 μm) of 12 Vega-like stars including the four 'prototypes' (Vega, β Pic, Fomalhaut and ϵ Eri) in search for silicates and PAHs features in debris discs. They found silicate dust emission towards two stars (HD 144432 and HD 139614), emission from carbon-rich molecules towards two others (HD 169142 and HD 34700) and emission from both towards HD 142666. For all their other stars, including the four 'prototypes', either only the photosphere is seen at these mid-infrared wavelengths, or some thermal featureless excess. The authors also present preliminary ISOPHOT maps at 60 and/or 90 μm, thus giving some insight in the extent and structure of the discs. The authors argue that the discs could be in the early stage of planet formation. However they give no accurate information on stellar age, hence the question: "Are the above features emitted by dust in a debris disc or in a much younger and thicker envelope or disc?".

3.2. α PsA

Fajardo-Acosta et al. (1997) have obtained P32 maps with ISOPHOT-C100 at 60 μm, with a spatial resolution of about 30″ for six Vega-type systems. At 60 μm there is no excess emission detected towards α CrB, σ Her or α Cen. There is a marginal detection of extended emission, out to $\sim$800 AU or 30″ from the star γ Oph. Only α PsA in their sample shows a convincing excess emission in the range $\sim$30″ to 80″ i.e. $\sim$210 to 560 AU, confirming the IRAS temperature of 58–75 K and suggesting grains up to $\sim$10 μm in size. They estimate a dust mass of $\sim$(2–6)$\times 10^{-3} M_{\oplus}$. A comparison with β Pic shows that both discs are similarly extended at 60 μm (400 AU for β Pic vs. 560 AU for α PsA).

3.3. ρ^1 CnC

The star ρ^1 CnC is among the first 10 stars found to host a planet. In 1996, following the news of a planet around ρ^1 CnC, a special set of ISO observations was requested and carried out to search for a disc. The star ρ^1 CnC was observed with ISOPHOT at 25 μm (PHT03), and at 60, 90, 135 and 170 μm (PHT22). Dominik et al. (1998) found an excess of 170 ± 30 mJy at 60 μm. They interpreted it as a debris disc located at about 60 AU from the star and containing at least $4 \times 10^{-5} M_{\oplus}$ of dusty material. The star is a G8V, slightly metal-rich, located at a distance of 12.5 pc from the Sun. From CaII H and K lines, its age was estimated to 5 Gyr. Butler et al. (1997) detected the presence of a planet of period 14,65 days, implying a semi major axis of 0.11 AU. The inferred mass is $M_2 \sin i = 0.84 M_{\rm Jup}$. The far-infrared ISO excess was interpreted as a disc after any other possible origin had been examined and eliminated (companion M5, planet, cirrus knot in the background). The far-infrared spectrum of the excess is best fitted using cometary icy dust grains from the dust model by Li & Greenberg (1997) as seen in Fig. 2 of Dominik et al. (1998). These observations brought the first evidence of the coexistence of a disc and a planet around a star other than the Sun.

3.4. HD 207129

This solar-type (G2V) star is particularly interesting because of its cold debris disc, maybe one of the coldest observed so far. It caught the attention of Jourdain de Muizon et al. (1999) when they found a clear excess not only at 60 μm, but also at 170 μm in their ISOPHOT-C200 data. Additional discretionary ISO observations were requested and obtained to get a more complete infrared spectrum of the disc. Based on the independent measurements of the CaII K line made by two groups of authors (Pasquini 1992 and Henry et al. 1996), Lachaume et al. (1999) determined a stellar age of 4.7 Gyr similar to that of the Sun, adopted by Jourdain de Muizon et al. (1999) and Habing et al. (2001). Zuckermann & Webb (2000) argue that the star is a member of the Tucanae stream and must be as young as the Tucanae association (10–50 Myr) which is located at $\sim$45 pc. That is 3 times further than HD 207129 which is located at 15.6 pc from the Sun, according to the Hipparcos Catalogue (Perryman et al. 1997a, 1997b). This significantly weakens the possibility of its belonging to the Tucanae stars. In any case the age of the star is less of an issue if it is young because it would then strengthen the case of Habing et al. (1999, 2001) that debris disc is the privilege of young stars (less than 400 Myr). HD 207129 is indeed one of the few puzzling exceptions in their study.

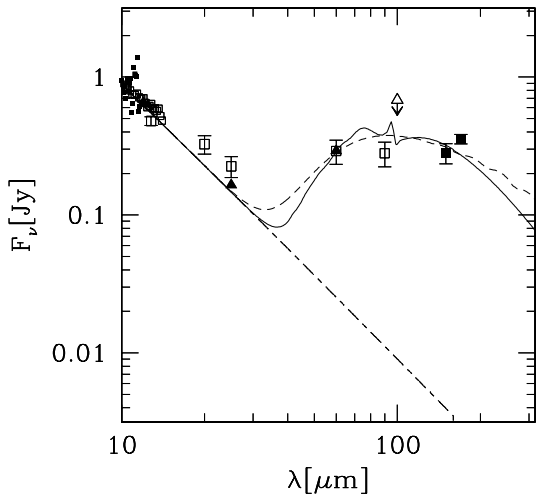

Figure 2. The infrared excess toward HD 207129. Comparison between two different dust compositions. The dashed line indicates a Draine & Lee (1984) interstellar grain model, the solid line a Li & Greenberg (1997) cometary dust model. The two cases differ most around 30–40 μm, but they both fit the remaining far-IR excess equally well. (from: Jourdain de Muizon et al. 1999)

The infrared excess around HD 207129 is shown in Fig. 2. The star emits approximately 1.1×10^{-4} of its luminosity longword of 25 μm. The excess emission is explained by assuming a disc of dust-like material equivalent to $2 \times 10^{-2} M_{\oplus}$. The dust temperature ranges from 10 to 50 K, which makes it the coldest debris disc around a Vega-like star known to date. The dust distribution in the disc presents a circular hole at a distance of $\sim$ 400 AU from the star. This hole should be filled within 10^{-3} of the stellar age by particles spiralling inward because of the Poynting-Robertson effect unless an agent sweeps it clean. It could thus be explained by the present of one or more planets.

4. DUST AND GAS COMPOSITION OF THE DISCS

Debris discs are essentially made of dust particles and larger bodies; however, these latter cannot be detected by ISO. In addition, the younger discs may still have a significant gas component. Before ISO, any attempt to trace the gas via CO molecular bands was unsuccessful. Direct measurement of H_2 with ISO–SWS (de Graauw et al. 1996) has made a real breakthrough toward understanding the gas composition of very young discs.

4.1. DUST COMPOSITION

Amorphous silicates (r$<$1 μm) were detected in the ISOPHOT-S spectra of 9 classical T Tauri stars in the Cham I dark cloud (Natta et al. 2000). They discuss a model which explains the origin of this material in a hot, optically thin surface layer of a disc around the star, i.e in the disc atmosphere.

Crystalline silicates were detected by van den Ancker et al. (2001) toward the pre-main-sequence (B9.5Ve, A0II-IIIe or AOV ?) star 51 Oph, using SWS01 and LWS01 full scans. The solid-state bands and energy distribution indicate that the dust has formed recently; it is a very young disc, not a debris disc. Other emission bands from hot gas ($\sim$ 350 K) such as CO, CO_2, H_2O and NO dominate the 4–8 μm spectrum. Both these gas and dust bands are unusual for a young star and are more typical of evolved AGB stars, although 51 Oph doesn't seem at all to belong to that class. The authors explore various possibilities for the nature of 51 Oph, among them a recent episode of mass loss from a Be star, the collision of two gas-rich planets and the accretion of a solid body as the star expends at the end of its short main-sequence life.

A variety of crystalline silicates, fosterite (Mg_2SiO_4), has been found toward the star HD 100546. Malfait et al. (1998) present SWS01 and LWS01 full scans of this isolated Herbig Ae/Be star. Fosterite is present in the micrometeorites and interplanetary dust of our Solar System. The ISO spectrum of HD 100546 is very similar to that of comet Hall-Bopp published by Crovisier et al. (1997). The amount of fosterite in the disc of HD 100546 is equivalent to 10^{13} comets Hale-Bopp, strengthening the hypothesis by Grady et al. (1997) that the disc around HD 100546 contains a huge swarm of comets similar to the Oort cloud in the Solar System. Crystalline silicates have also been found in several other comets such as P/Halley. Malfait et al. (1998) argue that the crystallisation process occurs during the early phases of disc evolution around young stars.

The ISO-SWS and -LWS spectra of an additional 14 isolated Herbig Ae/Be stars are presented in Meeus et al. (2001). These stars are believed to be the more massive analogs of T Tauri stars; they are seen as the progenitors of Vega-like stars (Waters & Waelkens 1998). Meeus et al. (2001) obtained a variety of mid-infrared spectra ranging from the amorphous silicates (as in the M supergiant μ Cep) to the crystalline silicates (as in comet Hale-Bopp). The variations in the shape of the 8–14 μm part of the spectra indicate the prominence of one or the other form of silicates. Four out of the fourteen stars have no silicates. In most silicate stars in their sample, crystalline silicates are present; this is confirmed by the shape of the 15–28 μm ISO–SWS spectra of the stars. PAH bands are also identified toward half of the stars, and all features are superposed on a near-IR to mid-IR continuum excess. The authors interpret the continuum in term of disc geometry: an optically thick, geometrically thin, power-law component and an optically thin flare region (black body component). Bouwman et al. (2001) got a further detailed insight into the 6–14 μm spectrum of these stars in order to study the silicate grain processing. The 10 μm silicate profile is modelled using three components: silica (SiO_2) responsible for the 8–9 μm blue shoulder in the silicate band, fosterite contributing to the 11.3 μm feature, and amorphous olivine with two typical grain sizes of 0.1 and 2.0 μm. They identify two causes for the observed shift in peak position of the silicate band: i) a change in average grain size from small (0.1 μm) to big (2 μm), as a result of the depletion of small grains in the inner region of the disc, due to coagulation and other effects, ii) a change in grain composition from amorphous silicate to a mixture of amorphous and Mg-rich crystalline silicate (fosterite) which could be the result of thermal annealing in the inner regions of the disc. However crystallisation occurs on a longer timescale than coagulation. There is no correlation between dust composition and disc geometry.

4.2. GAS COMPOSITION: H_2

Before ISO, any attempt to detect a gas component in Vega-like discs had been unsuccessful or inconclusive (see e.g. Liseau 1999). The classical method of tracing molecular hydrogen by observing CO, widely applied in the interstellar medium, did not seem to help. Thi et al. (1999) discovered molecular H_2 in the ISO–SWS spectra of the T Tauri star GG Tau. The detection of two pure rotational lines at 17.035 and 28.218 μm provided a direct measure of the total amount of warm molecular gas in the disc around the star. The same group (Thi et al. 2001a, 2001b) found H_2 lines in the SWS spectra of 4 T Tauri stars (spectral type K to M), 7 Herbig Ae stars (sp. type A to F), and 3 main-sequence stars including β Pic (sp. type A to F). Their data suggest the presence of warm gas (T$\approx$ 100 $-$ 200 K), which mass ranges from $\sim$ $10^{-4}M_{\odot}$ up to $8 \times 10^{-3}M_{\odot}$, around all the stars they observed. This mass corresponds to 1%–10% of the total disc mass inferred from millimeter continuum observations, and a much higher fraction in the case of debris discs. Additional CO observations show that CO is not a good tracer of the gas in circumstellar discs. The amount of CO gas is likely strongly affected by photodissociation due to the stellar and interstellar ultraviolet radiation in the surface layers of the disc and freeze-out onto grain surface in the mid-plane. Direct measurement of H_2 leads to a gas-to-dust ratio of ~ 100 in the debris discs of β Pic and HD 135344, similar to the interstellar medium ratio. The bulk of the gas around pre-main-sequence stars is cool (T$\approx$ 20 $-$ 80 K), while the warm gas (T$\approx$ 100 $-$ 200 K) may constitute the major gaseous component of debris discs around main-sequence star, thus providing a reservoir for the formation of Jovian planets.

5. CONCLUSION AND OPEN QUESTIONS

The ISO Data Archive has not yet been fully exploited as far as debris discs and their precursors are concerned. At least 85 hours of ISO observing time, distributed in some 15 proposals still remain to be explored on this topic. Several aspects of disc evolution are not well understood. Why and how do most discs disappear after about 400 Myr ? Why do some stars keep a disc for much longer, up to several Gyr ? Do discs coexist with

planets? Is it systematic, and if not, what conditions lead to a disc-planets or disc-only system ? Does it depend on the stellar spectral type ? Which physical and chemical processes occur during the evolution of a disc ? Although the ISO data has already provided partial answers to some of these questions, it is clear that our picture is still very basic. Beyond ISO, future space projects such as SIRTF and the Herschel Space Observatory will no doubt bring much new data on debris discs. SIRTF has a similar wavelength range as ISO but a higher sensitivity; it will be able to probe deeper and, hence, make the same kind of statistics but on a larger volume around the Sun. Herschel will open a new window since it extends to the submm. This will allow to trace the cold component of the discs such as the dust located in the Kuiper Belt, the Oort cloud and still further from the star.

REFERENCES

Aumann H.H., Gillett F.C., Beichman C.A., de Jong T., Houck J.R., Low F.J., Neugebauer G., Walker R.G., Wesselius P.R., 1984, ApJ 278, L23

Backman D., Paresce F., 1993, in "*Protostars and Planets III*", eds E. Levy & J. Lunine, Tucson: University of Arizona press, pp.1253-1304

Bouwman J., Meeus G., de Koter A., Hony S., Dominik C., Waters L.B.F.M., 2001, A&A 375, 950

Butler R.P., Marcy G.W., Williams E., Hauser H., Shirts P., 1997, ApJ 474, L115

Crovisier J., Leech K., Bockelee-Morvan D., Brooke T.Y., Hanner M.S., Altieri B., Keller H.U., Lellouch E., 1997, Science 275, 1904

Decin G., Dominik C., Malfait K., Mayor M., Waelkens C., 2000, A&A 357, 533

de Graauw Th., Haser L.N., Beintema D.A., Roelfsema P.R. et al., 1996, A&A 315, L49

Dominik C., Laureijs R.J., Jourdain de Muizon M., Habing H.J., 1998, A&A 329, L53

Draine B.T., Lee H.M., 1984, ApJ 285, 89

Fajardo-Acosta S.B., Stencel R.E., Backman D.E., 1997, ApJ 487, L151

Fajardo-Acosta S.B., Stencel R.E., Backman D.E., Thakur N., 1999, ApJ 520, 215

Grady C.A., Sitko M.L., Bjorkman K.S., Perez M.R., Lynch D.K., Russell R.W., Hanner M.S., 1997, ApJ 483, 449

Habing H.J., Dominik C., Jourdain de Muizon M., Kessler M.F., Laureijs R.J., Leech K., Metcalfe L., Salama A., Siebenmorgen R., Trams N., 1999, *Nature* 401, 456

Habing H.J., Dominik C., Jourdain de Muizon M., Laureijs R.J., Kessler M.F., Leech K., Metcalfe L., Salama A., Siebenmorgen R., Trams N., Bouchet P., 2001, A&A 365, 545

Heinrichsen I., Walker H.J., Klaas U., 1998, MNRAS 293, L78

Heinrichsen I., Walker H.J., Klaas U., Sylvester R.J., Lemke D., 1999, MNRAS 304, 589

Henry T.J., Soderblom D.R., Donahue R.A., Baliunas S.L., 1996, AJ 111, 439

Johnson H.M., Wright C.D., 1983, ApJS 53, 643

Jourdain de Muizon M., Laureijs R.J., Dominik C., Habing H.J., Metcalfe L., Siebenmorgen R., Kessler M.F., Bouchet P., Salama A., Leech K., Trams N., Heske A., 1999, A&A 350, 875

Jourdain de Muizon M., Laureijs R.J., Habing H.J., Leech K., Kessler M.F., Metcalfe L., Salama A., Siebenmorgen R, Dominik C., Trams N., Bouchet P., 2001, Earth, Moon and Planets 85–86, 201

Kessler M.F., Steinz J.A., Anderegg M.E., Clavel J., Drechsel G., Estaria P., Faelker J., Riedinger J.R., Robson A., Taylor B.G., Ximénez de Ferrán S., 1996, A&A 315, L27

Lachaume R., Dominik C., Lanz T., Habing H.J., 1999, A&A 348, 897

Lagrange A.-M., Backman D., Artymowicz P., 2000, in "*Protostars and Planets IV*", eds V. Mannings, A.P. Boss, S.S. Russell, Tucson: University of Arizona Press, 639

Laureijs R.J., Jourdain de Muizon M., Leech K., Siebenmorgen R., Dominik C., Habing H.J., Trams N., Kessler M.F., 2002, A&A 387, 285

Lemke D., Klaas U., Abolins J., Ábrahám. P. et al., 1996, A&A 315, L64

Li A., Greenberg J.M., 1997, A&A 323, 566

Liseau R., 1999, A&A 348, 133

Malfait K., Waelkens C., Waters L.B.F.M., Vandenbussche B., Huygen E., de Graauw M.S., 1998, A&A 332, L25

Meeus G., Waters, L.B.F.M., Bouwman J., van den Ancker M.E., Waelkens C., Malfait K., 2001, A&A 365, 476

Morbidelli A., Petit J.-M., Gladman B., Chambers J., 2001, *Meteorit. Planet. Sci.* 36, 371

Natta A., Meyer M.R., Beckwith S.V.W., 2000, ApJ 534, 838

Pasquini L., 1992, A&A 266, 347

Perryman M.A.C., Lindegren L., Kovalevsky J. et al., 1997a, A&A 323, L49

Perryman M.A.C., et al. 1997b, The Hipparcos and Tycho Catalogues, ESA SP-1200

Plets H., Vynckier C., 1999, A&A 343, 496

Robberto M., Meyer M.R., Natta A., Beckwith S.V.W., 1999, in "*The Universe as seen by ISO*", eds. P. Cox, M.F. Kessler, ESA SP-427, 195

Shoemaker E., Shoemaker C., 1999, in "*The New Solar System*" 4th edition, eds J.K. Beatty, C. Petersen, A. Chaikin, Sky Publishing Corporation and Cambridge University Press, 69

Spangler C., Sargent A.I., Silverstone M.D., Becklin E.E., Zuckerman B., 2001, ApJ 555, 932

Thi W.F., van Dishoeck E.F., Blake G.A., van Zadelhoff G.J., Hogerheijde M.R., 1999, ApJ 521, L63

Thi W.F., Blake G.A., van Dishoeck E.F., van Zadelhoff G.J., Horn J.M.M., Becklin E.E., Mannings V., Sargent A.I., van den Ancker M.E., Natta A., 2001a, Nature 409, 60

Thi W.F., van Dishoeck E.F., Blake G.A., van Zadelhoff G.J., Horn J.M.M., Becklin E.E., Mannings V., Sargent A.I., van den Ancker M.E., Natta A., Kessler J., 2001b, ApJ 561, 1074

van den Ancker, M.E., Meeus G., Cami J., Waters L.B.F.M., Waelkens C., 2001., A&A 369, L17

Walker H.J., Heinrichsen I., 2000, Icarus 143, 147

Waters L.B.F.M., Waelkens C., 1998, ARAA 36, 233

Zuckerman B., Webb R.A., 2000, ApJ 535, 959

Zuckerman B., 2001, ARAA 39, 549

STAR FORMATION AND EARLY EVOLUTION IN THE ISO DATA-BASE

Brunella Nisini

INAF-Osservatorio Astronomico di Roma, Via di Frascati 33, Monteporzio Catone, 00040 Italy

ABSTRACT

In this contribution, I will summarize the observations available in the ISO Data Archive concerning the different phases of the star formation process, focusing in particular on the low mass young stars. I will also address possible projects on specific issues of the young star evolution which remain still uncovered. As an example of a large project exploiting the ISO Data Archive I will finally show the results of a far infrared spectroscopic survey performed on a sample of 54 Young Stellar Objects (YSOs) in different evolutionary phases, from the youngest protostars to pre-main sequence stars. Such a study has allowed to define average spectroscopical properties of different classes of YSOs, which will be useful for the definition of programmes for future space missions.

Key words: ISO – star formation – pre-main sequence stars

1. INTRODUCTION

ISO has given a fundamental step towards enlarging the observational scenario for understanding the still poorly known field of the formation of a new star. Indeed, the spectral range from mid to far infrared is the most suited both to identify new cold and heavily extinct protostars and to probe the different processes characterizing the interaction between young stars and their parental cloud. In particular, in the infrared the gas and dust cooling from the close environment of YSOs can be traced, which is in turn a function of the different heating mechanisms and of their time evolution. In Fig. 1 a sketch is presented showing the prevailing heating channels of young stars circumstellar envelopes and how they change with the protostellar evolution. The formation of an isolated low mass star begins with the collapse of a cold dense core, which is only externally heated by the interstellar radiation field. As soon as a centrally condensed protostar developes, the main heating mechanisms of circumstellar gas and dust are shocks, either due to matter accretion onto the disk and the protostellar surface, or developing along the energetic outflows. Finally, when the protostellar phase is ending and the star becomes optically visible on its pre-main sequence evolutionary track, a well defined photosphere develops while the accretion/ejection mechanisms become less and less important; in this phase the stellar radiation field is the main source of heating. ISO has gathered observations over all these evolutionary phases which brings from a cold pre-stellar core to a well formed star in pre-main sequence phase. During its lifetime, ISO has performed about 2530 observations specifically devoted to star formation and early evolution, for a total of $\sim$ 830 hours of observing time. In this review I will try to summarize the available observations which address different aspects of the star formation process, mainly concentrating on the observations of low and intermediate mass young stellar sources.

1.1. PRE-STELLAR CORES

About 15 ISO Open Time (OT) proposals were devoted to the study of the initial conditions for star formation. These observations mainly use the PHT and CAM imaging capabilities to obtain maps of large samples of pre- and proto-stellar cores in different star forming regions. PHT maps at different wavelengths (90, 170 and 200μm) are aimed to study the cores emission and temperature distribution, as shown by Ward-Thompson et al. (2002), which have analyzed PHT observations of 18 pre-stellar cores to infer their SEDs and temperature profiles. This analysis have evidenced that most of these cores remain undetected in the 90 μm filter, implying that their temperature should be very low ($<$20 K, see Fig. 2). Moreover, the color temperature profiles derived across the cores shown that in many cases the temperature decreases towards the center, supporting the pre-stellar nature of these objects where the heating does not come from a central source but from the external radiation field.
A different approach for the study of the core internal structure have been to observe the pre-stellar cores in absorption against the background mid-infrared emission by CAM. Bacmann et al. (2000) have analyzed in this way the CAM mid-IR images of 24 cores showing that some of them present sharp edges and appear to be decoupled from their parent clouds, providing finite reservoirs of mass for subsequent star formation.

1.2. CENSUS OF PROTOSTARS, IMF

An important goal of the ISO mission in the star formation field, was the mid IR surveys of different star forming regions for the detection and classification of the young stellar and substellar population of embedded clusters. ISOCAM has mapped selected parts of the major nearby star forming regions in the two broad band filters LW2 and LW3. The main aim of these observations was to detect deeply embedded sources not ob-

Proceedings of the Symposium *"Exploiting the ISO Data Archive - Infrared Astronomy in the Internet Age"*,
24–27 June 2002, Sigüenza, Spain (C. Gry, S. B. Peschke, J. Matagne et al. eds., ESA SP-511)

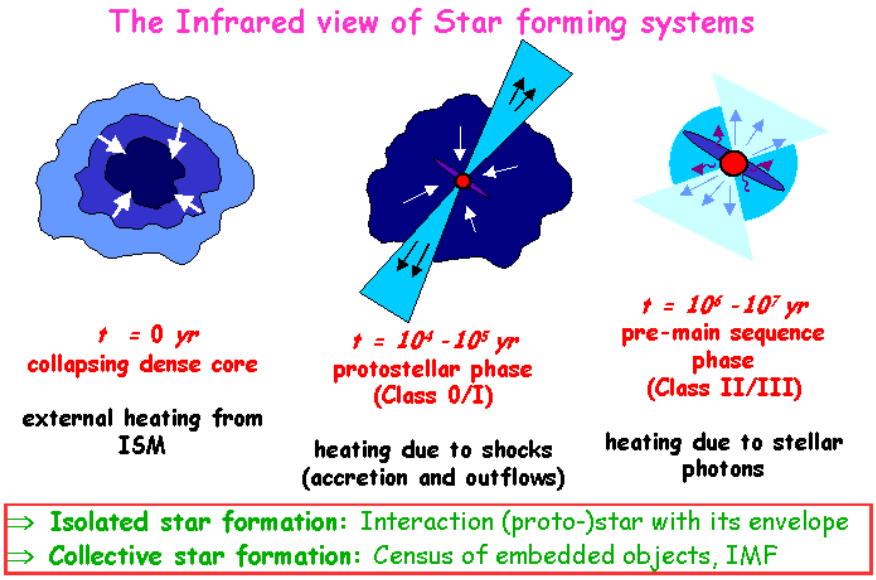

Figure 1. Sketch showing how the heating mechanisms of low-mass protostellar envelopes change with the evolution from a pre-stellar core to a pre-main sequence star. The main objective which can be addressed through the data gathered by ISO is how these different heating mechanisms affect the circumstellar gas and dust chemical and physical parameters during the young star evolution. At the same time the ISO data allow to perform an unprecedented census of the embedded population in different star forming regions.

servable in the near infrared and to extend the initial luminosity and mass function down to the brown dwarfs regime. An example of the nice results obtained from these data is given by the study performed by Bontemps et al. (2001) on the ρ Ophiuchi embedded cluster. The observations performed with ISOCAM increased the number of recognized YSOs by more than a factor of two extending the previously known Class I/II population of the ρ Oph cloud toward low IR fluxes (see Fig. 3). This, in turn, have allowed to construct the mass function for the Class II population down to a completeness level of 0.055 $M_\odot$, clearly showing that a flattening exists for masses lower than $\sim$0.5 $M_\odot$.

Other regions observed with CAM whose data have already been published are Chameleon (Persi et al. 2000), R CrA (Olofsson et al. 1999) and Serpens (Kaas et al. 1999), where similar results in terms of newly detected sources and the presence of a mass function flattening have been found. An extension of this kind of studies towards star forming regions with different masses and star formation rates will allow to test whether the derived mass and luminosity functions are universally defined or depends on the cloud star forming history. Moreover, important by-products of these observations will be flux limited catalogues of mid-IR sources, which will represent a unique database for future missions and follow-up observations.

1.3. Young Stellar Objects

A large fraction of the ISO observing time dedicated to star formation studies have been used to obtain spectroscopic and photometric observations of sample of young stellar sources in different star forming regions. In particular, 29 Guaranteed Time (GT) and OT proposals for a total of 260 hrs of observing time have been devoted to these kind of studies exploiting the four ISO instruments. So far, mainly the spectroscopic data obtained with SWS and LWS have been fully analyzed and published. ISO spectra have been obtained on a variety of sources with different luminosity and evolutionary stage, providing a fundamental data-base to probe the physical and chemical properties of the YSOs circumstellar regions. Indeed, the mid and far infrared spectral range include important lines of atoms and molecules which are able to discriminate among different excitation mechanisms, such as interstellar shocks driven by the source winds or UV radiation producing extended circumstellar photo-dissociation regions (PDRs) (e.g. van Dishoeck et al. 1999). In the ISO infrared spectra the dominant transitions are pure rotational lines of abundant molecules, such as H_2, CO, H_2O and OH, as well as atomic/ionic species such as [SiII]35μm, [OI]63,145, and [CII]158μm lines(see Fig. 4). The relative importance of the molecular over the ionic emission may depend on the luminosity as well as on the source evolutionary stage. Particularly important is the possibility offered by ISO to detect lines of water in gaseous form, which is predicted to be one of the major coolant of the warm circumstellar gas heated by both shocks and stellar radiation (i.e. Ceccarelli

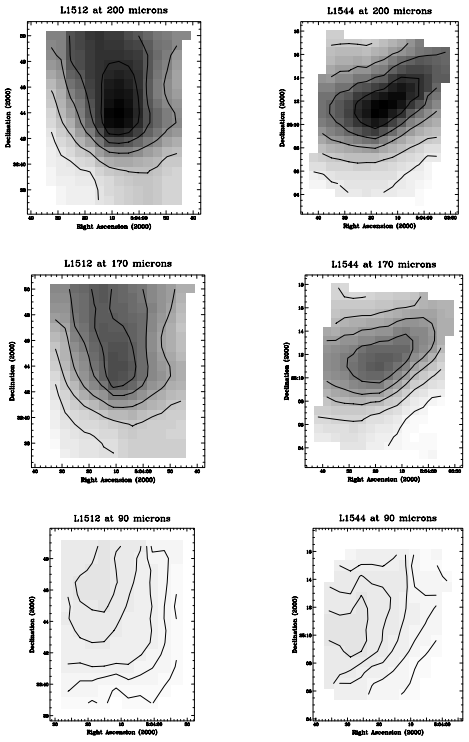

Figure 2. ISOPHT images at 90, 170 and 200μm of the pre-stellar cores L1512 (left) and L1544 (right). These images show clear emission only at 170 and 200μm, which implies temperatures of only $\sim$ 10–20 K (Ward-Thompson et al. 2002)

et al. 1996, Kaufmann & Neufeld 1996). Plenty of H_2O pure rotational lines have been indeed observed allowing for the first time to test the model predictions. Indeed, water has been found very abundant in warm regions around low mass protostars, with values ranging from $\sim 10^{-6}$ to $\sim 10^{-4}$ (e.g. Giannini et al. 2001, Ceccarelli et al. 1999). The higher values are found in very young protostars indicating that the water molecule is subject to a sensitive time dependent chemistry.

The SWS spectral range also includes plenty solid-state absorption features which uniquely probe the dust grain composition as well as their thermal history. As an example, Fig. 5 shows the SWS spectrum of the Class I source Elias 29 (Boogert et al. 2000), presenting strong ice features of H_2O, CO and CO_2. The possibility to observe in the same spectral range also the absorption from the same species in gas-phase, allows to measure, in sufficiently bright sources, the gas/dust ratio and to derive how it evolves with the luminosity and the age of the source (van Dishoeck et al. 1999).

Finally, an extremely interesting but so far rather unexplored subject, is the study of the YSO SEDs by means of both PHT and LWS spectrophotometric observations. Such observations extend the wavelength range reached by IRAS up to 200μm, allowing to trace the peak of the energy distribution in the coldest and youngest objects, like the Class 0 sources (see inset in Fig. 4), and thus to better define the temperature and density

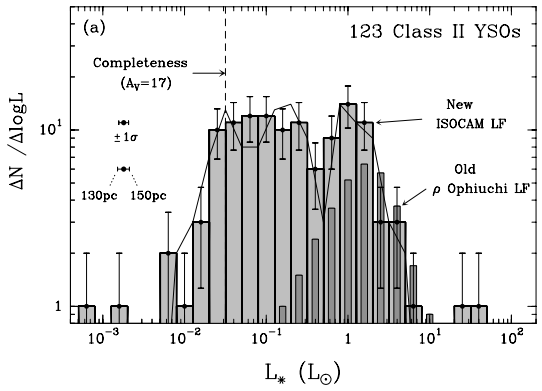

Figure 3. Luminosity function (LF) for the Class II YSOs population detected by ISOCAM in the ρ Ophiuci star forming region. The darker histogram shows the LF of the Class II sources previously known by means of ground based NIR observations. ISOCAM has more than doubled the number of identified objects, allowing to trace the LF down to the brown dwarf regime (Bontemps et al. 2001)

structures of their circumstellar envelopes (e.g. Larsson et al. 2000). In fact a large number of GT and OT observations devoted to the reconstruction of the young stars SEDs have been obtained, but need to be analyzed in a systematic way.

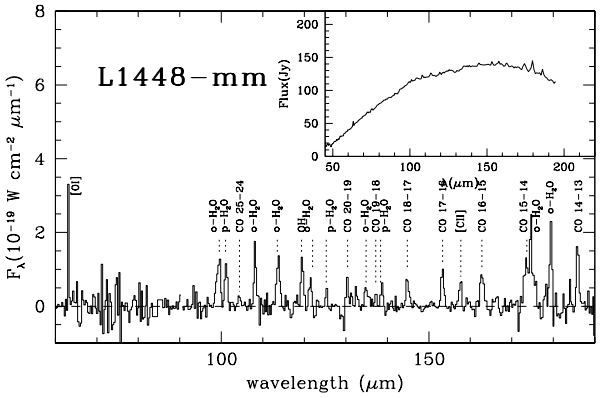

Figure 4. Continuum subtracted LWS spectrum of the Class 0 source L1448-mm, showing the strong emission from both the [OI]63μm and from CO and H_2O rotational lines (from Nisini et al. 1999). The inset show the far IR SED of the object reconstructed from the LWS data.

1.4. Outflows and Herbig Haro objects

Energetic mass loss phenomena in form of outflows and jets are present during all the stages of the star formation process. Shocks originated in outflows cools mainly radiatively through line emission in a wide range of wavelengths, from UV to the radio. The mid/far IR spectral range is particular important for the study of the outflow shocked regions, since allow to trace gas excited from few tens up to more than 2000

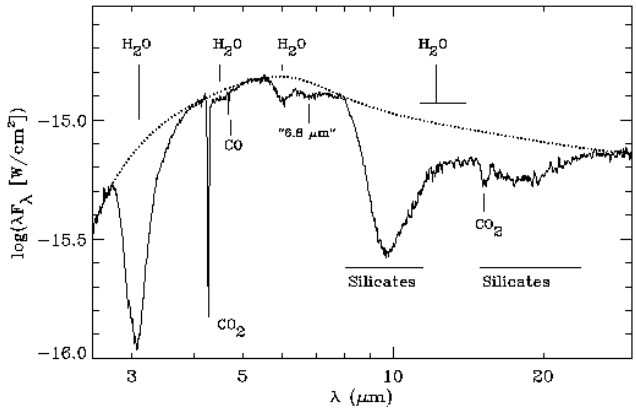

Figure 5. SWS spectrum of the Class I source Elias 29, showing strong absorption features from both ice mantles and silicates (Boogert et al. 2000)

Kelvin, which is mostly unaccessible from ground. In particular, shocks occurring in dense environments cool down preferentially through emission lines in the mid and far IR, mainly through the [OI]63μm transition and the pure rotational transitions of abundant molecular species, such as H_2, CO, H_2O (Nisini et al. 2000). The wavelength range covered by the ISO spectroscopic facilities, also include other transitions from the fundamental levels of ions, such as SIII, SiII, OIII, NII, which can be important to trace the presence of high temperature dissociative shocks in embedded outflows as well as to better constrain the excitation conditions in Herbig Haro objects (e.g. Molinari et al. 2001). About 15 ISO proposal exploiting SWS, LWS and CAM have been performed on selected samples of outflows from both low and high luminosity sources. The LWS spectra, in particular, show that the far infrared gas cooling can be a significant fraction of the total shock cooling in outflows from young embedded protostars, allowing to define the global energy budget in the interaction between the protostellar jet and the environment (Nisini et al. 2000, Giannini et al. 2001). With ISO has been also possible to test for the first time predictions about the water formation in non-dissociative shocks (Kaufmann & Neufeld 1996), and it has been found that it can be indeed the major coolant but only in specific conditions of low velocity shocks not-exposed to strong FUV fields (Giannini et al. 2001) A significant number of outflows have been also mapped with ISOCAM in CVF mode, allowing to have images in the pure rotational H_2 lines (i.e Wilgenbus et al. 2001, Moro-Martín et al. 2001). H_2 (0-0) spectra are also obtained with SWS in selected positions of different outflows. The emission from these lines, which trace shocked gas excited at temperatures ∼200–1000 K, is usually spatially correlated with the emission from the higher excitation H_2 1-0 S(1) line at 2.12μm, confirming that high and low velocity shocks coexist, probably in the form of bow shocks.

1.5. Pre-main sequence stars and disks

Large samples of pre-main sequence stars of both low (T Tauri) and intermediate (Herbig AeBe) mass have been observed by ISO with the four instruments. Such a database of infrared observations gives the possibility to investigate over the circumstellar structure of these stars and over their interaction with the ambient medium.

Photometric and spectrophotometric observations at different wavelengths allow to accurately define the source infrared excesses which can be in turn compared with models considering different circumstellar morphologies, i.e. disks vs dusty envelopes and a combination of the two. Elia et al. 2002, modelled the SEDs from the optical to the radio of all the Herbig AeBe stars observed by SWS and LWS with a spherical circumstellar envelope, fitting the temperature and density structure of the circumstellar regions. Models of passive circumstellar disks have been also used to fit the mid and far IR SEDs observed in few Herbig AeBe stars (Natta et al. 2001, Creech-Eakman et al. 2002).

The gas emission from circumstellar envelopes and disks of both T Tauri and Herbig AeBe stars have been probed with both SWS and LWS. Pure rotational H_2 line emission from disks around pms stars have been tentatively detected (Thi et al. 2001 and Fig. 6) from which an unexpectedly large amount ($0.1–10\,10^{-3}$ $M_\odot$) of molecular gas at ∼ 100–200 K has been deduced, giving strong constraints on the mass of the disk. A more detailed discussion about observations of circumstellar disks by ISO is given by Jourdain de Muizon in this conference proceedings. The presence of photodissociation regions created by the star FUV photons have been also evidenced from observations of the [OI]63,145μm and [CII]158μm lines with LWS (Lorenzetti et al. 2002 and this conference.) Finally, ISO has also gathered a wealth of spectroscopic data on dust and ice features in pre-main sequence circumstellar envelopes, able to address the issue of the dust re-processing due to the star UV photons. Other contributions in this meeting (i.e. from Joblin and Waters) specifically address these studies.

2. FAR INFRARED SPECTRA OF LOW MASS YSOs

As an example of a survey program exploiting the ISO database, I am presenting a spectroscopic survey done on the ISO-LWS spectra of 54 YSOs in different evolutionary phases, from the Class 0 protostars to pre-main sequence stars. The aim of this survey was to study, on a statistical basis, which are the main gas excitation mechanisms and cooling channels in the circumstellar environments of young stars, and see whether any evolutionary trend can be defined by means of the far infrared spectra. The adopted sample is composed by 17 Class 0 sources (all the Class 0 objects listed in André et al. 2000 observed by LWS), 11 Class I sources (all the low mass Class I observed under the LWS GT on Star Formation, Saraceno et al. 1999) and 26 pre-main sequence Herbig Ae/Be stars (all the AeBe listed by Thè et al. (1994) observed by LWS). For the sources of this sample, we have analyzed both the spectra obtained on-source and along the source outflow, considered as part of the young

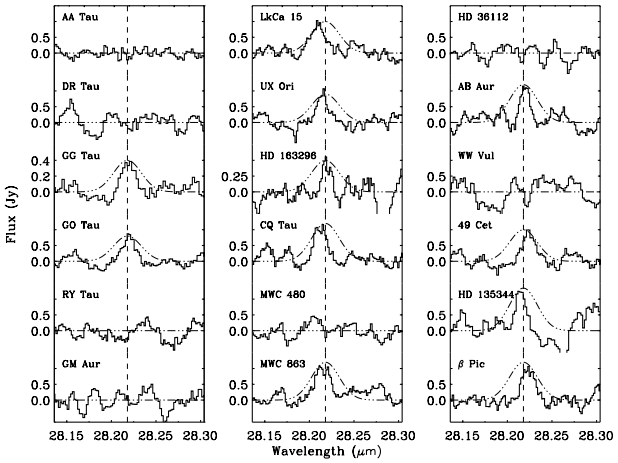

Figure 6. H_2 S(0) 28μm spectra observed with SWS toward a sample of pre-main sequence and debris-disk stars (Thi et al. 2001).

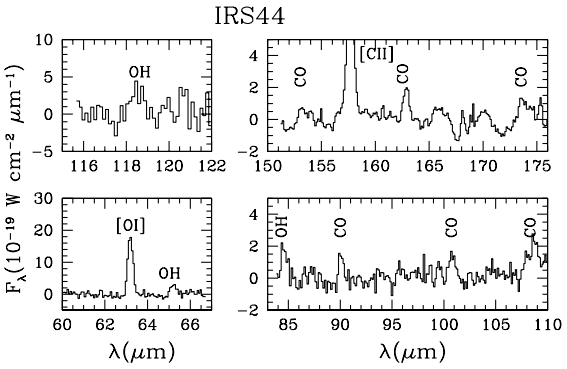

Figure 8. Continuum subtracted LWS spectrum of the Class I YSO IRS44. Molecular emission is observed in form of CO and OH, but no water emission lines are detected.

star system. The main results of this analysis have been presented in Giannini et al. (2001), Nisini et al. (2002) and Lorenzetti et al. (2002).

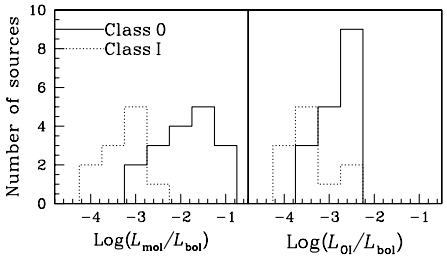

Figure 7. Histograms of the molecular ($L_{\rm mol}$) and [OI] ($L_{\rm OI}$) coolings with respect to ($L_{\rm bol}$), for Class 0 and Class I sources observed by LWS.

.

The spectra from the Class 0 sources are dominated by both [OI]63μm emission and molecular emission from the abundant species CO, H_2O and OH. The molecular lines are consistent with emission from a moderately warm and dense gas (n=10^4-10^6 cm^{-3}, T=300-1500 K). The same physical conditions are derived for the molecular emission observed along the associated outflows and this is a strong indication that in the large LWS field of view the dominant excitation mechanisms in circumstellar envelopes of low mass stars are shocks developed along the protostellar jets; other evidences in this direction are the found correlation between the total luminosity radiated by the traced gas component, $L_{\rm rad}$, and the outflow kinetic luminosity. A further evidence in this sense is that when stronger emission is observed on-source with respect to the outflow lobes, it is usually associated with the presence of dense and warm molecular bullets of outflowing material, like in the case of L1448 (Nisini et al. 2000).

At variance with the Class 0 spectra, the spectra of Class I sources present a lower contribution due to molecular emission. Fig. 7 shows how the total cooling due to molecular emission with respect to the bolometric luminosity decreases by about an order of magnitude going from Class 0 to Class I sources. In a framework where most of the observed molecular emission originate in shocks, this trend can be explained by a lower ambient density encountered by the stellar wind, which gives rise to preferentially dissociative shocks, causing a significant decrease of the contribution of the molecular luminosity to the total gas cooling.In addition, when molecular emission is observed in Class I sources, this is due only to CO and sporadically to OH lines (Fig. 8), while water lines are not detected in any of the considered sources. This can be due to two different effects connected with the source evolution. First of all as the source evolves from the Class 0 to the Class I phase, its envelope becomes more diffuse and excavated. In this situation, the smaller optical depth intervening between the shocked gas and the FUV interstellar field, may easily dissociate the water produced during the early phase of energetic shocks. Moreover, a decrease in the water abundance is also helped by its depletion on dust grain mantles on timescales of the order of 10^5–10^6 yr.

At variance with the Class 0 and Class I sources, the far IR spectra of the more evolved Herbig AeBe stars are largely dominated by atomic/ionic emission lines (mainly [OI]63μm, 145μm and [CII]158μm) which appear well reproduced assuming an excitation in a circumstellar PDR. The weak molecular transitions observed in few objects are consistent with the presence of density peaks in a clumpy circumstellar PDR (Giannini et al. 1999). Therefore, the evolution from the protostellar phase to the pre-main sequence phase is reflected in the far infrared spectra of young stars with an evolution from a shock excited gas emission to a UV photon excited emission, as expected as the outflow power decreases with time while the stellar photons are more able to heat larger regions of the more and more diffuse circumstellar envelope.

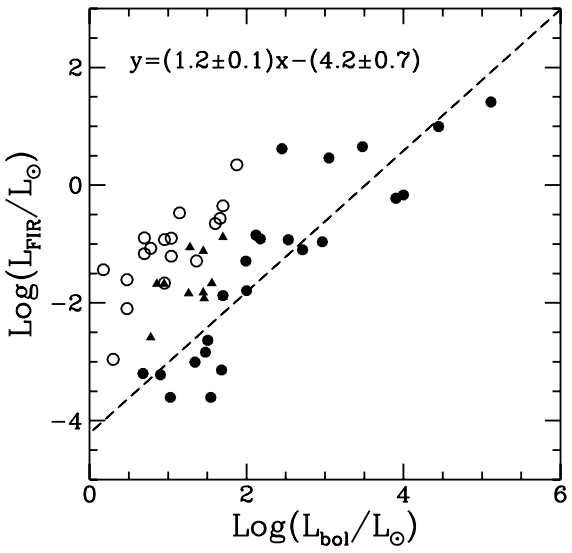

Figure 9. Far IR lines luminosity vs source bolometric luminosity for the sample of Class 0 (triangles), Class I (open circles) and Herbig AeBe stars (filled circles).

Finally, we have compared the far infrared radiated luminosity ($L_{\rm FIR}$) , computed as the total luminosity due to all line emission contributions (fine structure emission and total molecular cooling), of the different classes of sources. In Fig. 9 the $L_{\rm FIR}$ values are plotted as a function of the bolometric luminosity of the central object. From this Figure we can see that the $L_{\rm FIR}/L_{\rm bol}$ ratio tends to decrease with the evolution, with a value $\sim 10^{-2}$ for the Class 0, $\sim 10^{-3}$ for the Class I and $\sim 10^{-4}$ for the Herbig AeBe stars. This evidence indicates that in young sources, the conversion of the bolometric luminosity into far IR line cooling in the circumstellar envelope becomes less and less efficient with the evolution. This fact extends to the FIR gas cooling the well consolidated statement according to which the relevance of the circumstellar vs stellar properties diminishes during pre-stellar evolution.

REFERENCES

André P.,Ward-Thompson D., Barsony M. 2000, "Protostar & Planets IV", eds Mannings V., Boss A.P., Russell S.S., p.59
Bacmann A., André P., Puget J.L., Abergel A., Bontemps S., Ward-Thompson D., 2000, A&A, 361,555
Boogert A.C.A. et al., 2000, A&A, 360, 683
Bontemps S. et al., 2001, A&A 372, 173
Ceccarelli C., Hollenbach D.J, Tielens A.G.G.M, 1996, ApJ 309, 827
Ceccarelli C. et al., 1999, A&A, 342, L21
Creech-Eakman M.J., Chiang E.I., Joung R.M.K., Blake G.A., van Dishoeck E.F., 2002, A&A 385, 546
Elia, D. et al., 2002, this volume
Giannini T. et al., 1999, A&A 346, 617
Giannini T., Nisini B., Lorenzetti D., 2001, ApJ 555, 40
Kaas, A.A. et al., 1999, in "The Universe as Seen by ISO", Eds. P. Cox & M. F. Kessler. ESA-SP 427, p. 493
Kaufman M.J., Neufeld D.A., 1996, ApJ, 456, 611
Larsson B. et al., 2000, A&A 363, 253
Lorenzetti D. et al., 1999, A&A 346, 604
Lorenzetti D. et al., 2002, A&A in press
Molinari S., Noriega-Crespo A., Spinoglio L., 2001, ApJ 547, 292
Moro-Martín A., Noriega-Crespo A., Molinari S., Testi L., Cernicharo J., Sargent A., 2001, ApJ 555, 146
Natta A., Prusti T., Neri R., Wooden D., Grinin V.P., Mannings V., 2001, A&A 371, 186
Nisini B. et al., 1999, A&A 350, 529
Nisini B. et al., 2000, A&A 360, 297
Nisini B. et al., 2001, The Promise of the Herschel Space Observatory. Eds. G.L. Pilbratt, J. Cernicharo, A.M. Heras, T. Prusti, & R. Harris. ESA-SP 460, p. 211
Nisini B., Giannini T., Lorenzetti D., 2002, ApJ, 574,
Olofsson G. et al., 1999, A&A 350, 8830
Persi P. et al., 2000, A&A 357, 219
Saraceno P. et al., 1999, in "The Universe as seen by ISO", eds Cox P. & Kessler M., ESA-SP 427, p. 575
Thè P.S., de Winter D., Perez M.R. 1994, A&AS, 104, 315
Thi, W.F. et al., 2001, ApJ, 561, 1074
van Dishoek E. et al. 1999, in "The Universe as seen by ISO", eds Cox P. & Kessler M., ESA-SP 427, p. 437
Ward-Thompson D., Andrè P., Kirk J.M., 2002, MNRAS 329, 257
Wilgenbus D., Cabrit S., Pineau Des Forêts, Flower D., 2001, "From Darkness to Light: Origin and Evolution of Young Stellar Clusters", ASP Conference Proceedings, Vol. 243, p.347

THE IR CONTINUUM OF THE HERBIG AE/BE STARS AS SEEN BY THE ISO SPECTROMETERS: A CONTRIBUTION TO THE MODELING OF THE CIRCUMSTELLAR ENVIRONMENT

Davide Elia[1], Loretta Campeggio[1], Francesco Strafella[1], Teresa Giannini[2], Dario Lorenzetti[2], Brunella Nisini[2], and Stefano Pezzuto[3]

[1]Dipartimento di Fisica, Università di Lecce, C.P.193, I-73100 Lecce, Italy
[2]Osservatorio Astronomico di Roma, via Frascati 33, I-00040 Monte Porzio, Italy
[3]IFSI-CNR, via Fosso del Cavaliere, I-00133, Roma, Italy

ABSTRACT

We present a study of the whole sample of the Herbig Ae/Be stars observed with the spectrometers (SWS+LWS) on board of the Infrared Space Observatory (ISO). These objects have been studied not only by considering their IR continuum emission but also taking into account all the available photometric data, collected from the optical region to the radio wavelengths. In this way their global spectral energy distributions (SEDs) have been compared with the results of the radiative transfer calculations in the context of a model for the circumstellar environment. Besides different density laws and dust types, this model considers also the possibility for the presence of:

1) different radial density distributions describing respectively the inner and outer regions of the envelope;

2) polar cavities that could be evacuated by the action of the stellar wind associated with the pre-main sequence phases.

We present the result of a selection for the best models which has been done by considering both the spectral fit to the observed SEDs and the consistency between the model parameters and the corresponding observable quantities as the spectral type, the distance and the extinction. A possible relationship is noted between the geometry of the CS matter distribution and the evolutionary stage of the Herbig Ae/Be stars.

Key words: Stars: pre-main sequence – circumstellar matter – Infrared: stars

1. INTRODUCTION

The class of the Herbig Ae/Be stars (HAEBE) was defined by Herbig (1960) to identify the precursors of main-sequence objects of intermediate mass ($M \sim 2 - 10\ M_{\odot}$). Since then the group has grown from the original 26 sources to include more then 300 members and candidates (Thé et al. 1994) revealing a great degree of heterogeneity in many properties. Among the most debated points is the spatial distribution (spherical envelopes versus discs) of the circumstellar (CS) dust, whose presence is shown by the IR excess, a common characteristic of the HAEBEs.

In most cases, because of the distance of the objects and the consequently inadequate spatial resolution of the observations, theoretical models have been used to reproduce the observed SEDs. This still remains a very important tool to infer on the geometry of the CS matter.

The Infrared Space Observatory (ISO, Kessler et al. 1996) has produced spectrophotometric data in the range between 2 and 200 μm, where the HAEBEs emit the bulk of their radiation: the ISO observations allow us to put more tight constraints for the modeling of the CS environment.

In Section 2 we report the sample of the observed sources, we describe the data reduction procedure, and we present the results. In Section 3 the ISO data are complemented with ground based photometry from the optical to radio wavelengths. The SEDs obtained in this way have been then compared with synthetic spectra computed by means of a CS model. We also briefly discuss the results of the fitting procedure.

2. DATA REDUCTION

The ISO Data Archive has been searched for Short Wavelength Spectrometer (SWS) and Long Wavelength Spectrometer (LWS) observations related to HAEBEs. We found 36 objects, which are listed in Table 1.

Table 1. The observed sample of HAEBE

LkHα 198	He 3-1191
V376 Cas	HD 150193
Elias 3-1	CoD -42°11721
AB Aur	HD 163296
MWC 480	MWC 297
HD 34282	MWC 300
HD 36112	TY CrA
CQ Tau	R CrA
MWC 137	HD 179218
Z CMa	WW Vul
HD 97048	BD +40°4124
HD 100546	LkHα 224
HD 104237	PV Cep
IRAS 12496-7650	HD 200775
HD 141569	V645 Cyg
HD 142666	LkHα 234
HD 14443	LkHα 233
HR 5999	MWC 1080

The SWS spectra were taken in the range 2.3–45 μm with low resolution ($\lambda/\Delta\lambda \sim 250$) and a typical field of view increasing with wavelength from $14'' \times 20''$ to $20'' \times 33''$ (de Graauw et al. 1996), while the LWS spectra were obtained in the range 43–196.7 μm, $\lambda/\Delta\lambda \sim 200$, (Clegg et al. 1996). In the LWS spectral range the instrumental beam size is $\sim 80''$ so that in some cases (12 objects) the observations were carried out also at off-source positions to account for the contamination due to the local background.

Proceedings of the Symposium *"Exploiting the ISO Data Archive - Infrared Astronomy in the Internet Age"*, 24–27 June 2002, Sigüenza, Spain (C. Gry, S. B. Peschke, J. Matagne et al. eds., ESA SP-511)

The raw SWS and LWS data were processed using version 10 of the off-line pipeline, which produces series of repeated spectral scans, each composed of 12 and 10 sub-spectra for SWS and LWS, respectively. These corresponds to different spectral ranges, that are arranged to be partially overlapping.

The data were further reduced and analysed in subsequent steps:

- removing bad points (glitches, residual detectors responsivity drifts);
- averaging of the many scans obtained on each sub-spectrum;
- removing of the low-frequency fringes, whose presence affects particularly the LWS spectra (Swinyard et al. 1998).
- smoothing of averaged spectra (SWS only).

Whenever possible, the off-source LWS spectra were subtracted from the correspondent on-source data. Notwithstanding accurate data reduction, the sub-spectra obtained appear in many cases not perfectly overlapping together, probably because of the variation of the beam size with the wavelength (de Graauw et al. 1996, Swinyard et al. 1998). In our experience it was not possible to deal with this effect other than shifting the 10 sub-spectra, using one detector as reference and scaling the intensity from the others using overlapping spectral ranges.

In Fig. 1 we show examples of two reduced source spectra.

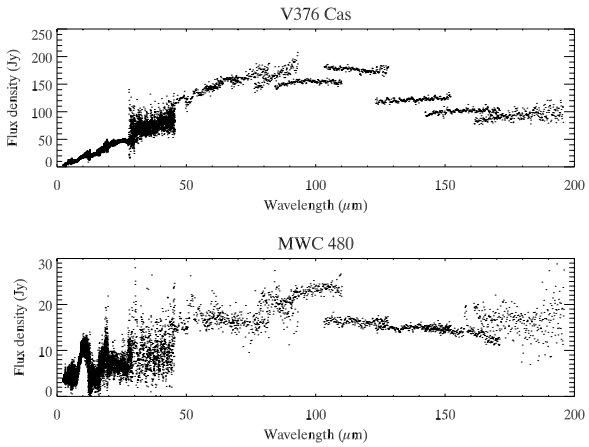

Figure 1. ISO spectra. Both sources show a good continuity between SWS and LWS fluxes despite the different beamsize involved. On the other hand they clearly present discontinuities in the LWS respective sub-spectra.

3. MODEL AND OBSERVATIONS

The SEDs emerging from CS envelopes have been computed by means of a model based on a spherical geometry of the CS environment.

The model is characterized by a density distribution $n(r)$ around a central star and by the presence of an HII region whose radius is determined by the ionizing luminosity of the central star. A temperature profile $T(r)$ is also considered for the dust component while for the gas we assumed $T = 10^4$ K in the HII region.

The gas emission processes considered in the radiation transfer are: free-free, free-bound and electron scattering, while for the dust component the emissivity is computed on the basis of the "astronomical silicate" defined by Draine & Lee (1984). Cases with a modified dust emissivity (at $\lambda > 20\mu$m) have also been computed to take into account the fact that in star forming regions the average dust grain size can be larger than in the diffuse IS medium and consequently the opacity can be described by a $k \propto \lambda^{-\beta}$ law; in our case, β = 1.2, 0.8, 0.6 (see Pezzuto et al. 1997 for a more complete model description). In addition we also consider:

1) the possible presence of cavities in the CS envelope as can be evacuated by the strong stellar wind associated with the pre-main sequence;
2) the possibility of two different density distributions describing the inner and outer parts of the envelope, respectively.

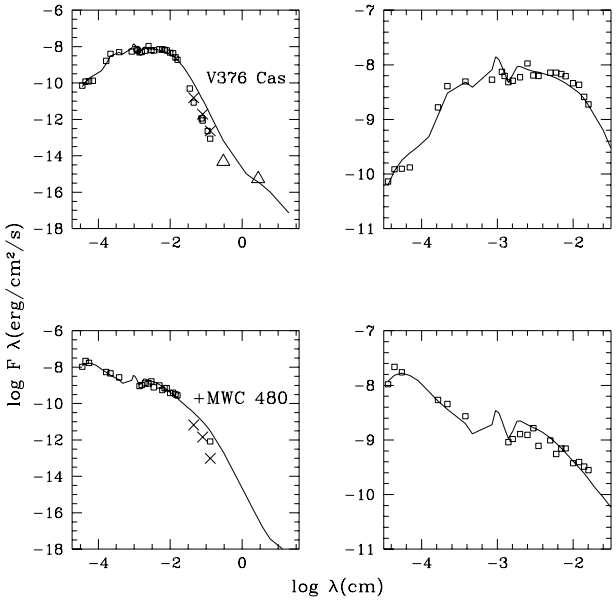

Figure 2. Spectral fits. Computed SEDs (solid line) are superimposed to the observed fluxes (squares; triangles are upper limits). Crosses represent submillimetric model fluxes corrected for diffraction effects due to the instrumental beamsize.

Varying the model parameter values, we explored a reasonable volume of the parameter space in order to create a large bank of continuum spectra, to be subsequently compared with the observed SEDs, obtained by complementing the ISO spectral data with the available photometric data from optical to radio wavelengths. Such a comparison, made by means of a "chi square like" method, allows the selection of the best models for each object. Among the best fit models we further selected the realistic ones by considering the compatibility with other

Table 2. Fit parameters and correspondent observables

Source	β	q	p	n_0	Spectral type		A_V (mag)			Distance (pc)	
				(cm^{-3})	Calc.	Obs.	CS	IS	Obs.	Calc.	Obs.
V376 Cas	1.2	0.5	0.8	$3{\cdot}10^8$	B5	B5[1]	4	2.5	2.9-5.2[3,4]	724±32	600[3]
MWC 480	0.6	0.6	1.3	$3{\cdot}10^{10}$	A3	A3[2]	1	0	0.25-0.4[5,6]	101±5	131[5]

NOTES: V376 Cas was fitted with a purely spherical model, MWC 480 with a "two polar cavities" model.
REFERENCES TO THE TABLE: 1. Herbig 1960; 2. Jaschek et al. 1991; 3. Hillenbrand et al. 1992; 4. Pezzuto et al. 1997; 5. van den Ancker et al. 1998; 6. Miroshnichenko et al. 1999.

observable quantities, as spectral type, visual absorption, and distance.

As an example, in Fig. 2 we show the results obtained for two of the HAEBE stars, while in Table 2 we list the corresponding best fit model parameters as well as the observed values of visual extinction, distance, and spectral type.

This work is in progress and we are planning to extend this approach to the whole sample of HAEBE listed in Table 1 with the aim to obtain statistical informations on the environments of these objects.

REFERENCES

Clegg, P.E., Ade, P.A.R., Armand, C., et al. 1996, A&A 315, L38

de Graauw, T., Haser, L.N., Beintema, D.A. et al., 1996, A&A, 315, L49

Draine, B.T., Lee, H.M., 1984, ApJ, 285, 89

Herbig, G.H., 1960, ApJS 4, 337

Hillenbrand, L.A., Strom, S.E., Vrba, F.J., Keene, J., 1992, ApJ, 397, 613

Jaschek, M., Jaschek, C., Andrillat, Y., 1991, A&A, 250, 127J

Kessler, M.F., Steinz, J.A., Anderegg, M.E. et al., 1996, A&A 315, L27

Miroshnichenko, A., Ivezić , Z., Vinković, D., & Elitzur, M., 1999, ApJ, 520, L115

Pezzuto, S., Strafella, F., Lorenzetti, D., 1997, ApJ 485, 290.

Swinyard, B.M., Burgdorf, M.J., Clegg, P.E., Davis, G.R., Griffin, M.J., Gry, C., Leeks, S.J., Lim, T.L., Pezzuto, S., Tommasi, E., 1998. In: Proc. SPIE, A.M. Fowler (Ed.), Vol. 3354, Pag. 888

Thé, P.S., de Winter, D., Pérez, M.R., 1994, A&AS 104, 315

van den Ancker, M.E., de Winter, D., Tjin A Djie, H.R.E., 1998, A&A, 330, 145

LUMINOSITY FUNCTIONS OF YOUNG STELLAR CLUSTERS: ISO DATA ARCHIVE AS A PART OF THE VIRTUAL OBSERVATORY

Timo Prusti

Herschel Science Centre, Astrophysics Missions Division, Research and Scientific Support Department of ESA, ESTEC, Noordwijk, The Netherlands

ABSTRACT

We have examined the use of ISO data for statistical studies of young stellar clusters. The need for the ease of usage is emphasised as the ISO observations form just one part of the full data set needed for luminosity function studies. The automatically produced point source list from the ISOCAM pipeline is looked in more detail. A comparison is made with interactively extracted point source list to that of the pipeline with data from the Chameleon I star forming region. Recommendations are given to deal with the pipeline produced list for luminosity function applications. Finally, suggestions are made for the ISO Active Archive Phase to improve the pipeline produced point source list to allow a wider use of this data product in the Virtual Observatory.

Key words: Luminosity Function — Pipeline Processing — Star Formation — Virtual Observatory

1. INTRODUCTION

Luminosity functions provide a statistical method to address questions of star formation in clusters. By concentrating to young clusters it is possible to have access to the very low mass stars and brown dwarfs as they are most luminous at their young age. The drawback of young clusters is extinction as the cloud from which the stars were born is still around with its associated dust. Therefore infrared observation are needed and ISO observations have proved to be an important source of data (e.g. Bontemps et al. 2001).

Luminosity function itself is not an interesting quantity. Its importance lies in the fact that it is a tool to compare observations to theory. An observer constructs the luminosity function in three steps. Firstly, one needs to find all members of a young cluster. Secondly, one needs to gather sufficient amount of photometric data for each member. Thirdly, one needs to estimate the bolometric luminosity from the available photometry. After that the luminosity function deduction is a simple summing of the number of stars in each luminosity bin. A theoretical luminosity function can be constructed by convolving estimates of initial mass function, star forming history within the sample and pre-main sequence tracks. By comparing the observed and theoretical luminosity functions it is then possible to test the validity of e.g. the assumed initial mass function.

In the context of the ISO Data Archive as a part of the Virtual Observatory the most relevant step is the gathering of photometry. The following sections will concentrate on this step of the work the observer has to do when constructing a luminosity function.

2. COLLECTING PHOTOMETRY

In young clusters with ages of the order of few million years, the most dominant young stellar population consists of T Tauri stars. T Tauri stars are often characterised with a broad spectral energy distribution with significant contribution to the luminosity in optical, near-, mid- and far-infrared wavelengths. For accurate estimates of the bolometric luminosity it is therefore often necessary to combine ground based optical and near-infrared data with satellite data (e.g. ISO) in the mid- and far-infrared ranges. The key point is that ISO data is an important part of the full picture, but not the only part.

There are different types of sources for the photometric data. An observer may choose to use literature data only for collecting the measurements. This has the advantage that typically the flux or magnitude is directly given to a named target. The drawbacks are that this way only published data can be accessed and often significant amounts of re-typing are needed as only recently the astronomical literature has started to provide data tables also in electronic format.

When collecting photometry from catalogues, an observer has couple of advantages with respect to gathering data from literature. Typically catalogues are provided in electronic format making it easier to ingest relevant photometric points. Also a catalogue often provides a homogeneous data set for many objects increasing the reliability of results. However, there are complications as well. An observer is still left to do the object to object correlation between different catalogues. This can be tedious especially when positional accuracies are poor or spatial resolving powers differ significantly. E.g. in Chameleon I there is a match between T Tauri star T42 and far-infrared source IRAS 11083–7618 and only a more careful analysis with additional ground based mid-infrared data reveals that part of the IRAS flux is coming from the close by T Tauri star WW Cha (Prusti et al. 1992). This is a common problem in young clusters with high stellar densities.

Other sources of photometric data are archives of various observatories. If the ISO archive is examined then vast amount of mid- and far-infrared data of young stellar clusters can be found. The problem, by no means genuine to ISO, is that the

Proceedings of the Symposium *"Exploiting the ISO Data Archive - Infrared Astronomy in the Internet Age"*, 24–27 June 2002, Sigüenza, Spain (C. Gry, S. B. Peschke, J. Matagne et al. eds., ESA SP-511)

data need to be reduced first. The pipeline processing is not considered to be of high enough quality to allow direct publishing of the results. This is a fundamental problem for studies of luminosity functions because each wavelength regime — optical, near-infrared, mid-infrared and far-infrared — needs its special methods and software. This way a task of getting good spectral energy distributions to all member stars becomes huge if archive data alone is used. The obvious advantage is the availability of all data instead of the published data alone.

The problem of using archives can be expressed in other words too. Archive interfaces are usually very good in telling whether "observations covering the target at the requested wavelengths exist" while the question of the astronomer is "is my source detected at requested wavelengths and with what fluxes". For ISO observations the first part is indeed easily done with the ISO Data Archive while the fluxes are recommended to be reduced interactively by the observer. However, the ISOCAM pipeline produces an automatically extracted point source catalogue from the images. As luminosity function is used as a statistical tool, the automatically extracted source fluxes may be acceptable with their larger errors as long as no undesirable biases are introduced. However, before using the pipeline list its accuracy, completeness and reliability has to be assessed.

3. THE ISOCAM POINT SOURCE LIST

The ISOCAM pipeline produces various kinds of products from each of the observations. One of the products is the point source list. The point sources are extracted from every stable pointing of an observation. This means that e.g. in the case of a two by two mosaic, there will be four separate point source lists each corresponding to one of the four stable pointings. The consequence of this extraction method is that for mosaics with redundancy the potentially deeper overlap region is not searched for fainter targets as the extraction algorithm is not executed on the final mosaic. On the other hand the stronger point sources in the overlap region should be detected more than once providing an additional check on reliability.

In order to examine the overall quality of the automatically extracted ISOCAM sources, we have made a case study of the observations made from the Chameleon I star forming region. Chameleon I was included in the observing programme with mapping of 0.59 square degrees at 6.7 and 14.3 μm. The observations have already been reduced with interactive analysis by Persi et al. (2000) who detected 282 sources at 6.7 μm. Out of the 6.7 μm detections 103 sources were detected also at 14.3 μm, but we concentrate on the 6.7 μm detections in this comparison study. The 282 sources can be traced back to near-infrared detections in 96 % of the cases. This suggests a low false alarm rate in the source list by Persi et al. (2000).

The ISOCAM automatically extracted list contains 182 sources at 6.7 μm after merging the multiple detections of the same object in different raster points. The statistical flux uncertainty in the ISOCAM list is about 2 mJy with the weakest detections at 6 mJy level. For comparison it is good to note that the Persi et al. (2000) list contains sources down to 2 mJy at 3 sigma detection level. The higher sensitivity is based on the earlier mentioned advantage of extracting the sources from the final mosaic which has lower noise at the regions where different raster pointings overlap.

The astrometry in the automatically extracted source list is in order as there was no problem to merge the sightings of the same source between different raster points. For the same reason there was no problem to identify the common sources between the pipeline list and the list of Persi et al. (2000). At 6.7 μm there are 143 common sources between the two source lists. With these common sources it is possible to examine the flux calibration of the automatically extracted sources. Figure 1 shows the correlation between the pipeline and Persi et al. (2000) fluxes (excluding one source which is marked as saturated in the pipeline list). Figure 2 shows the same correlation at low flux levels. In general the correlation is good with relative uncertainty increasing toward lower fluxes.

In Fig. 3 the 6.7 μm sources are grouped into three categories: sources detected only by Persi et al. (2000), sources detected only by the pipeline (OLP) and the earlier mentioned 143 common sources. At first glance it looks like both interactive analysis and pipeline fail seriously in completeness. However, unlike the sources found by Persi et al. (2000), the sources detected only by the pipeline do not have near infrared matches. This hints toward high false alarm rate in the case of the pipeline. A more detailed look reveals that most of the pipeline only detected sources are transients from strong point sources in raster points prior the raster point where the detection has been made. Therefore we can interpret the source list of Persi et al. (2000) to be reliable and complete at the flux levels of the weakest pipeline detections. This allows to estimate the reliability of the pipeline deduced point source list. In the case of Chameleon I the reliability is 80 %. This figure cannot be generalised as the contamination due to transients depends on the number of strong sources in the field and the details of the raster pattern for a specific observation.

By assuming the Persi et al. (2000) list to be complete above 10 sigma level it is possible to estimate the completeness of the pipeline list. At 10 mJy bin only half of the "true" sources are detected. This means that at 5 sigma level the pipeline point source list can be expected to be 50 % complete. At 10 sigma level the completeness level has increased to 96 %.

4. CONCLUSIONS

In studies of luminosity functions of young stellar clusters data is needed from various sources. Therefore an important aspect to consider is the effort one needs to put in each data set to pull out the publishable numbers. With ISO the recommendation for observers is to reduce their data themselves despite the pipeline end products. In this study the point source list from the ISOCAM pipeline has been evaluated against manually reduced data set. The quality is sufficient for statistical work when the following is taken into account

– the pipeline warnings of saturation have to be taken into account

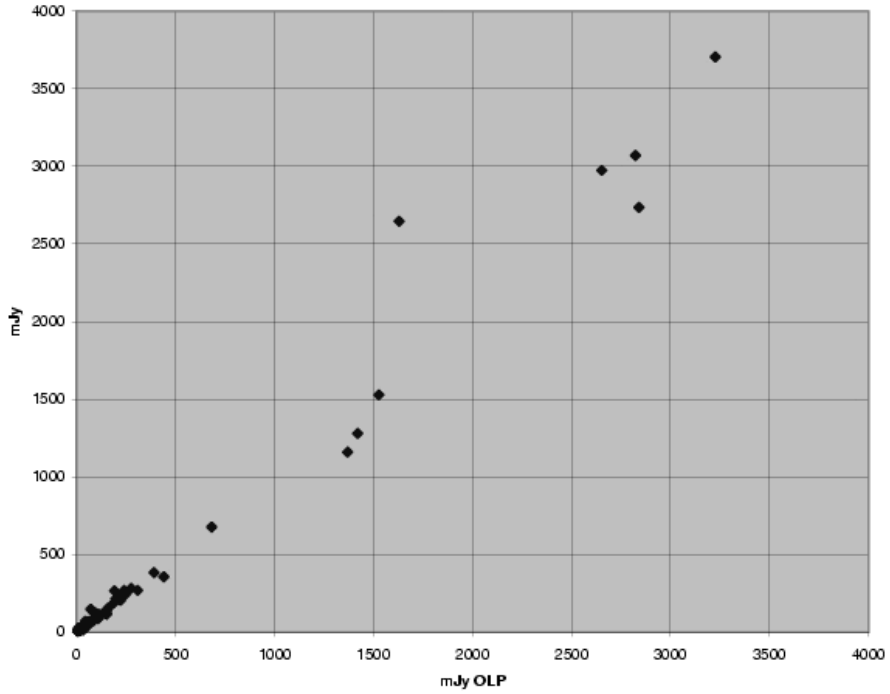

Figure 1. Persi et al. (2000) vs. ISOCAM pipeline (OLP) fluxes

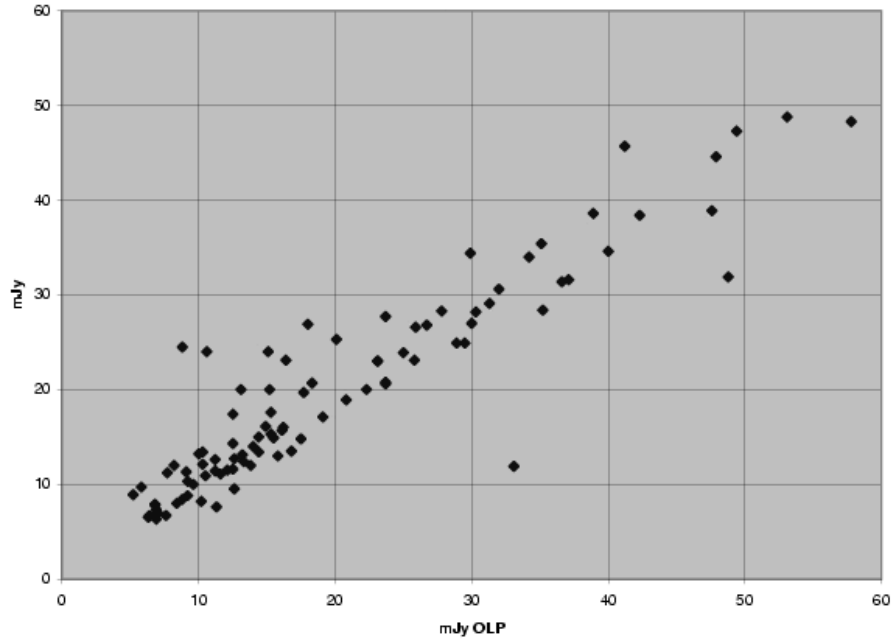

Figure 2. As Fig. 1 but for sources with flux below 60 mJy

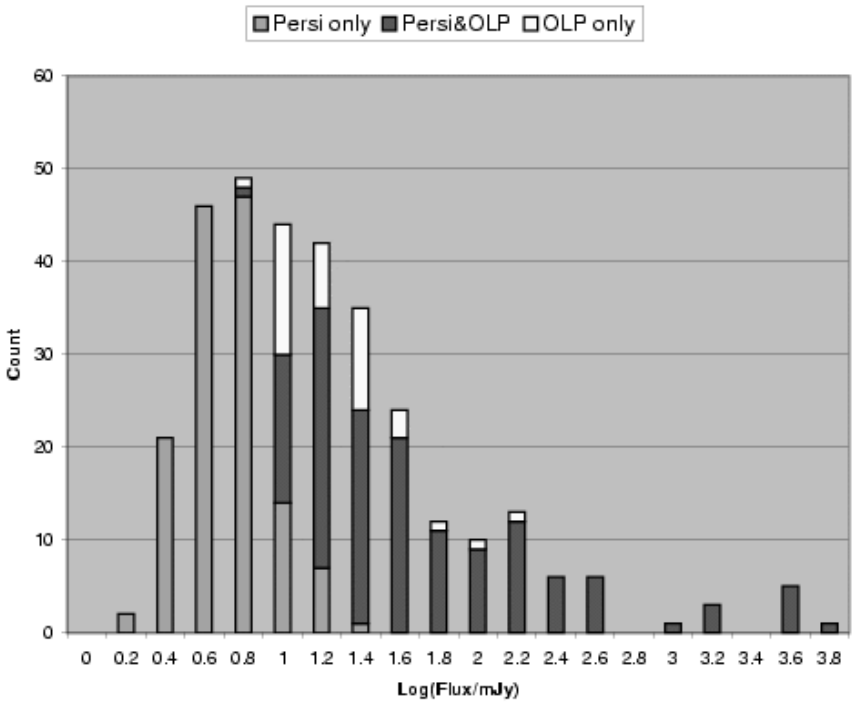

Figure 3. 6.7 μm flux distribution of detections

– transients have to be taken into account by removing spurious sources from raster positions following bright sources (by taking the array column pixel numbers and checking the same pixel position in the next sky position)
– the lower sensitivity has to be accepted due to point sources being from raster positions rather than from combined mosaic

Especially the removal of spurious sources due to transients is a tedious manual operation. During the ISO Active Archive Phase one should consider whether this false source indication could be removed automatically from the pipeline products: either by flagging detections following bright sources in the same pixel position or by running the point source extraction to transient corrected images. The point source extraction from the mosaics may be a more difficult task with a danger of creating many more false alarms at raster map borders of the mosaic images, but it would be desirable to get the weak sources detected automatically as well. From user point of view it is frustrating to see a pipeline product which is almost there to be used directly, but the final touch is missing so that manual work is needed after all. By being able to give this missing final touch during the ISO Active Archive Phase would increase the accessibility significantly with a great potential to even wider use of ISO data in astronomical research of young stellar clusters.

REFERENCES

Bontemps S., André P., Kaas A.A., Nordh L., Olofsson G., Huldtgren M., Abergel A., Blommaert J., Boulanger F., Burgdorf M., Cesarsky C. J., Cesarsky D., Copet E., Davies J., Falgarone E., Lagache G., Montmerle T., Pérault M., Persi P., Prusti T., Puget J.L., Sibille F., 2001, A&A 372, 173

Persi P., Marenzi A.R., Olofsson G., Kaas A.A., Nordh L., Huldtgren M., Abergel A., André P., Bontemps S., Boulanger F., Burgdorf M., Casali M., Cesarsky C.J., Copet E., Davies J., Falgarone E., Montmerle T., Perault M., Prusti T., Puger J.L., Sibille F., 2000, A&A 357, 219

Prusti T., Whittet D.C.B., Wesselius P., 1992, MNRAS 254, 361

A STAR FORMATION/ISM ASTRONOMICAL DATABASE

Sergio Molinari[1], **Babar Ali**[2], **John Good**[2], **and Alberto Noriega-Crespo**[3]

[1]Istituto di Fisica Spazio Interplanetario-CNR, Via Fosso del Cavaliere 100, 00133 Rome, Italy
[2]Infrared Processing and Analysis Center, Caltech, Pasadena CA-91125
[3]SIRTF Science Center, Caltech, Pasadena CA-91125

ABSTRACT

The **Star Formation/ISM Astronomical Database** (hereafter SFD) will be a set of on-line services adding value to existing data archives and published journals, along the lines of the very successful NASA/IPAC Extragalactic Database (NED) and SIMBAD projects but with a focus on star formation an the interstellar medium (ISM) within the Milky Way. Unlike NED and SIMBAD, however, the SFD must deal with multi-wavelength measurements of **extended** regions and cross--correlative relationships between disparate measurements. The SFD will rely heavily on existing databases, primarily adding data content and connectivity between datasets around the world, and custom tailoring of existing tools to provide interfaces (programming API, Web, and JAVA GUI) specific to this application.

We consider the SFD as a valuable component in the broader context of a future Virtual Observatory.

1. INTRODUCTION

As in all areas of modern science, the ongoing development of new technologies in the optical, infrared, millimeter and submillimeter astronomy has resulted in an explosion of digital data relating to the interstellar medium in general and star formation in particular. These data are suitable for ingestion into archives and for sharing over computer networks; in fact, the volume of data is now such that it has become impossible to use effectively by non-digital means.

Luckily, information systems technology has also reached the point where reliable remote access to archive datasets (on a variety of scales) is not only possible but a standard (if currently fragmented) approach to performing astronomical research. What this massive body of data currently lacks is a logical and efficient "directory"; services which not only capture the knowledge of the existence of data but provide the added value of efficient search and interrelationship mechanisms.

The SFD would build on database and interface activities and expertise all around the world to provide efficient location and access information for all existing data on large spatial and complex morphological region (e.g., molecular clouds, SNRs, HII regions, *etc.*) with cross-referencing mechanisms based on scientific criteria to capture interrelationships between datasets.

2. A SCIENCE DRIVEN APPROACH

Virtual observatories are the new paradigm of interaction with the present explosion of the available astronomical data from multi-wavelength, ground-based and satellite observatories. While the technical challenge of setting up such a "virtual" observatory is enormous, it is important to emphasize that science must remain the primary motivation for approaching these technical problems in a way to ensure that this will meet the scientist needs.

The immediate scientific benefit available from combining a large collection of astrophysical data and advanced computing technology will be a flexible, fast and efficient interface for astronomical research. One which allows the user to take full advantage of as much knowledge-base and information as possible on astronomical objects, regions, wavelengths, parameter space. The NASA Extragalactic Database (NED, Helou & Madore 1988) pioneered such services on extragalactic objects. Although very complex in nature, the objects contained in NED are well defined physical entities. However, the research on interstellar medium and the formation of stars deals in many cases with entities which are not bound as single objects.

On the one hand the traditional association between object name and sky coordinates has to be abandoned when we start dealing with entities like giant molecular clouds, molecular outflows, reflection nebulae and SNRs. As an example, an astronomically meaningful association of stellar objects with a molecular cloud should not assume the cloud as a rectangular box but must take into account the cloud's complex morphology. On the other hand, the criteria linking objects with datasets, as well as different datasets together cannot be limited to the simple positional coincidence. As an example, the physical association between a Young Stellar Object and the bow-shock produced by its jet cannot be established on the basis of spatial superposition (e.g., the case of HH34IRS, Devine et al. 1997), because they are several arcminutes away from each other. The link connecting the two objects together (and the related datasets) can only be established based on astrophysical considerations; the SFD will capture that information (including all necessary bibliographical references), allowing the user to navigate through multi-wavelengths and multi-instruments datasets in an astrophysically meaningful way.

Proceedings of the Symposium *"Exploiting the ISO Data Archive - Infrared Astronomy in the Internet Age"*,
24–27 June 2002, Sigüenza, Spain (C. Gry, S. B. Peschke, J. Matagne et al. eds., ESA SP-511)

3. SFD BUILDING BLOCKS

3.1. The Sources

One of the most important and novel aspects of the SFD will be its ability to deal with extended objects, such as giant molecular clouds, dense cores, shock-excited nebulosities. The issue of the (boundary) "definition" of complex entities, whose morphology changes dramatically depending on the observational tracer used, is less academic than it may seem. From a technical standpoint, building an information system like the SFD will require the creation of "standards" (like the "definition" of extended sources). It is highly probable that the everyday, widespread, use of the service may slowly shift the standards' validity from the technical to the scientific ground. For this reason the standards' definition will need to be addressed with a set of clear and astrophysically meaningful criteria, and *with the concourse of the astronomical community*. As an example, the definition of the NGC1333 and Serpens molecular clouds in the on-line prototype of the SFD is based on maps of low critical density molecular tracers, like CO(1–0).

Specialized name resolution capabilities, in addition to those provided by SIMBAD (Egret, Wenger & Dubois 1991), will also be offered.

3.2. Database Contents

Three classes of archive data should be accessible (directly or indirectly) through SFD services:

i) Space Mission Archives: IRAS, 2MASS, MSX, ISO (the Browse Products), ROSAT, HST, *etc.* All these archives have been (or are being) produced and maintained by their responsible institutions/groups.
ii) Ground-Based Observatory Archives. For Palomar (Digital Sky Survey), NRAO/VLA-FIRST/NVSS and the James Clerk Maxwell Telescope (JCMT), data archives exist and are already available on-line. For Owens Valley Radio Observatory (OVRO), the IRAM/Plateau de Bure, Caltech Submillimeter Observatory (CSO), Five College RadioAstronomy Observatory (FCRAO), the archives exist but are not yet on-line.
iii) Databases Derived from the Literature, including the following four subclasses:
   a - Data from large ground-based ISM standalone projects such as the Stony Brook CO (Solomon, Sanders & Rivolo 1985) and the Leiden/Dwingeloo HI (Burton & Hartmann 1994) galactic surveys, the K′-band imaging survey of molecular outflows exciting sources (Hodapp 1994).
   b - Astronomical catalogs/archives created and maintained on a private basis (although accessible to the public), such as the Herbig-Haro objects catalog created and maintained by B. Reipurth at http://casa.colorado.edu/hhcat/
   c - Data published in major observational papers that are currently made available to the community in electronic form at CDS-Strasbourg and ADC at NASA/GSFC.
   d - Catalogs that will need to be compiled containing data and information about photometry, spectroscopy and imaging of YSOs and related objects and regions from the UV to the radio, which are not otherwise available in electronic form. Data will be stored in files which will also contain, in the form of FITS-like headers, all the parameters charaterising the dataset (see §3.3).

The task of setting up all the infrastructure needed to access data archives (i), (ii) and (iiic) and to make them interoperable is a formidable technological and conceptual challenge. It constitutes most of the effort being spent by "Virtual Observatory" projects like NVO (in the USA) and AVO (in Europe, see contribution by P. Benvenuti in these proceedings). The aim is to build the necessary interfaces to issue direct queries to the appropriate remote archives, augmenting the standard interactive query mechanisms available at each site by making this integrated data retrieval process as transparent as possible to the user.

Item (iiid) is the only case where catalogs will have to be built from scratch. As with NED and SIMBAD, however, this effort adds enormous value to the literature from which it derives.

3.3. The Metadata

The focus of a Star Formation/ISM database is not primarily the collection of datasets but rather the *generation of a complete set of basic information and metadata pointers to the data, wherever it resides*. Such searchable information for an object, diffuse region or includes not only sky coverage but also their properties when known; such things as distance, luminosity, radial velocity, and proper motion. Clearly, metadata will be built also for datasets and will include all information useful to characterise them: wavelength, resolution, molecular/atomic species, photometric band, beam-size, *etc.*

However, a major goal of this work is to avoid archive duplication by making use of existing databases residing at their original site. In case of existing archives the task of the project will be to build the necessary interfaces to associate sky coverage information with each data element. The information needed to establish this data↔sky-region dependency is either available with the data themselves or can be derived knowing the instrument used to collect those data:

- In the case of image data (*i. e.* FITS files), the needed information is stored in the header of the file containing the image; this is the case for IRAS, 2MASS, MSX, ISO-CAM, *etc.*
- In the case of photometric/spectral data (the actual data collected at the telescope), the information is simply the field of view of the instrument used; this is the case for ISO, the JCMT photometer and spectral receivers, and similar data.
- In the case of data from the literature (images, spectra and tables), the needed information will have to be extracted

from the data as published or from other information in the papers.

Data concerning star formation and studies of the ISM taken prior to the era of electronic publishing are generally not digitally archived, so the project must provide a "digital home" for them. It is recognized that this is a challenging job, but it is crucial that this considerable and historically critical information be stored and made **searchable** in digital form. Contour maps will be 'digitized' and tables will be casted into ASCII format using relatively cheap off-the-shelf commercial hardware and software products (following the methods currently used by the NED project). Metadata pointers will then be built in exactly the same way as for existing digital catalogs.

3.4. Access and Interface

To be as effective as possible, the SFD must be accessible through a variety of methods. These include WWW HTML form-driven CGI programs and custom JAVA client-environment applications. All of these can be layered on top of the same basic database search and access components described above. As also mentioned earlier, the SFD will in turn rely on external archives for much of the real data and on SIMBAD for resolution of point-like object names; instead, the name resolution for extended objects will perforce be handled as part of the SFD effort.

It is expected that the bulk of the access by the research community will follow one of two primary tracks. A **"Batch" Mode** is the most efficient way for users to collect information and datasets where the parameters defining the request are known *a priori*. Here, the query will normally be constructed by filling out a Web form or, for more expert users, directly through custom HTTP POST messages or e-mail using extended SQL. An **Interactive Java-based GUI** for efficient but reasonably simple client-side interaction with the database. The use of mouse-driven events will allow to limit to a minimum the number of Web layers of the database front-end. This mode allows a wide variety of usage patterns. For instance, the user might construct an image or a contour plot overlaid on a pre-existing plot or image, a list of bibliographic references (directly linked to NASA/ADS) pertaining to the objects selected, information and data tables, plots of spectra, line fluxes and photometric data complete with essential information about instrumental parameters used, and so on.

4. A SFD PROTOTYPE

Since many of the concepts (e.g., the handling of extended sources and the building of astronomically meaningful metadata) were relatively new, we felt necessary to develop a prototype in order to bring those ideas to a certain level of maturity as early as possible in the project. The SFD prototype (Fig. 1) implements many of the building blocks described above; a demo has been given during the conference.

The contour map represents the CO(1–0) line integrated intensity from Loren (1976), while the yellow asterisks are the K-band sources identified in the pioneering study of Strom, Vrba & Strom (1976). Every contour of the original CO map has been digitised and stored in an ASCII file. The top right table is the "Layer Control Window" which controls the visualization of the different stored datasets on the plot window. The lower table summarizes information (coordinates, magnitudes, etc.) on all near-IR sources plotted.

5. PERSPECTIVES

The project is still at the beginning, but the SFD prototype already implements some of the key features. The most challenging task for the future will be to capture the scientific knowledge that will allow linking of objects to datasets, and of datasets to datasets. For a Star Formation/ISM database the extent of sky to be covered is virtually the whole 2π; clearly, priorities will have to be set starting, e.g., from the best known and representative star forming regions (Orion, Ophiuchus, portions of the Galactic plane, etc.). The scientific knowledge-base at the foundation of the SFD is not frozen once and for all but will have to be maintained, in parallel with increasing the sky coverage, as new results will become available in the literature. If the SFD, in its initial and limited sky coverage which we plan to be available in the near future will prove useful to the community, it may likely evolve into the Galactic analogue of NED as an everyday astronomical research tool.

REFERENCES

Burton W.B., Hartmann D., 1994, Ap&SS 217, 189
Devine D., Bally J., Reipurth B., Heathcote S., 1997, AJ 114, 2095
Egret D., Wenger M., Dubois P., 1991, Ap&SS Library v. 171, p. 79
Helou G.X., Madore B., 1988, ESO Proceedings #28, p. 335
Hodapp K.-W., 1994, ApJS 94, 615
Loren R.B., 1976, ApJ 209, 466
Solomon P.M., Sanders D.B., Rivolo A.R., 1985, ApJ 292, L19
Strom S.E., Vrba F.J., Strom K.M., 1976, AJ 81, 314

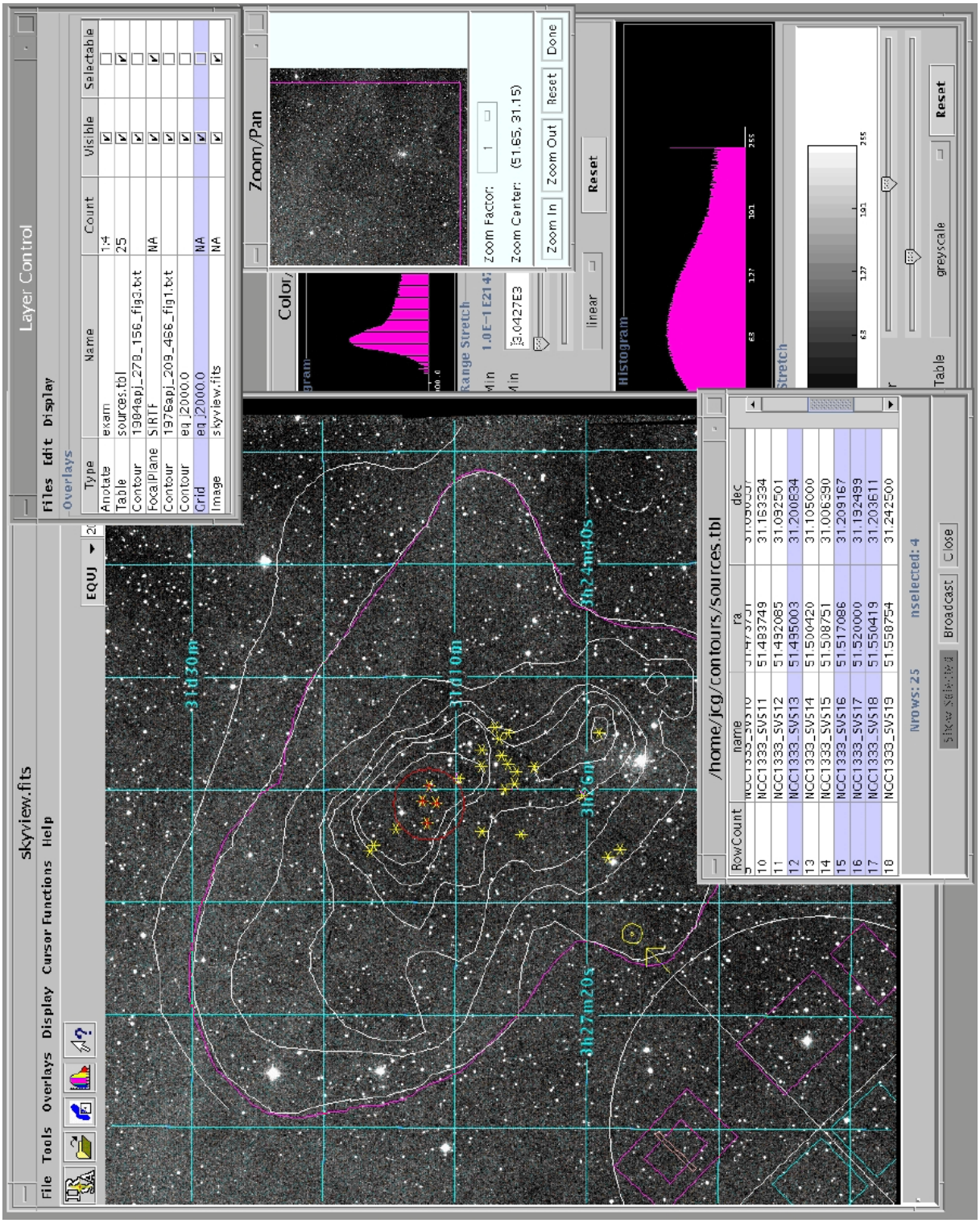

Figure 1. Screen dump from a typical SFD prototype session. The region is NGC 1333. See text for more details.

CIRCUMSTELLAR DUST AROUND MAIN-SEQUENCE STARS: WHAT CAN WE LEARN FROM THE ISOPHOT ARCHIVE?

Péter Ábrahám[1], Attila Moór[1], Csaba Kiss[1], Philippe Héraudeau[2], and Carlos del Burgo[2]

[1]Konkoly Observatory of the Hungarian Academy of Sciences, PO Box 67, H-1525 Budapest, Hungary
[2]Max-Planck-Institut für Astronomie, Königstuhl 17, D-69117 Heidelberg, Germany

ABSTRACT

Circumstellar dust around main-sequence stars, the *Vega phenomenon*, was the topic of a number of ISOPHOT key projects. The results of these projects were published in separate papers without combining their data. In this contribution we discuss the possible merit of collecting and re-analysing all normal star observations from the ISOPHOT archive, and present preliminary results extracted from a collection of minimap observations performed with the ISOPHOT C100 camera at 60μm.

Key words: Vega phenomenon - circumstellar dust - far-infrared photometry

1. INTRODUCTION

One of the main discoveries of the IRAS mission was that main-sequence stars can be accompanied by circumstellar dust disks (Vega phenomenon, Aumann et al. 1984; for reviews see Backman and Paresce 1993, Zuckerman 2001). Systematic searches in the IRAS catalogues resulted in several lists of candidate stars (Fajardo-Acosta et al. 2000, Mannings & Barlow 1998 and references therein) and come to the conclusion that 10-20% of main-sequence stars harbour dust disk (Plets & Vynckier 1999).

The sensitivity and spatial resolution of the IRAS detectors have imposed limitations on the study of the Vega phenomenon. Higher angular resolution coronagraphic observations at optical wavelengths indicated that in some cases the far-infrared excess observed by IRAS is of interstellar, rather than of circumstellar origin, leading to false entries in the Vega-candidate lists (e.g. Kalas et al. 2002). For sensitivity reasons several important questions could not be properly addressed from the IRAS data, e.g.: "Does the presence of a disk depend on the stellar age?" or "Is the incidence of disks the same in clusters and multiple systems as among single field stars?". Taking advantage of the higher sensitivity and spatial resolution of ISOPHOT (Lemke et al. 1996), the photometer onboard the Infrared Space Observatory (Kessler et al. 1996), a number of key observing programmes were devoted to the Vega phenomenon. The aims of these programmes were to obtain multi-wavelength photometry and resolved maps of the most famous Vega-type stars at far-infrared wavelengths, and also to address the questions outlined above, especially to determine the temporal evolution of the disks. The results of the different programmes, however, were published in separate papers and no attempt has been made up to now to combine all available data sets.

In this contribution we discuss the possible merit of collecting and re-analysing all normal star observations obtained with ISOPHOT (regardless of the original observer) being available in the ISO data archive. In particular, we discuss two major potential projects:

The first project is to re-process all observations according to our latest knowledge on the ISOPHOT instrument, and to compile a catalogue of Vega-candidate stars by applying identical detection criteria to all stars from all programmes. Such a study could give an independent confirmation of the number of excesses found in the original papers, and the resulting list would be an important input for the next infrared space missions. Beside the extracted fluxes we would include additional data in the catalogue which are helpful for the interpretation: spatial extent of the emitting region; sky background fluctuation, other ISO measurements, IRAS photometry, etc.

The second project comprises several statistical investigations aiming at answering the fundamental questions concerning temporal evolution of the circumstellar matter and concerning the incidence of disks in different environments. However, one has to be careful with this kind of studies: though an increase of the number of stars should improve the statistical significance of the results, one has to check the various biases and selection effects of the individual samples.

In order to demonstrate the possible potential of these projects we present some preliminary results extracted from minimap observations performed at 60μm with the ISOPHOT C100 camera.

2. OBSERVATIONS AND DATA REDUCTION

2.1. DATA BASE AND PROCESSING STEPS

Querying the ISO data archive we built up a data base containing 354 minimap observations of 198 normal stars taken with the ISOPHOT C100 camera, including 204 observations performed at 60μm. Minimaps with a raster stepsize of ΔM=ΔN=46$''$ and an odd number of raster steps M,N were selected. Thus, for each detector pixel a central pointing on the target was included. Despite different observers (most observations belong to HHABING, EBECKLIN, CWAELKEN, and PHT_CAL) the data base turned out to be rather homo-

Proceedings of the Symposium *"Exploiting the ISO Data Archive - Infrared Astronomy in the Internet Age"*, 24–27 June 2002, Sigüenza, Spain (C. Gry, S. B. Peschke, J. Matagne et al. eds., ESA SP-511)

geneous both in terms of observing time per sky position and read-out parameters. A more detailed description of the data base is given in Moór et al. (this volume).

For each star we predicted the far-infrared flux density of the photosphere from the K- (or V, when K was not available) magnitudes and from the B-V colour indices. The relations were set up from and tested on a collection of stellar model predictions produced by M. Cohen and P. Hammersley (available on the ISO Data Centre home page). The accuracy at 60 micron is estimated to be around 3% if predicted from the K-magnitudes and 8% if only V-magnitudes are available.

The data were processed in batch mode with the PHOT Interactive Analysis software V9.1 (Gabriel et al. 1997) using calibration files compatible to OLP V10. In addition we applied the new dynamic transient correction developed recently at the ISOPHOT Data Centre (see del Burgo et al, this volume).

2.2. Detection limits

From a comparison of the observed and predicted flux densities at 60μm we derived an empirical photometric correction curve. This can be used to correct – at least in an average sense – for the systematic discrepancies of the minimap photometry (for details see Moór et al., this volume). The standard deviation of the measurements around the empirical curve defines an average error bar (21 mJy at faint level and 3.1% at bright level) which is representative for the sample, although it may not be valid for each individual measurement. This flux limit can be translated to detection limits in terms of fractional luminosity τ and dust mass M_d of the Vega disks. Since there is no standard way to perform these transformations, for the present study we adopt the formulae used in Ábrahám et al. (1998):

$$\tau = \frac{(3.1e_{25} + 1.4e_{60} + 0.3e_{100}) \times 10^{-4}}{10^{[0.4(4.75 - m_V - B.C.)]}} \quad (1)$$

(from Backman and Gillett, 1987) where e_λ are the excess fluxes at different wavelengths in Janskys; and

$$M_d = \frac{e_{60} D^2}{\kappa(\nu) B_\nu(T_d)} \quad (2)$$

where D is the distance of the star, $B_\nu(T_d)$ denotes the Planck function, and κ is the dust absoption coefficient. We assumed $\kappa(\nu) \sim \nu^{+1}$ with $\kappa(850\mu m) = 1.7\,\mathrm{cm^2 g^{-1}}$. As a representative value for all disks $T = 70\,\mathrm{K}$ was adopted.

In order to estimate detection limits, e_{60} was replaced by the 3σ average error bar, e_{100} was predicted from e_{60} using the modified blackbody of Eq. 2, and e_{25} was set to zero. Figure 1 shows the 3σ thresholds as a function of distance and V-magnitude, respectively. For reference the corresponding values of the zodiacal cloud of our solar system are also marked. We note that formulae different from Eqs. 1-2 (e.g. the ones used in Habing et al. 2001) lead to somewhat different relations.

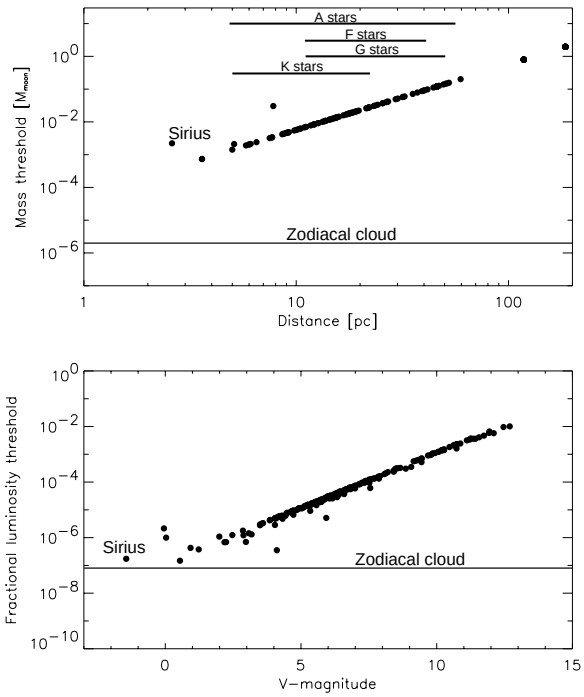

Figure 1. (a) 3σ detection threshold for disk mass as a function of distance, assuming an average 1σ flux error of 21 mJy at low flux and 3.1% at high flux at 60μm. Horizontal lines indicate the typical distance ranges for stars of different spectral types in our sample. (b) 3σ threshold for fractional luminosity as a function of V-magnitudes of the stars, based on the same average error bars as in Fig. 1a. The scatter is partly related to variations in the bolometric correction $B.C.$. Representative values of the solar system zodiacal cloud are marked in both plots.

3. A CATALOGUE OF VEGA-CANDIDATE STARS

3.1. Confirmation of previous detections

Adopting an average error bar of 21 mJy at faint level and 3.1% at bright level we counted all stars exhibiting an excess above the 3σ level at 60μm as Vega-candidate. In total 34 Vega-candidates were selected from the sample. Table 1 lists the number of detections claimed in the original papers together with the number of detections found by our data reduction. Because in general the list produced with our reduction technique contains less stars than the published lists, and we claim no new detections, our approach seems to be more conservative. Computing individual error bars for each observation, the next step in our project, will certainly change the number of candidates. Nevertheless, the fact that the final list is sensitive to details of the data analysis points to the need of a homogeneous processing of all data in order to accomplish a final consolidated list of Vega-like stars detected by ISOPHOT.

3.2. Spatial extent of the disks

Using dedicated high resolution observing modes it was possible to resolve several Vega-type disks with ISOPHOT (e.g.

Table 1. Detections of Vega-like stars published in the original ISOPHOT papers and found in our analysis

Original paper	This study
19 Vega candidates seen by IRAS	13
2 new candidates in Habing et al. (2001)	1
3 new candidates in Decin et al. (2000)	1
15 new candidates in Spangler et al. (1999)	14
14 new candidates in Spangler et al. (2001)	5

Walker & Heinrichsen 2000). Although minimaps do not belong to these modes, we tested if they contain enough information to provide an estimate for the sizes of the objects.

Since the footprint of the C100 detector is broader than the pixel size, a small fraction of the source flux is still observable on raster positions $\pm 46''$ apart. As an example Fig. 2 shows these measured fractions for the particular case of Pix. 8 and DY=46″, DZ=0″ (plus signs) as a function of the source flux. Overplotted is the fraction expected from the footprint of a true point source, and also the expected fractions if the source were extended with a FWHM=20″,30″,40″,50″.

In the case of faint sources (<1Jy) the noise is too high to make any statement. Among the bright stars the two prototype Vega stars (Vega, αPsA) are clearly extended. Assuming spherical symmetry and averaging the measurements of all pixels and all appropriate raster positions we get a FWHM of 19.8″ and 21.3″, respectively, for the extents of the two stars. For comparison, at submillimetre wavelengths Vega was measured to be 24″x21″, while αPsA has an extent of 41″x18″ (Holland et al. 1998). The edge-on disk of β Pic is 22″x11″ at submillimetre wavelengths, while only 14.5″x6.1″ at 60μm as determined from high-resolution ISOPHOT scans (Heinrichsen at el. 1999). With our method β Pic is not resolved showing the limitations of this technique.

4. STATISTICAL ANALYSES

There are a number of issues related to the Vega phenomenon which can only be studied in a statistical way:

- the distribution of disks per spectral type;
- the evolution of the disks with stellar age, and dependence of the characteristic timescale on spectral type;
- the influence of the environment (cluster, multiple system) on the incidence of the disks;
- the correlation with planets;
- the correlation with the rotational velocity of the stars;
- do very faint disks exist, and are they ubiquitous?
- ...

Before performing any of these analyses for the combined sample one has to address the issue of statistical completeness and that of different biases implied by the selection criteria of the different observers for the subsamples.

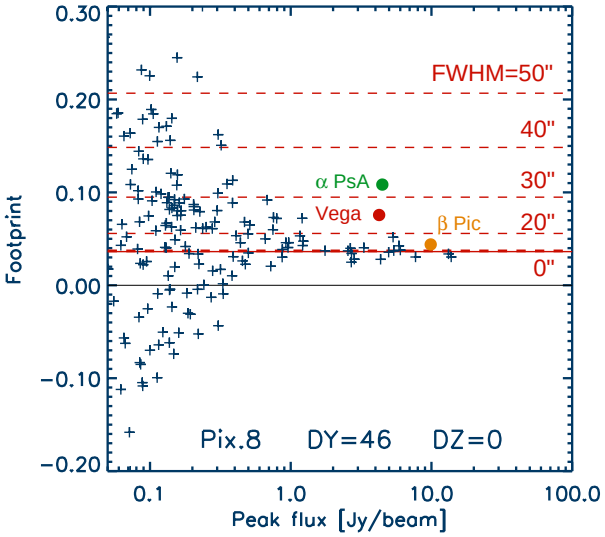

Figure 2. Measured fractions of the peak flux for Pix.8 at DY=46″, DZ=0″. Dashed lines mark the fraction expected from a theoretical beam profile convolved with a Gaussian of FWHM=20″,30″,40″,50″.

4.1. THE EXISTENCE OF VERY FAINT DISKS

The Vega-type disks discovered by IRAS were all in the range where the disk re-processes a fraction of about 10^{-5} of the star's optical and UV radiation. One could expect that even more transparent disks - more similar to the Kuiper belt of the solar system - exist too, and that they may even be ubiquitous.

Fig. 1*b* shows that this hypothesis can only be checked with ISOPHOT for the brightest stars. We computed the measured vs. predicted (photospheric) fluxes for Sirius and Altair as well as for several standard stars. The fact that no excess was observed gives 3σ upper limits of $f = 1.7 \times 10^{-7}$ and 4.3×10^{-7} for the fractional luminosities of the disks towards Sirius and Altair, respectively. Although two stars do not form a statistical sample, the resulting limits – which are not far from the value of the zodiacal cloud in our solar system – might indicate that a fraction of stars harbour only very faint disks or have no disks at all, and the observed Vega stars do not necessarily correspond to the bright tail of a broad mass distribution, but may represent a separate disk evolutionary track.

4.2. EVOLUTION OF DISK MASS WITH STELLAR AGE

Evolution of disk mass with stellar age was the central topic of two ISOPHOT papers which were based on observations made in minimap mode (Spangler et al. 2001, Habing et al. 2001). The two groups have come to so remarkably different conclusions, that the combination of all observations may be necessary to consolidate the results.

In Figure 3*a–d* we plot the disk mass, determined from the 60μm excess and expressed in Moon masses, versus the age of the stars. Unlike in the original papers, we divided the stars according to their spectral types of A, F, G, and K, respectively.

The following remarks on the plots indicate which kind of issues have to be taken into consideration in a future analysis of the complete sample (which will include significantly more data than the C100 minimap data base presented in this paper):

– since the main-sequence lifetime of a star depends on the spectral type, the early part of the evolutionary trend proposed by Spangler et al. (2001, dashed line) is defined more by A-type stars while the old part is based more on low-mass stars (although F- and G-stars provide overlap). Thus, the physical significance of the trend is based on the assumption of a universal, stellar mass-independent disk evolutionary timescale;
– a comparison of the evolutionary trend with the detection limit indicates that for A-type stars the sample becomes incomplete already at about 5×10^8 yrs, which has to be taken into account e.g. in the kind of cumulative analyses performed by Habing et al. (2001);
– The upper limit for Sirius and the zodiacal cloud are significantly below the main trend, indicating that some stars loose their disks faster than suggested by the trend, or do not develop one at all.

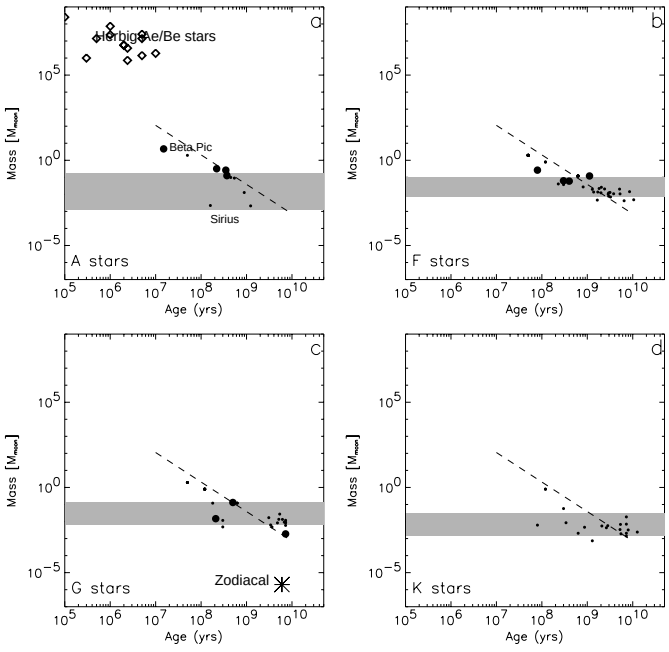

Figure 3. Disk mass, determined from the 60μm excess versus the age of the stars. The stars are divided according to their spectral types. Big dots: detected Vega-type disks; small dots: upper limits. The detection limits depend on the distances of the stars, and within our sample are the lowest for K-dwarfs (see Fig. 1a). Shaded strips mark the representative range of detection limit values for each spectral class.

ACKNOWLEDGEMENTS

This research was partly supported by the ESA PRODEX programme (No. 14594/00/NL/SFe) and by the Hungarian Research Fund (OTKA No. T037508). P.Á. acknowledges the support of the Bolyai Fellowship.

REFERENCES

Ábrahám, P., Leinert, Ch., Burkert, A., Lemke, D., Henning, Th., 1998, A&A 338, 91-96

Aumann H.H., Gillett F.C., Beichman C.A., de Jong T., Houck J.R., Low F.J., Neugebauer G., Walker R.G., Wesselius P.R., 1984, ApJ 278, L23

Backman, D.E., Gillett, F.C. 1987, in Cool stars, stellar systems, and the Sun (eds.: Linsky, J.L., Stencel, R.E), 340

Backman D.E., Paresce F., 1993, in *Protostars and Planets III* (Eds.: Levy E.H., Lunine J.I.), 1253

Decin G., Dominik C., Malfait K., Mayor M., Waelkens Ch., 2000, A&A 357, 533

Fajardo-Acosta S.B., Beichman C.A., Cutri R.M., 2000, ApJ 538, L155

Gabriel C. et al, 1997, in Proc. of the ADASS VI conference (Eds.: G. Hunt, H.E. Payne, ASP Conf.Ser. 125), 108

Habing H.J., Dominik C., Jourdain de Muizon M., Laureijs R.J., Kessler M.F., Leech, K., Metcalfe, L., Salama, A., Siebenmorgen, R., Trams N., Bouchet P., 2001, A&A 365, 545

Heinrichsen, I., Walker, H.J., Klaas, U., Sylvester, R.J., Lemke, D., 1999, MNRAS 304, 589

Holland W.S., Greaves J.S., Zuckerman B., Webb R.A., McCarthy C., Coulson I.M., Walther D.M., Dent W.R.F., Gear W.K., Robson I., 1998, Nature 392, 788

Kalas P., Graham J.R., Beckwith S.V.W., Fewitt D.C., Lloyd J.P., 2002, ApJ 567, 999

Kessler M.F. et al., 1996, A&A 315, L27

Lemke D. et al., 1996, A&A 315, L64

Mannings V., Barlow M.J., 1998, ApJ 497, 330

Plets H., Vynckier C., 1999, A&A 343, 496

Spangler C., Silverstone M.D., Becklin E.E., Hare J., Zuckerman B., Sargent A., Goldreich P., 1999, Proc. of "The Universe as seen by ISO" (Eds. P. Cox and M.F. Kessler), ESA SP-427, 405

Spangler C., Sargent A.I., Silverstone M.D., Becklin E.E., Zuckerman B., 2001, ApJ 555, 932

Walker H.J., Heinrichsen I., 2000, Icarus 143, 147

Zuckerman B., 2001, ARAA 39, 549

FOLLOW-UP STUDIES OF VERY YOUNG INTERMEDIATE AND HIGH MASS STAR FORMING REGIONS DETECTED BY THE ISOPHOT SERENDIPITY SURVEY

Oliver Krause[1], L. Victor Tóth[1,2], Roland Vavrek[1], Manfred Stickel[1], and Dietrich Lemke[1]

[1]Max-Planck-Institut für Astronomie, Königstuhl 17, D-69117 Heidelberg, Germany
[2]Department of Astronomy, Loránd Eötvös University, Pázmány Péter sétány 1/a, H-1117 Budapest, Hungary

ABSTRACT

We report results from our search for very young high-mass star forming regions using the 170 μm ISOPHOT Serendipity Survey. A total sky coverage of 15 % makes this survey of the ISO satellite the largest one ever performed in the unexplored FIR beyond the IRAS 100 μm band. It is particularly sensitive to cold dust condensations with a dust temperature below 18 K. The cold and luminous FIR emitters of our sample were identified by a cross-correlation of cold sources in the ISOSS database coinciding with infrared sources detected by the 2MASS, MSX and IRAS surveys. The low temperature and large mass of the cold circumstellar matter in these objects, which has not yet been dispersed, indicates a recent begin of star formation. In order to explore the early evolutionary stage of these objects, we have initiated follow-up campaigns at (sub)mm (SCUBA, MAMBO), infrared (MAX, TIMMI2) and radio wavelengths (Effelsberg 100m–telescope). While ISOPHOT allowed us to measure the peak of thermal dust emission, the combination with ground based mm-continuum measurements of high spatial resolution is essential for investigating the morphology of the dust component. Optical and infrared observations were targeted on embedded (proto)stellar sources, ammonia observations were performed in order to probe the dense gas. Our approach of multi wavelength characterization is demonstrated in detail for the newly discovered object ISOSS J 20298+3559. The observations revealed the presence of a molecular cloud complex with a total mass of 760 $M_\odot$ and an average dust temperature as low as 16 K. Several massive cold cores without infrared counterparts have been found in coexistence with a luminous Herbig B2 star, which is the most evolved object in that complex. Spectroscopic signatures for ongoing mass infall towards the Herbig star give further evidence for the young age of the system.

Key words: stars: formation – ISM: clouds – dust – Instruments: ISO – ISOPHOT

1. INTRODUCTION

It is a challenge to identify massive young stellar objects during their early evolution. The youngest protostars form deeply embedded in their cold (T $\sim$ 10-20 K) parental clouds. The association with dense ambient material makes such objects best detectable as cold condensations at far-infrared and (sub)millimeter wavelengths. The short evolutionary timescales (Palla & Stahler 1993) and low spatial density of massive objects require large scale surveys for their identification. Many of the known intermediate- and high-mass protostellar candidates have therefore been discovered by follow-up studies towards IRAS sources (eg. Shepherd et al. 2000, Cesaroni et al. 1997, Molinari et al. 1998, Beuther et al. 2002), which were selected on the basis of color and flux density criteria.

A number of studies of high-mass star forming regions probe the surroundings of ultra-compact HII regions (UCHII). Due to the fast early stellar evolution of massive stars, usually there is little trace left of the initial conditions in the parental molecular cloud. Our goal is to detect and study the status before the onset of the UCHII phase. Among the most promising candidates at present are the mid-infrared dark clouds found by the MSX mission (Carey et al. 1998). Their detection is however limited to rather nearby objects on a bright galactic background.

2. SEARCH STRATEGY

The earliest stages of massive star formation are characterized by the initial conditions of their parental cloud cores with spectral energy distributions peaking beyond 100 μm (Evans et al. 2002). In order to unveil such young objects we are using the ISOPHOT (Lemke et al. 1996) 170 μm Serendipity Survey (ISOSS) (Bogun et al. 1996), which is the largest high spatial resolution survey performed beyond the IRAS 100 μm band. In order to identify young massive star forming regions in this early evolutionary phase we selected candidate regions by the following criteria:

- Bright ($F_{170\mu m} \sim$ 100 Jy) and compact (diameter $<$ 2.5 arcmin) sources detected by ISOSS and IRAS with a flux ratio $F_{170\mu m}/F_{100\mu m} > 2$, implying a low dust temperature T $<$ 18 K and a large mass of the cold ISM in these objects.
- No associated mid-infrared point source with colors typical of UCHII regions (Wood & Churchwell 1989) and no coincident radio continuum source (RMS noise $\sim$ 0.45 mJy beam^{-1} at 1.4 GHz) from the NVSS survey (Condon et al. 1998)
- Detection in ^{12}CO or ^{13}CO (Yang et al. 2002, Wouterloot & Brand 1989, Lee et al. 2001).

The sources have kinematic distances of 2 to 14 kpc, masses of $5\cdot 10^2$ - 10^4 $M_\odot$ and bolometric luminosities of 10^3 - $3\cdot 10^4$ $L_\odot$

Proceedings of the Symposium *"Exploiting the ISO Data Archive - Infrared Astronomy in the Internet Age"*, 24–27 June 2002, Sigüenza, Spain (C. Gry, S. B. Peschke, J. Matagne et al. eds., ESA SP-511)

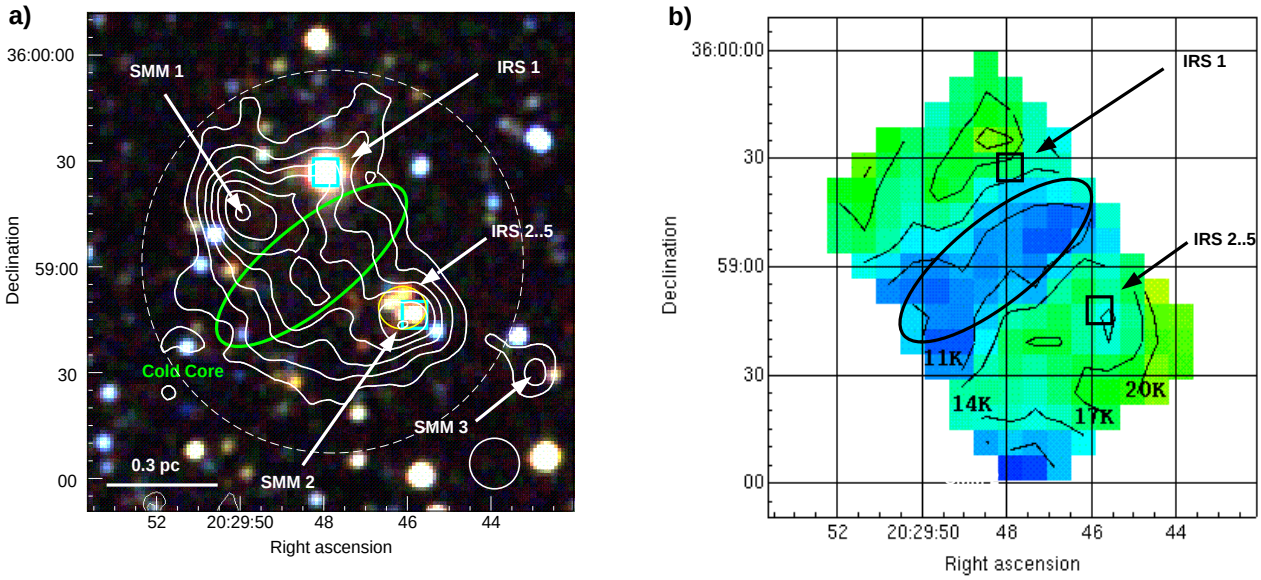

Figure 1. JHK$_S$-composite of the source ISOSS J 20298+3559, constructed from 2MASS data. Contours of the 850 μm continuum are overlaid. Three compact dust condensations (SMM1, SMM2 and SMM3) are detected, which are located in a diffuse extended emission. Mid-infrared sources detected by the MSX-satellite are marked with boxes. The submillimeter knot SMM2 is associated with a small cluster of embedded NIR sources (IRS2..5) as detected by the 2MASS and MSX surveys. IRS1 was identified as a very young Herbig B2 star by our follow-up spectroscopy. The two compact submillimeter sources SMM1 & SMM3 without any infrared counterparts are candidate Class 0 objects. The very cold cloud core is indicated by a green ellipse. The size of the SCUBA beam is indicated in the lower right, the dashed circle corresponds to the ISOPHOT beam. b) The SCUBA based dust color temperature distribution across FIR1 shows the presence of a very cold ($T_d \sim 11$ K) core at the center of the cloud. The temperature profiles towards north-east and south-west indicate an external heating by the infrared sources IRS1-5. The temperature is calculated from the submillimeter spectral index between 450 μm and 850 μm, assuming a dust emissivity β=2.

3. FOLLOW-UP OBSERVATIONS

Ground-based 450 μm, 850 μm and 1.2mm continuum observations with high spatial resolution have been obtained with the SCUBA bolometer array (Figs. 1+2a) at the JCMT on Mauna Kea, Hawaii, and MAMBO at the IRAM 30m telescope on Pico Veleta, Spain. Our ISOPHOT data point near the peak of the thermal dust emission in combination with the proper sampling of the Rayleigh- Jeans part from the SCUBA/MAMBO observations allow a precise color temperature determination of the involved dust components (Fig. 1b) It is important to approve the low cloud temperatures from the dust continuum by observing lines which reflect the physical conditions of the gas phase ISM. NH_3 is a very useful indicator of molecular cloud temperatures and column densities (e.g., Walmsley & Ungerechts 1983). We therefore started to map the clouds in NH_3 inversion lines in order to uncover the dense gas distribution in the targets. Our recent Effelsberg-100m measurements of 2 regions in the NH_3 (1,1), (2,2), (3,3) and (4,4) lines allowed us to conclude on the gas temperatures. We have detected (1,1), (2,2), (3,3) lines with high S/N in several positions of the objects (Fig. 2b).

4. RESULTS

Our follow-up observations confirmed the presence of cold and massive molecular cloud cores (Tab. 1). The dust temperatures are consistent with the gas temperatures derived from our ammonia measurements.

Table 1. Properties of dense gas and dust

Object ISOSS...	T_{dust} [K]	T_{gas}	Mass [$M_\odot$]	Column density [10^{22} cm^{-2}]
04225+5151	16	18	140	2
20298+3559	17	16	4700	15

ISOSS20298+3559-SMM1 and -SMM3 are two candidate Class 0 objects of intermediate mass. The region is associated with an optical dark cloud complex in the Cygnus X giant molecular cloud. The externally heated cloud core with a mass of 50 $M_\odot$ is gravitationally bound and good candidate for a massive pre-protostellar core. Several very young embedded objects have been detected in ISOSS20298+3559, the most luminous one is the Herbig B2e star IRS1 ($M_\star = 6.5 M_\odot$) with a luminosity of 2200 $L_\odot$ and age of less than 40000 years as inferred from evolutionary tracks (Krause et al. 2002).

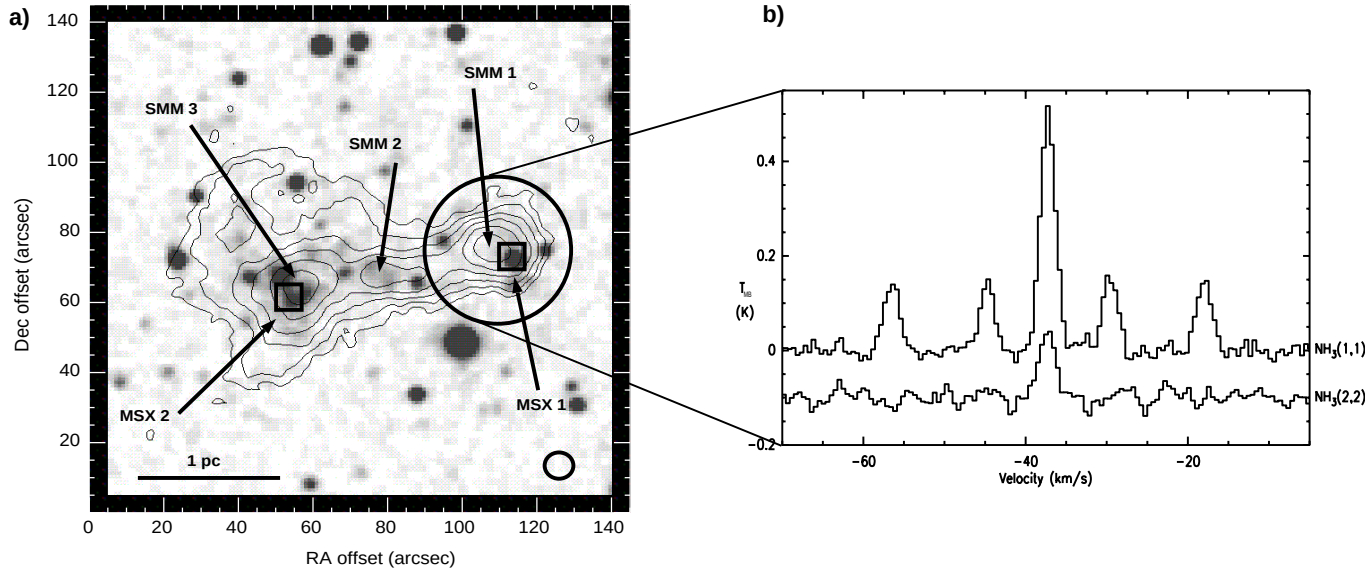

Figure 2. 450 μm continuum map of the cold ($T_d \sim 16$ K) and massive ISO cloud ISOSS 04225+5151, overlaid on a near-infrared K_S-band image from 2MASS. Three compact dust condensations (SMM1, SMM2 and SMM3) are detected, which are located in a diffuse extended emission. Mid-infrared sources detected by the MSX-satellite are marked with boxes. While SMM3 is associated with a warm near- and mid-infrared source, SMM1 is a good candidate for a massive core in the region. The mass of the region determined from our 170 μm, 450 μm and 850 μm photometry is $M(_{H_2}) \sim 4700\ M_\odot$. Recent ammonia spectra obtained with the Effelsberg 100m-telescope confirmed a gas temperature of 16 K towards the core SMM1, while the NH_3(3,3) and NH_3(4,4) emission is weak (T_{MB}(3,3) $\sim$ 40 mK, T_{MB}(4,4) $<$ 35 mK).

5. OUTLOOK

Our follow-up observations gave evidence for the low age of star forming regions with red FIR colors ($F_{170\mu m}/F_{100\mu m} > 2$) detected by the ISOPHOT Serendipity Survey. All objects so far have been selected to contain near- and mid-infrared sources being signposts for ongoing clustered star formation. We plan to extend our sample of cold ISOSS sources without evidence for stellar counterparts but only coinciding with molecular clumps detected by ^{12}CO, ^{13}CO and CS line surveys. These objects are expected to be further candidates for studies of the earliest stages of massive star formation.

ACKNOWLEDGEMENTS

The ISOPHOT Data Center at MPIA is supported by Deutsches Zentrum für Luft- und Raumfahrt e.V. (DLR) with funds of Bundesministerium für Bildung und Forschung, grant No. 50QI0201. OK thanks the Wernher von Braun-Stiftung zur Förderung der Weltraumwissenschaften e.V. for financial support. This study made use of the SIMBAD database operated at CDS, Strasbourg, France. HIRES images were provided by the Infrared Processing and Analysis Center. This publication makes use of data products from the Two Micron All Sky Survey, which is a joint project of the University of Massachusetts and the Infrared Processing and Analysis Center/California Institute of Technology, funded by the National Aeronautics and Space Administration and the National Science Foundation.

REFERENCES

Beuther, H., Walsh, A., Schilke, P. et al., 2002, A&A 390, 289
Bogun, S., Lemke, D., Klaas, U. et al., 1996, A&A 315, L71
Carey, S., Clark, F., Egan, M., 1998, ApJ 508, 721
Cesaroni, R., Felli, M., Testi, L., 1997, A&A 325, 725
Condon, J., Cotton, W., Greisen, E. et al., 1998, AJ 115, 1693
Evans , N. J. Shirley, Y.L., Mueller, K.E. et al, 2002, in Proc."Hot Star Workshop III: The earliest phases of massive star birth, ed. P.A. Crowther, ASP Conference Series
Krause O., Lemke, D., Tóth, L.V. et al., 2002, A&A in press
Lee, Y., Stark, A., Kim, H. et al., 2001, ApJS 136, 137
Lemke, D., Klaas, U., Abolins, J., 1996, A&A 315, L64
Molinari, S., Testi, L., Brand, J., et al., 1998, ApJ 505, L39
Palla, F. & Stahler, S., 1993, ApJ 418, 414
Shepherd, D. S., Yu, K. C., Bally, J. et al, 2000, ApJ 535, 833
Walmsley, C. M. & Ungerechts, H., 1983, A&A, 122.164.
Wood, D.O.S., Churchwell, E., 1989, ApJ 340, 265
Wouterloot, J. G. A., Brand, J., 1989, A&AS 80, 149
Yang, J., Jiang, Z., Wang, M. et al., 2002, ApJS 141 ,157

THE COMPLETE FAR INFRARED SPECTROSCOPIC SURVEY OF HERBIG AEBE STARS OBTAINED BY ISO-LWS

Dario Lorenzetti[1], Teresa Giannini[1], Brunella Nisini[1], Milena Benedettini[2], Davide Elia[3], Loretta Campeggio[3], and Francesco Strafella[3]

[1]INAF - Osservatorio Astronomico di Roma, via Frascati 33, I-00040 Monte Porzio, Italy
[2]Istituto di Fisica Spazio Interplanetario - CNR Area Ricerca Tor Vergata, via Fosso del Cavaliere, I-00133 Roma, Italy
[3]Università degli Studi di Lecce - Dipartimento di Fisica, via Arnesano, I-73100 Lecce, Italy

ABSTRACT

The ISO-LWS archive has been systematically searched in order to obtain a complete far IR spectrophotometric survey of Herbig AeBe (HAEBE) stars. The investigated sample is constituted by 15 objects which, together with the 11 HAEBE we have published in two previous papers, represents about 25% of all the known HAEBE. The [OI] 63 μm and the [CII] 158 μm lines are observed in many of the investigated sources, while the [OI] 145 μm remains often undetected, due to its relative faintness. Molecular lines, in form of CO high-J rotational transitions are detected in only three cases and appear associated to local density peaks. A new class of ISO-LWS spectra of HAEBE emerges, constituted by objects without any detected gas feature either in emission or in absorption. Not unexpectedly, these HAEBE are isolated from molecular clouds and, as such, lack of the cold circumstellar material probed by far IR ionic and molecular transitions. By comparing line intensity ratios with model predictions we find that photodissociation caused by the stellar photons and active in a clumpy medium is likely the prevalent excitation mechanism for the far IR lines. Finally, an evolutionary trend is found according to which the contribution of the far IR line emission to the total emitted energy is less and less important with time.

Key words: circumstellar matter – pre-main sequence – Infrared lines – ISO

1. INTRODUCTION

A significant fraction of the HAEBE's emitted power is released in the far IR range that is inaccessible from the ground (i.e. 45 – 200 μm) and that contains many emission lines which are unique tracers of the circumstellar gas physical conditions. The first spectrophotometric survey of HAEBE stars in this range has been obtained thanks to the ISO Long Wavelength Spectrometer (LWS) observations (Lorenzetti et al. 1999; Giannini et al. 1999; Papers I and II, respectively).

Our aim is to complete and extend our previous analysis to all the far IR spectra of HAEBE stars through an unbiased search from the ISO archive, in order to derive the far IR behaviour of HAEBE as a class. It is worthwhile noting that the same spectral range will be investigated at a much higher spectral ($\mathcal{R} \simeq 10^7$) and spatial ($\sim 9''$) resolution with the instruments on board Herschel (Pilbratt, 2001), hence the results of this spectroscopic survey can be considered as a useful database for planning future far IR observations.

Table 1. Parameters of the investigated HAEBE.

Source	Spectral Type	$L_{\rm bol}$ ($L_\odot$)	$A_{\rm V}$ (mag)	Dist. (pc)
AB Aur	B9-A0	48	0.50	140
MWC 480	A2/3	32	0.25	131
HD 34282	A0V	4.8	0.59	160
MWC 758	A3	22	0.22	200
CQ Tau	A8-F2	8	0.9	140
MWC 137	B0	2.8 10^4	4.5	900
He 3-672	B9V	32	0.28	103
He 3-741	A4	35	0.31	116
HD 141569	A0V	32	0.47	99
HD 142666	A8V	10.7	0.71	116
He 3-1141	A7V-F0	> 30	0.56	> 200
TY CrA	B9	98	1.5	140
BD+40°4124	B2V	3 10^3	3.0	1000
MWC 361	B2/3V	8 10^3	1.92	430
LkHα233	A7	100-150	2.6	800

2. SELECTED SAMPLE AND OBSERVATIONS

We have searched the ISO Data Archive ($http://www.iso.vilspa.esa.es/ida/index\_us.html$) for LWS grating spectra of the objects listed in the most complete HAEBE stars compilation available to date (Thé et al. 1994, their Table 1). The archive search was simply made by centering a circular box on the HAEBE coordinates, whose size is the same of the LWS field of view ($80''$). We have found LWS spectra of 26 HAEBE out of the 108 catalogued objects. In Papers I and II we have presented the LWS data of 11 HAEBE along with two spectroscopic far IR maps (NGC 7129 and MWC 1080): these observations constituted part of the ISO guaranteed time program. In the following we present LWS observations of the remaining 15 objects which belonged to different proposals. Including these objects allows to more than double the so far available sample, thus achieving a significant coverage ($\sim 25\%$) of all the known HAEBE stars. The 15 new objects are listed in Table 1: the astrophysical parameters (distance, luminosity, $A_{\rm V}$, etc.) have been taken by both Hipparcos (van den Ancker et al. 1998) and literature data.

Proceedings of the Symposium *"Exploiting the ISO Data Archive - Infrared Astronomy in the Internet Age"*, 24–27 June 2002, Sigüenza, Spain (C. Gry, S. B. Peschke, J. Matagne et al. eds., ESA SP-511)

The observations were carried out with the Long Wavelength Spectrometer (LWS: Clegg et al. 1996; Swinyard et al. 1996) on board the Infrared Space Observatory (ISO: Kessler et al. 1996) in full grating scan mode (LWS01 AOT). This configuration provides coverage of the 43−196.7 μm range at a resolution $\mathcal{R} \sim 200$, with an instrumental beam size of $\sim 80''$. All the details about the data reduction can be found in Papers I/II.

3. RESULTS

Figs. 1 and 2 show the portions of the continuum subtracted spectra where the [OI] 63μm and the [CII] 158μm lines with S/N ratio ≥ 3 have been detected.

The emission spectra are dominated by the presence of fine structure lines of both [OI] and [CII]. Molecular emission, in form of high-J CO rotational transitions, occurs in those cases where the column density ($A_{\rm V}$) is relatively large. Indeed the decreasing prevalence of molecular in favour of atomic line emission is a well recognized evolutionary trend, as already pointed out by Nisini et al. (2002), which is evident in going from the earliest phases of the protostellar evolution (Class 0 objects) toward Pre-Main Sequence stars (Class I/II objects).

The spectroscopic data indicate that a sub-class of HAEBE stars exists constituted by objects which show either no far IR emission line (MWC 480, HD 141569 and He 3-1141) or only small [CII] contributions marginally above the ubiquitous interstellar value (HD 34282, MWC 758, CQ Tau and HD 142666). The above mentioned HAEBE have an A-spectral type and an $A_{\rm V}$ value less than unity, conditions which both inhibit the excitation of the cold circumstellar material by stellar photons. Basically these objects are the least luminous ones among our sample, having all $L_{bol} \approx 30$ $L_{\odot}$ (see Table 1). From an observational point of view this limit represents an important prescription for selecting targets of future space missions.

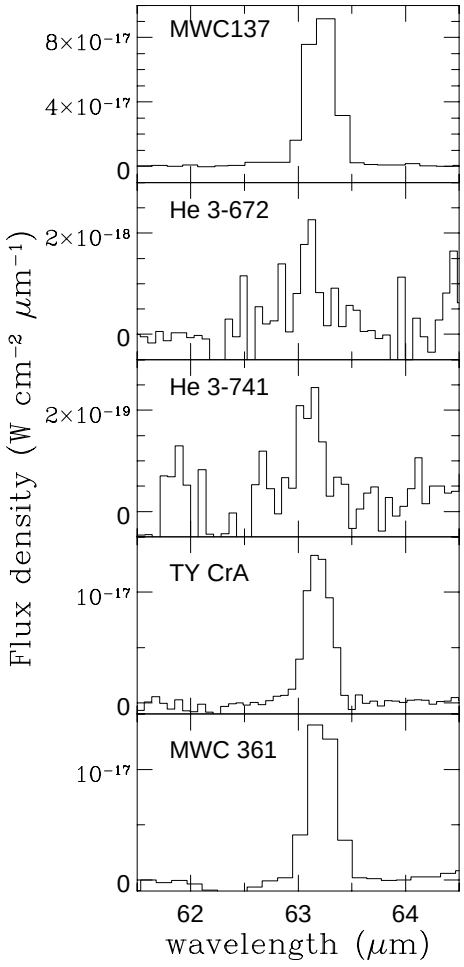

Figure 1. Continuum subtracted LWS spectra of the investigated HAEBE stars: selected ranges containing the [OI] 63μm line. Lines already presented in the previous literature are not re-depicted here.

4. DISCUSSION

4.1. [OI] AND [CII] LINES

The [OI] 63, 145 μm and [CII] 158 μm are the strongest features observed and have been used in Paper I as a diagnostic of the excitation mechanism and then of the physical conditions. Here we intend to follow the same method, namely to check whether or not the HAEBE of the present sample behave as the objects considered in Paper I. Line ratios and corresponding errors of the stars presented here are indicated in Fig. 3, where those already presented in Paper I are also reported for completeness but without any flag.

The observed line intensity ratios are superimposed in Fig. 3 on a grid of photodissociation models (Kaufman et al. 1999). The location of the data points, although in two cases (identified by the letters c and e) not perfectly coincident with the model grid, gives further support to our previous interpretation in favour of photodissociation as dominating mechanism for far IR line excitation. Our hypothesis about the existence, around the HAEBE stars, of a PDR originated by stellar rather than interstellar FUV photons has received further support by the correlation between [CII] 158 μm luminosity vs. the bolometric luminosity of the central source shown in Fig. 5 of Paper I. With reference to that plot, we note that the values ($L_{\rm bol}$, $L_{\rm [CII]}$) of the new sources investigated here are perfectly aligned along the already presented relationship.

Alternative models do not seem so much promising: J-shock models (e.g. Hollenbach & McKee 1989) can be ruled out, since they predict substantially different line ratios whose intersection with our PDR plane is indicated in Fig. 3 as the hatched area at the top right corner. Since a considerable fraction of the HAEBE is expected to drive molecular outflows, the role of non dissociative C-shocks (e.g. Draine et al. 1983) has been discussed in more detail in Paper I, where we conclude that possible contributions of C-shocks to the far IR emission lines cannot be ruled out, but such mechanism can be considered as

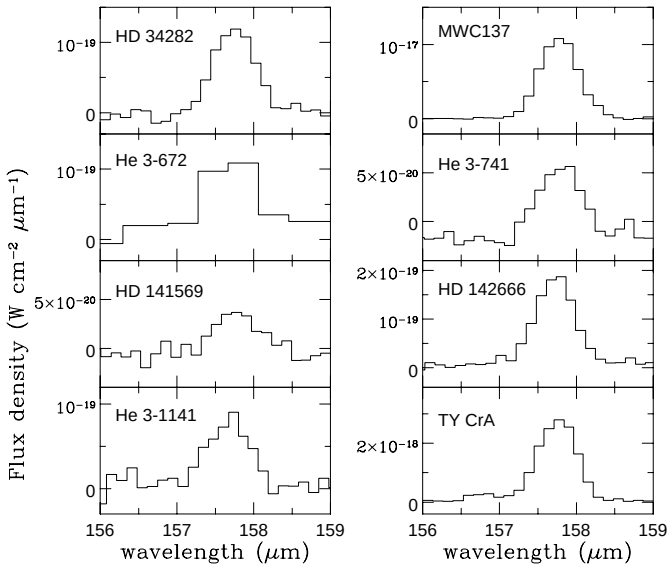

Figure 2. As in Fig. 1 for the [CII] 158μm line. The spectrum of He 3-672 has been re-binned at a lower resolution in order to increase the signal to noise ratio.

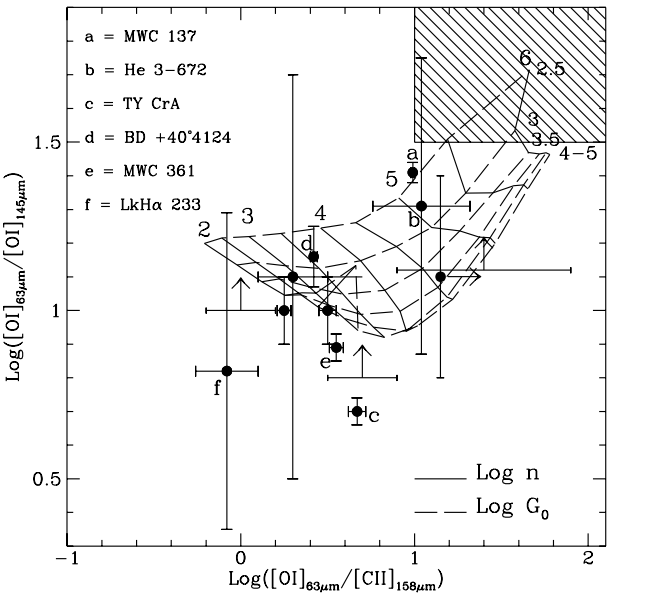

Figure 3. Observed line ratios superimposed to PDR models by Kaufman et al. (1999). The hatched area identifies the locus pertaining to the J-shock model predictions.

the main responsible for the gas excitation just in a narrow region of the parameter space (shock speed, magnetic field, pre-shock density).

4.2. Molecular emission

Out of the 15 considered HAEBE, we found molecular emission in form of CO rotational transitions in three objects: TY CrA, BD+40°4124 and MWC 361; hence the detection rate of molecular emission estimated on the overall sample is about 25 % (6 out of 26 objects). Although molecular lines are usually weak (see Table 3 and Paper II), we do not believe the lack of detection in other sources is due only to an instrumental sensitivity limit, but it is also related to an intrinsic property of the circumstellar environment, namely the existence or not of some compact density peaks near the source where the column density is expected to substantially increase. This occurrence has been already discussed in Paper II and our aim is to check this point on the three objects considered here.

To do that we have calculated the CO luminosity starting from the detected rotational lines (Paper II), then we have plotted $L_{\rm CO}/L_{\rm [OI]145}$ vs. $L_{\rm CO}/L_{\rm [CII]}$ in Fig. 4 along with the clumpy PDR model predictions by Burton et al. (1990). This plot offers the advantage of providing a diagnostic of the physical conditions by means of both atomic and molecular line emission; moreover it uses transitions not affected (as the [OI] 63 μm) by possible self-absorption problems. In Fig. 4 all the HAEBE showing molecular emission are depicted, although three of them (R CrA, IRAS 12496 and LkHα 234) were discussed in Paper II. The newly considered objects (TY CrA, BD+40°4124 and MWC 361) trace densities of the order of 10^6 cm^{-3} or less and G_o between 10^3 and 10^4, confirming the association between molecular emission and high density condensations. If molecular emission originates close to density peaks it could be associated, rather than to the HAEBE itself, to a nearby and more embedded companion of the kind that has sometimes been discovered in HAEBE neighbourhoods (e.g. Font et al. 2001).

Apart from photodissociation, a deeper discussion on the remaining alternatives is done in Paper II. Here we remember that molecular emission can also occur in C- or J-shocks. However, J-shocks at low values of the pre-shock density ($n_0 \simeq 10^4$ cm^{-3}) predict $L_{\rm [OI]}/L_{\rm CO} >> 1$, while we have for TY CrA, BD+40°4124 and MWC 361 quite low values for the $L_{\rm [OI]}/L_{\rm CO}$ ratio (0.7, 0.2, 0.3, respectively). According to both C-shocks and J-shocks at high values of the pre-shock density ($n_0 \simeq 10^6$ cm^{-3}), water should be the main coolant with a predicted cooling ratio $L_{\rm H_2O}/L_{\rm CO} \sim 10$, clearly in contrast with the absence of water emission in all the 26 HAEBE. In conclusion, the combined diagnostic provided by fine structure and molecular line emission tends to favour the photodissociation mechanism possibly operating in a clumpy medium.

4.3. An evolutionary trend

Since our complete ISO-LWS sample (26 HAEBE out of 108) can be considered representative enough of the entire class, we have tried to derive some general trend to be compared with similar behaviours from classes of younger objects. We have computed the far IR luminosity ($L_{\rm FIR}$) as due to all line emission contributions (fine structure line emission and total molec-

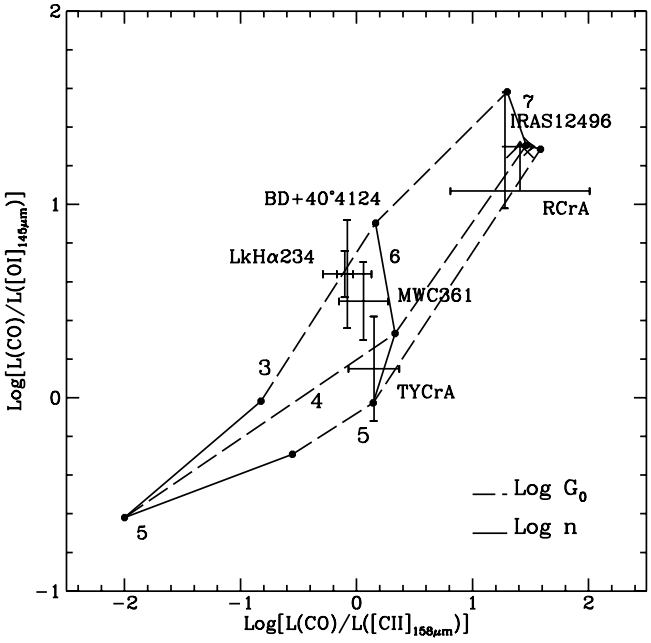

Figure 4. Observed ratios between molecular CO lines and fine structure [OI] 145 μm and [CII] 158 μm superimposed on clumpy PDR models.

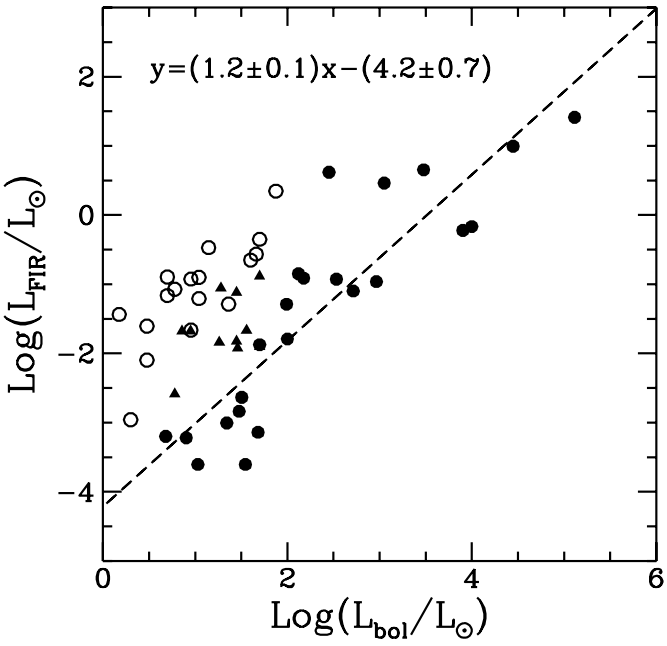

Figure 5. Far IR lines luminosity vs. bolometric luminosity of the central star.

ular cooling). In Fig. 5 these values are plotted as a function of the bolometric luminosity of the central object; the straight line, whose equation is given in the upper part of the Figure, represents the best linear fit to the points. A similar plot for the younger Class 0 objects (Nisini et al. 2002, here depicted as open circles) indicates $L_{\rm FIR} \simeq 10^{-2}$ as the intercept value. An intermediate value of 10^{-3} is attributable to the Class I objects (triangles), which are expected to be somehow younger than HAEBE and approaching to their evolutionary stage. It is worthwhile noting how $L_{\rm FIR}$ is a decreasing fraction of $L_{\rm bol}$ while the evolution goes on, although the different phases obey to different physical mechanisms. The conversion of the bolometric luminosity of the central object into far IR line cooling in the circumstellar envelope occurs at progressively lesser efficiency while time elapses.

REFERENCES

Burton M.G., Hollenbach D.J., & Tielens A.G.G.M. 1990 ApJ 365, 620

Clegg P.E., Ade P.A.R., & Armand C. 1996 A&A 315, L38

Draine B.T., Roberge W.G., & Dalgarno A. 1983 ApJ 264, 485

Font A.S., Mitchell G.F., & Sandell G. 2001 ApJ 555, 950

Giannini T., Lorenzetti D., Tommasi E., et al. 1999, A&A 346, 617 (Paper II)

Hollenbach D., & McKee C.F. 1989 ApJ 342, 306

Kaufman M.J., Wolfire M.G., Hollenbach D.J., & Luhman M.L, 1999 ApJ 527, 795

Kessler M., Steinz J.A., & Anderegg M.E. 1996 A&A 315, L27

Lorenzetti D., Tommasi E., Giannini T., et al. 1999 A&A 346, 604 (Paper I)

Nisini B., Giannini T., & Lorenzetti D. 2002 ApJ, in press

Pilbratt G.L. 2001 in: *The promise of the Herschel Space Observatory* - ESA-SP 460, Eds. G.L.Pilbratt, J.Cernicharo, A.M.Heras, T.Prusti, R.Harris, p.13

Swinyard B.M., Clegg P.E., Ade P.A.R. et al. 1996 A&A 315, L43

Thé P.S., de Winter D., & Pérez M.R. 1994 A&AS 104, 315

van den Ancker M.E., de Winter D., & Tjin A Djie, H.R.E. 1998 A&A 300, 145

FEATURES OF OXIDE DUST PARTICLES IN CIRCUMSTELLAR SHELLS OF AGB STARS

Thomas Posch[1], Franz Kerschbaum[1], Harald Mutschke[2], Dirk Fabian[2], Dominik Clément[2], and Johann Dorschner[2]

[1] Institut für Astronomie, Türkenschanzstraße 17, A-1180 Wien, Austria
[2] Astrophysikalisches Institut, Schillergässchen 2-3, D-07745 Jena, Germany

ABSTRACT

We give an overview of the dust emission features that oxide dust particles which are expected to form in circumstellar shells of AGB stars can produce. The dust species considered here are titanium oxides, Ca-Al-oxides, Mg-Al-oxides, Mg-Fe-oxides and amorphous alumina. At least for the presence of the latter three classes of solids, clear observational evidence exists. Some of those stars which form Mg-Al-oxide and Mg-Fe-oxide dust do not show any or do show very little amorphous silicate emission. This raises the question whether there exists a class of low-mass-loss dust shells dominated by oxides and not by silicates.

Key words: stars: circumstellar matter – stars: formation – stars: AGB and post-AGB – methods: laboratory

1. INTRODUCTION

According to ISO-SWS observations, oxygen-rich Asymptotic Giant Branch (AGB) stars with low mass-loss rates show a number of emission bands which can be attributed to minute solid oxide dust particles:

(1) The 13 μm feature (see Posch et al. 1999) usually occurs together with two additional emission bands observable in the spectra of oxygen-rich dust shells at wavelengths of 16.8 and 31.8 μm. All three bands can be assigned to resonance vibrations of $MgAl_2O_4$ (spinel) particles (Fabian et al. 2001).

(2) Many of the sources that show the 13, 16.8 & 31.8 μm emission features exhibit a broad emission band centered at 19.5 μm. We propose that small spherical particles of $Mg_{0.1}Fe_{0.9}O$ are the carrier of this feature.

(3) Various other oxides – among them amorphous Al_2O_3, $CaAl_{12}O_{19}$ and all known TiO_2 modifications – can emit rather efficiently in the 11-17μm range (see Tab. 1). This has also become clear from new results of experiments on vapour-condensed oxide nanoparticles.

2. THE FEATURES OF SPINEL ($MgAl_2O_4$)

It is rather difficult to identify a dust species on the basis of only one observed feature. However, the 13 μm emission feature turned out to often occur together with a minor feature at λ = 16.8 μm and a major one at λ = 31.8 μm. This is especially the case for bright sources of the 13 μm feature for which spectra with a good signal-to-noise ratio exist, e. g. for T Cep, R Dor, R Hya, W Hya, T Mic and S Pav (see Figs. 1 and 2).

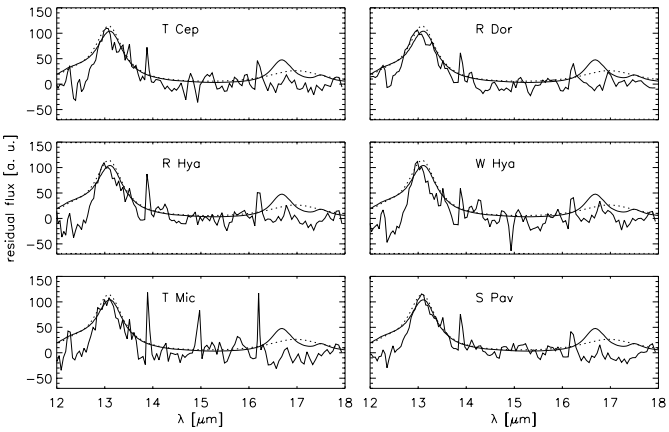

Figure 1. The 13 & 16.8 μm features in ISO-SWS spectra (rebinned to a resolution R=200) compared to the emissivity of natural (solid line) and annealed spinel (dotted line). The emissivity of natural spinel has been derived from the reflectance spectra measured by Fabian et al. (2001) by means of a Lorentz oscillator fit.

All three emission bands can be attributed to $MgAl_2O_4$ (spinel). The optical constants depend significantly on formation temperatures, stoichiometry and annealing effects (Fabian et al. 2001). Spinels that have been cooled down very rapidly after formation (like the Al-enriched spinel shown in Fig. 2) have an internal disorder which makes their resonance bands broader than for the case of natural spinels. The observed 13, 16.8 and 31.8 μm bands have rather small widths (FWHM $\approx$ 0.5 μm both for the 13 and the 31.8 μm feature), which is better compatible with the optical properties of natural spinels. However, the band positions can be better reproduced using the optical constants of spinels formed at (or heated to) temperatures between 1220 and 2400 K. Further experiments will make it clear whether spinels heated to slightly lower temperatures match the observed emission features both with respect to the band positions and the band widths.

3. THE $Mg_{0.1}Fe_{0.9}O$ EMISSION AT 19.5 μm

At 19.5 μm, a rather prominent flux maximum is present in most of those circumstellar shells which show the spinel bands

Proceedings of the Symposium *"Exploiting the ISO Data Archive - Infrared Astronomy in the Internet Age"*, 24–27 June 2002, Sigüenza, Spain (C. Gry, S. B. Peschke, J. Matagne et al. eds., ESA SP-511)

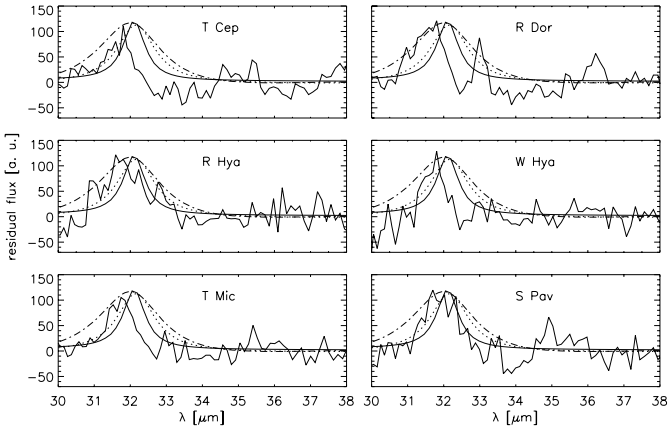

Figure 2. The 31.8 μm feature compared to the emissivity of natural (solid), annealed (dotted) and slightly Al-enriched spinel (dash-dotted line). The annealing temperature was 1220 K, the formation temperature of the Al-rich spinel was about 2400 K (which explains the large bandwidth that is due to a temperature-induced internal disorder of the crystal).

at 13, 16.8 and 31.8 μm. The reality of the 19.5 μm peak is supported by comparison with results of ground-based spectroscopy (see, e. g., Bagnulo & Doyle 1997). This feature is especially prominent in spectra of AGB stars with comparatively low mass-loss rates, indicating that its carrier is one of the first dust species to form in oxygen-rich circumstellar shells.

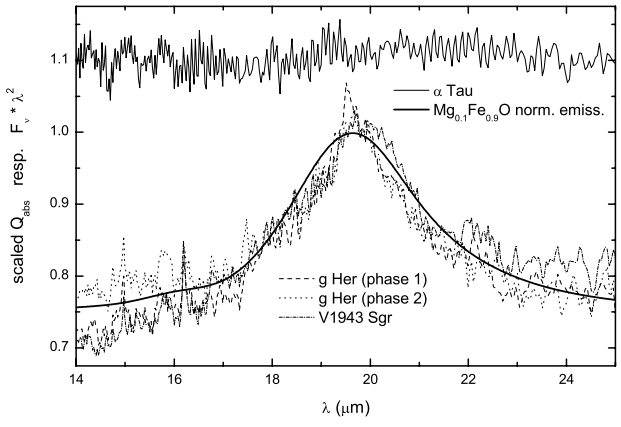

Figure 3. The 19.5 μm emission feature in ISO-SWS spectra of the semiregular variables g Her and V1943 Sgr compared to the emissivity of $Mg_{0.1}Fe_{0.9}O$ (which has been normalized and added to the underlying dust continuum). An ISO-SWS spectrum of α Tau has been overplotted to make it clear that the 19.5 μm is not an artifact, even though it is unfortunately centered very close to the border of the ISO-SWS bands 3C and 3D.

Solid solutions of MgO and FeO (which are also called magnesiowustites) emit very efficiently between λ=16 μm and λ=20 μm (Henning et al. 1995). Small spherical grains of $Mg_{0.1}Fe_{0.9}O$ can indeed produce a feature peaking at 19.5 μm with a FWHM of 3.2 μm. The influence of the dust temperature on the feature shape and position is rather small (see Posch et al. 2002). This is in excellent agreement with the results of ISO-SWS observations of g Her and V1943 Sgr (see Fig. 3), θ Aps, EP Aqr, RX Boo and SV Peg (see Fig. 4). From the spectral energy distributions plotted in these figures, the stellar photospheric continuum has already been subtracted (under the assumption that the the photospheric flux dominates over the dust emission for wavelengths $\lambda \leq 7\mu$m). For the purpose of this continuum subtraction, hydrostatic models calculated by B. Aringer (see e. g. Aringer et al. 2002) have been used which take into account molecular absorption due to H_2O, CO and SiO.

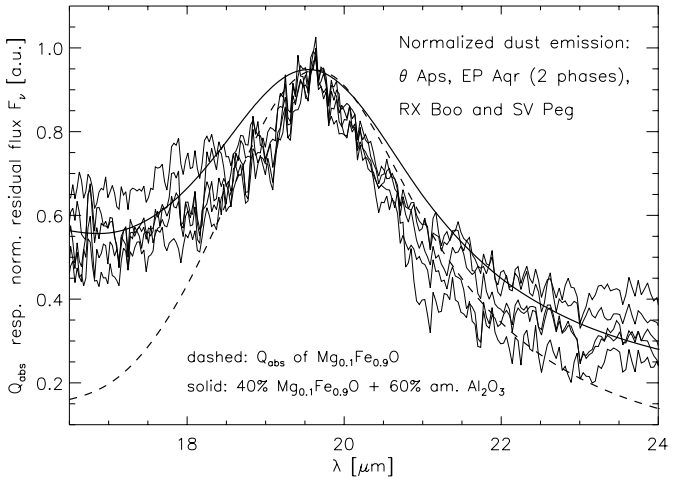

Figure 4. The 19.5 μm emission feature in ISO spectra of the AGB stars θ Aps, EP Aqr, RX Boo and SV Peg compared to the normalized emissivity of $Mg_{0.1}Fe_{0.9}O$.

4. LASER ABLATION EXPERIMENTS ON Al_2O_3

Al_2O_3 is one of the first solids expected to form in oxygen-rich circumstellar shells. However, it is not clear which form of Al_2O_3 (amorphous or crystalline) is the dominant one in the outflows of late-type stars. Small spherical particles of crystalline α-Al_2O_3 (corundum) produce very sharp emission features at 12.7, 15.9, 19.9, 21.0 and 25.6 μm (see Tab. 1) which have, however, not been observed in the IR spectra of AGB stars.

In order to better understand the formation of alumina dust, we performed the following experiment: we synthesized Al_2O_3 by laser-ablating aluminum in a 10 mbar O_2-atmosphere. For this purpose, a Nd:YAG-laser (λ=532nm) with a pulse duration of 10ns and a pulse energy of 250mJ has been used.

The comparison of the inverted transmission spectrum of the condensed particles with the emissivity of amorphous Al_2O_3 (Begemann et al. 1997) makes it clear that the laser-ablation-synthesized Al_2O_3 is not crystalline (see Fig. 5).

Amorphous Al_2O_3 is likely to be the carrier of the broad $\sim$11.5 μm emission observed in the spectra of many oxygen-rich AGB-stars like, e. g., R Cas (Fig. 6). It probably serves as

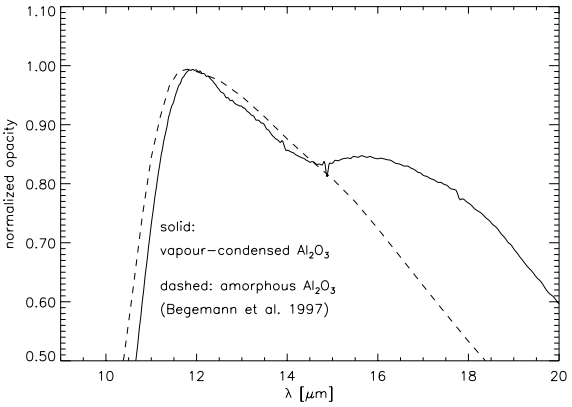

Figure 5. Inverted transmission spectrum of Al_2O_3 synthesized by means of laser ablation compared to the opacity of amorphous Al_2O_3.

an essential reagent for the formation of crystalline $MgAl_2O_4$, e. g. by the chemical reaction

Al_2O_3 (solid) + Mg + $H_2O \rightarrow MgAl_2O_4$ (solid) + H_2 (after Gail & Sedlmayr 1998).

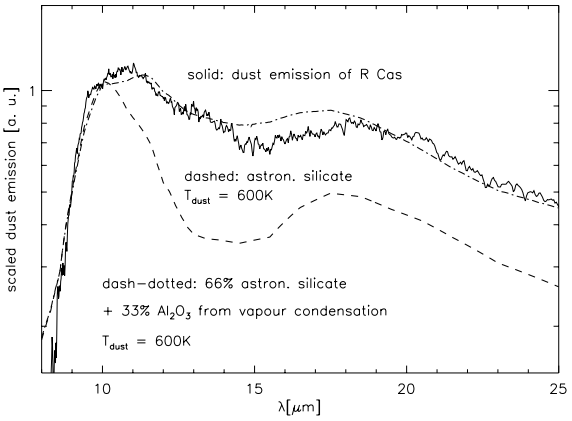

Figure 6. The dust emission of R Cas compared to the emissivity of astronomical silicate (after Ossenkopf et al. 1992) and of a mixture of 66% astronomical silicate dust + 33% Al_2O_3 dust.

Since there exist stars like g Her with spectra that are dominated by the ∼11.5, 13, 19.5 and 31.8 μm emission bands and that show only very weak silicate features around 10 and 18 μm, the question has to be raised: Does there exist a class (or an evolutionary stage) of AGB stars with dust shells dominated by oxides and not by silicates? On the basis of currently available mid-IR spectra of AGB stars, it seems as if this were the case. Already on the basis of IRAS-LRS spectra, Stencel et al. (1990) came to a similar hypothesis. They suggested that due to the higher electron affinity of aluminum (compared to silicon) for oxygen, silicates will only form after most of the available aluminum has been oxidized.

5. CIRCUMSTELLAR HIBONITE?

Hibonite ($CaAl_{12}O_{19}$) is a calcium-aluminum-oxide which has recently been detected in meteoritic presolar grains originating from AGB stars (Choi et al. 1999). At pressures above 2×10^{-3} bar, it is the very first condensate to form (at T>1770 K) from a cooling composition gas with solar elemental abundances. At lower pressures, hibonite is expected to form by reaction of corundum (α-Al_2O_3) with gas-phase calcium.

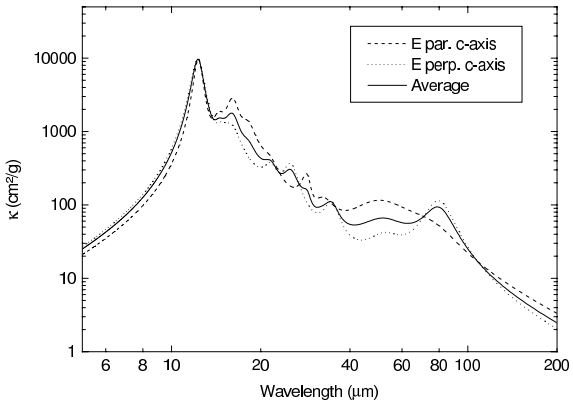

Figure 7. The emissivity of $CaAl_{12}O_{19}$ in the Rayleigh case (after Mutschke et al. 2002). The dashed and dotted lines represent the decomposition of the emissivity into the two principal orientations of the electric field vector relative to the crystallographic axis.

Since no optical constants of this mineral were available as yet, reflection measurements on samples from Madagascar have been performed in the Jena laboratory, and the dielectric functions have been derived from them. Fig. 7 shows the absorption efficiency of small spherical hibonite particles resulting from these dielectric functions. The strongest maximum of the absorption efficiency is situated at a wavelength of 12.3μm. Some of the sources of the 13 μm feature do show something like an additional 12 μm peak in their spectra; however, at the same wavelength, the relative spectral response function of SWS shows some irregularities, and therefore, it is not yet clear whether hibonite is among the major components of circumstellar oxide dust (see Mutschke et al. 2002).

6. TITANIUM OXIDES

Titanium oxide nanoparticles are expected to be among the first solids that form in oxygen-rich circumstellar shells (e. g. Jeong et al. 1999). However, the infrared-optical properties of titanium oxides have not yet been explored sufficiently.

We derived the optical constants of the comparatively rare TiO_2 modifications anatase and brookite and calculated small particle spectra from them. Additionally, the emissivities of Ti_2O_3 (based on the optical constants published by Lucovsky et al. 1977) and $CaTiO_3$ (based on powder transmission spectra) have been derived. The results are summarized in Tab. 1 (which also lists the feature positions of the oxides discussed in the previous sections).

Anatase, the low-temperature modification of tetragonal TiO_2, which is stable at temperatures below 800 K, is among the potential carriers of the 13 μm emission feature. Its secondary emissivity peaks at 15 and 27.4 μm, though, have not been observed in the spectra of circumstellar shells. Therefore, anatase can not be considered as a real alternative to spinel as carrier of the 13 μm feature.

Among the other features expected to be produced by the above mentioned solid titanium compounds, none could be identified as yet in the spectra of any circumstellar shell. Maybe this is due to the fact that titanium oxides serve as seed nuclei for the condensation of other oxide and silicate dust species such that they are not detectable in (spatially not resolved) spectra. By means of high resolution spectroscopy, titanium compounds may become detectable in the inner parts of circumstellar dust shells.

Table 1. Feature positions of selected oxide dust species in the Rayleigh limit (for spherical particles). The respective main features have been emphazised in italics. Those dust species for which we claim observational evidence have been marked with an asterisk (*).

Dust species	feature pos. [μm]
$MgAl_2O_4$ (spinel)*	*13.1*, 16.8, 31.8
$Mg_{0.1}Fe_{0.9}O$*	*19.5*
amorphous Al_2O_3*	$\sim$ *11.5*
α-Al_2O_3 (corundum)	*12.7*, 15.9, 19.9, 21.0, 25.6
$CaAl_{12}O_{19}$ (hibonite)*	*12.3*, 15.9, 78.7
TiO_2 (rutile)	*13.4*, 23.0, 27.4
TiO_2 (anatase)	*13.0*, 15.0, 27.4
TiO_2 (brookite)	*13.5*, 18.5, 22.0, 26.7, 31.2, 33.0
Ti_2O_3	18.3, *18.8*, 20.0, 25.6, 28.5, 35.7
$CaTiO_3$ (perovskite)	*17.3*, 22.3, 26.3, 34.1
amorphous SiO_2	*8.8*, 12.3, 20.5

ACKNOWLEDGEMENTS

T.P. received a DOC grant from the *Doktorandenprogramm der Österreichischen Akademie der Wissenschaften* and travel grants from the project FIRST-PACS/Phase$\sim$I, financed by the Austrian Federal Ministry of Transport, Innovation and Technology (bm:vit). This work was also supported by grant number Mu 1164/5-1 of the *Deutsche Forschungsgemeinschaft*, DFG.

REFERENCES

Aringer, B., Kerschbaum, F., Jørgensen, U.G., 2002, A&A, in press
Bagnulo, S. & Doyle, J.G. 1997, Ap&SS 251, 177
Begemann, B., Dorschner, J., Henning, Th. et al., 1997, ApJ 476, 199
Choi, B.-G., Wasserburg, G.J., Huss, G.R., 1999, ApJ 522, L133
Fabian, D., Posch, Th., Mutschke, H. et al., 2001, A&A 373, 1125
Gail, H.-P. & Sedlmayr, E., 1998, in: Hartquist T.W., Williams D.A. (eds.), The molecular astrophysics of stars and galaxies, Claredon Press, Oxford
Henning, Th., Begemann, B., Mutschke, H., Dorschner, J., 1995, A&AS 112, 143
Jeong, K. S., Winters, J. M., Sedlmayr, E. 1999, in: Le Bertre T., Lèbre A., Waelkens C. (eds.), Asymptotic Giant Branch Stars, Proc. IAU Symp. 191, ASP Conf. Ser. p. 233
Lucovsky, G., Sladek, R. J., Allen, J. W. 1977, Phys. Rev. B, Vol. 16, 5452
Mutschke, H., Posch, Th., Fabian, D., Dorschner, J., 2002, A&A, in press
Ossenkopf, V., Henning, T., Mathis, J. S., A&A 261, 567
Palik, E.D. (ed.), 1985-1998, Handbook of Optical Constants of Solids, 3 vols., Academic Press, Boston
Posch, Th., Kerschbaum, F., Mutschke, H. et al., 1999, A&A 352, 609
Posch, Th., Kerschbaum, F., Mutschke, H., Dorschner, J., Jäger C., 2002, A&A 393, L7
Stencel, R., Nuth, J.A., Little-Marenin, I., Little, S.J., 1990, ApJ 350, L45

LOW MASS LOSS IN LATE TYPE STARS

Aafifa Ramdani

Département de Physique, Université Mohamed 1er, PO Box 524, 60000 Oujda, Morocco

ABSTRACT

The spectra of 83 giant stars obtained by the ISO/SWS covering the wavelength range 2.4 - 45 μm have been analysed. The stars of our sample have been selected on the basis of their IRAS colors as low mass loss candidates ([12]-[25] $<$ 0 and [25]-[60] $<$ -1.8, where $[12]-[25] = 2.5\ log(\frac{F_{25}}{F_{12}})$ and $[25]-[60] = 2.5\ log(\frac{F_{60}}{F_{25}})$). The sample includes 10 supergiants, 30 Miras, 27 Semiregular Variables (SRVs) , 5 irregulars (IRVs) and 12 IRAS objects of different types, all these stars are surrounded by oxygen-rich dust shells characterized by silicate emission.

The spectra are analysed in terms of a spherical radiative transfer model based on the DUSTY code. The model fits to the SED restricted to the ISO/SWS wavelength range allow us to evaluate reasonably well the optical depth at 10 μm, especially since the present study is a differential analysis of the mass loss versus variability properties for stars with small mass-loss rates. In addition, taking into account the spectral type of the star, the presence of 10 and 18 μm silicate emission features constrains drastically the other model fit parameters. The optical depth at 10 μm spans the range 0.01 to 1.8 for all the stars of our sample, with the upper limit corresponding in fact to the value where in average the 10 μm dust feature shows in self absorption and translates to a dust mass loss rate $\dot{\mathrm{M}}_{\mathrm{d}}$ around 10^{-7} $\mathrm{M}_{\odot}\mathrm{y}^{-1}$ for an optically visible Mira whose luminosity equals 10^{4} $\mathrm{L}_{\odot}$. The optical depth distribution peaks abruptly around 0.05 both for Miras and SRVs, whereas supergiants are apparently more uniformly distributed in the full range. Almost all our stars have HIPPARCOS derived distances so an accurate determination of mass loss rates will be made.

The ISO/SWS spectra are compared to their equivalent IRAS/LRS in order to account for variability of the SED in the near and mid-infrared and to check for long-term changes of the circumstellar material surrounding these stars.

Key words: infrared: spectra - stars: circumstellar matter - stars: mass loss - stars: variables

1. INTRODUCTION

The general picture of the mass loss process occurring at the end of the Asymptotic Giant Branch is well understood in terms of a two-step process. First, stellar pulsation drives strong shock waves into the photosphere. The shock waves then transport mass to large distances from the star where condensation of dust particles takes place and radiation pressure accelerates these dust grains outwards. The gas density needs to be large enough for the dust grains to couple to the gas and to drag it outwards. The existence of a lower limit of mass loss rate for radiation-driven winds around 10^{-7} $\mathrm{M}_{\odot}\mathrm{y}^{-1}$ derived from theoretical considerations (Gail & Sedlmayr 1987; Netzer & Elitzur 1993) indicates that different physical mechanisms must operate in stars undergoing mass loss at a rate below this limit. Such a mechanism responsible for low mass loss rates should be noticeable as a discontinuity in the evolution of mass loss. Indeed the presence of a gap in the distribution of sources observed in the IRAS two-colour diagram is interpreted along these guidelines (van der Veen & Habing 1988). The transition from low mass loss rate to high mass loss rate must occur at some point in the evolution along the Asymptotic Giant Branch, yet it is still not clear for what type of variables and whether there is a lower limit to the mass of main sequence stars that will go through this transition as derived by Schröder et al. (1999) from evolutionary models of carbon stars. An analysis of the variability properties of low mass losing stars is of special importance in this respect because it is well known from an observational point of view that all the mass losing stars are variables and that at least some SRVs are the immediate precursors of Miras (e.g. Lloyd Evans & Menzies 1973). The present study is an observational investigation of low mass loss in different groups of LPVs and includes some supergiants and irregular variables. Thanks to the large infrared spectrum data base collected by the two spectrometers on board of ISO, it is possible to perform a statistical analysis comprising most groups of variables.

2. OBSERVATIONS

2.1. ISO DATA

From the IRAS sky survey, we have selected a number of stars with circumstellar envelope characterized by silicate dust emission. The selection criteria of these stars based on their location in region II and IIIa of the IRAS two-colour diagram as defined by van der Veen & Habing (1988) restrict the sample to stars with low mass loss rates (see figure 1). Only were considered those stars with spectra showing at the same time the 10 and 18 μm silicate dust feature.

Proceedings of the Symposium *"Exploiting the ISO Data Archive - Infrared Astronomy in the Internet Age"*, 24–27 June 2002, Sigüenza, Spain (C. Gry, S. B. Peschke, J. Matagne et al. eds., ESA SP-511)

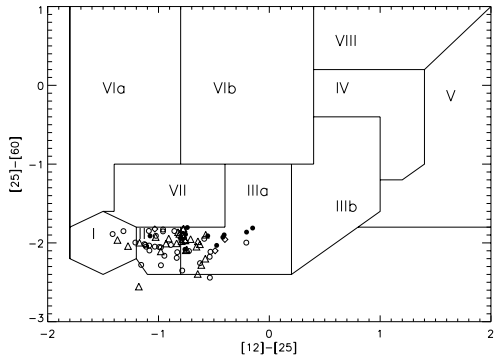

Figure 1. IRAS two-colour diagram: filled circles, squares, triangles and open circles represent respectively supergiants, IRVs, SRVs and Miras.

The spectra analysed in the present study were obtained by the ISO/SWS (de Graauw et al. 1996), covering the wavelength range 2.4 - 45 μm. The spectra were reduced by the SWS offline processing software, version 10.1, for the photometric calibration procedure see Schaeidt et al. (1996). Some spectra still show a jump in flux level at the sub-band edges due to either imperfect flux calibration or dark current subtraction or pointing problems. In most cases, the jump occurs at the edge of bands 3D and 3E, the correction was done by scaling the flux level in the longer wavelength band to the shorter one. In case of negative flux in band 4, an additive correction was applied. The spectra were then smoothed and rebinned to a resolution of 100.

2.2. Method for the model fitting

The fit procedure is based on models computed from the stationary DUSTY code for spherical radiative transfer (Ivezic et al. 1997). The major problem in fitting the SED for optically thin shells is to restrain the set of input parameters because in this case the emerging spectrum is more sensitive to the stellar and circumstellar parameters. The input parameters necessary in DUSTY are, in addition to the dust composition and the optical depth, the photospheric temperature T_* and the dust temperature at the inner boundary of the dust shell T_c. For a Mira, the photospheric temperature can vary by up to 650 K on average during a light cycle as deduced from the mean V - K color of the sample studied by Smith et al. (2002) and the synthetic V-K colors given by Bessell et al. (1998). It is therefore necessary to derive this parameter from the spectrum itself. Fortunately for optically thin shells the shape of the continuum at near infrared wavelengths (below $\sim$ 5.5 μm) is practically insensitive to the dust shell parameters (T_c) and dust composition contrary to the OH/IR stars. The NIR region is used here to derive the photospheric temperature through a fit to the synthetic spectra given by Fluks et al. (1994).

The same dust composition and properties were assumed for all the stars: the dust is composed by 80% of amorphous silicate from Ossenkopf et al. (1992) and 20% of amorphous silicate from Draine & Lee (1984) with a single grain size of 0.05 micron. The shape of the 10 and 18 μm silicate features and the presence of secondary features are disregarded in the fit procedure, these two last characteristics are mainly related to the presence of other dust species.

The shape of the continuum at mid infrared as well as the relative strength of the 18 to the 10 μm silicate feature are essentially sensitive to T_c, whereas the strength of the 10 μm silicate feature is well correlated to the flux averaged optical depth (Ivezic & Elitzur 1995).

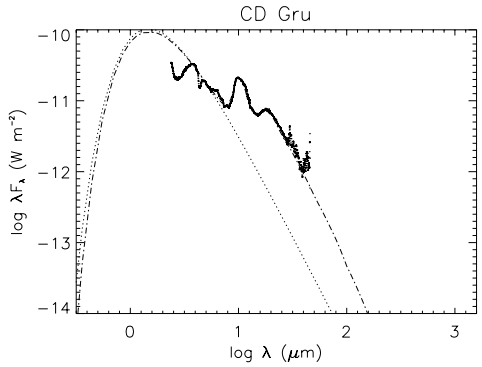

Figure 2. Best fit to the ISO/SWS spectrum of the Mira CD Gru with T_*=2667 K and T_c=500 K, the model is represented by the dot-dashed line, the dotted line represent the black body assumption of the photospheric spectrum

Figure 2. shows the observed and modelled spectrum of the Mira CD Gru with a dust shell with relatively moderate optical depth [$\tau(10\ \mu\mathrm{m}) = 0.2$]. The overall shape of the SED is rather well reproduced by the modelled spectrum. A comprehensible deviation between the modelled and the observed spectrum can be seen in the 2.38 to $\sim$3.8 μm wavelength region due to the molecular absorption bands of CO and H_2O not taken into account by the black body assumption.

Figure 3. presents the model fit for two stars with dust shells of low optical depths [$\tau(10\ \mu\mathrm{m}) = 0.02$ and 0.01 for RT Pav and ST Her, respectively]. In the case of ST Her there is an evident discrepancy between the observed and the modelled spectra since the model fails to reproduce the strength and the shape of the 10 μm feature. This behavior observed for some stars which exhibit also the 13 μm feature is due probably to a very different dust composition especially since the maximum of the 10 μm feature is shifted to the red in this case.

The assumption of a same dust composition and grain size properties for all the stars is certainly not realistic and might lead to an erroneous optical depth values for those stars with very different dust composition and/or grain size properties and for which the model fit is relatively poor. Generally this applies to dust shells with very low optical depth ($\tau(10\ \mu\mathrm{m}) \leq 0.02$). Nevertheless, it is expected that even if the very low optical depth values derived in this way suffer a 100% uncertainty, the

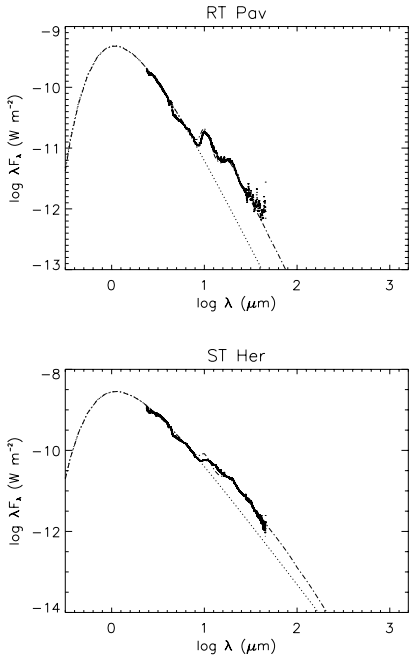

Figure 3. Same as figure 2. for the Semiregular Variable RT Pav with T_*=3396 K and T_c=500 K and for the Semiregular Variable ST Her with T_*=3100 K and T_c=500 K.

overall shape of the optical depth distribution will not be affected (See section 3.).

2.3. Model fit paramaters

In table 1. we give the fit parameters for 7 stars together with the corresponding mass loss rates obtained from the literature. However, a straightforward comparison with the optical depth is difficult owing to a difference in the parameters especially the luminosity and distance derived by these authors. It is noteworthy that the low value found for the temperature at the inner boundary of the dust shell $T_{\rm c} = 500$ K gives the best fit in the majority of the model fits in contradiction with a higher nucleation temperature in the range 700 - 1000 K (see, e.g., Sedlmayr 1994). However if we consider the optical properties of amorphous silicates from Dorschner et al. (1995) instead of those from Ossenkopf et al (1992) and Draine & Lee (1984), comparable model fit parameters are derived except for $T_{\rm c}$ which increases by 200K in average.

A characteristic value of 3100 K is derived for the photospheric temperature of the SRVs in our sample which is consistent with their corresponding spectral type in most cases. On the contrary Miras have lower photospheric temperatures spanning the range 2000 - 2700 K. More generally we confirm the result of Hron et al. (1997) according to which Miras form an extension of the SRVs towards lower effective temperature and slightly higher flux averaged optical depth, the latter parameter correlating with the optical depth at 10 μm.

3. OPTICAL DEPTH DISTRIBUTION

In the right panel of figure 4., we present the optical depth distribution for Miras and SRVs, which reflects also the mass loss rate distribution for these variables since they have roughly the same luminosity.

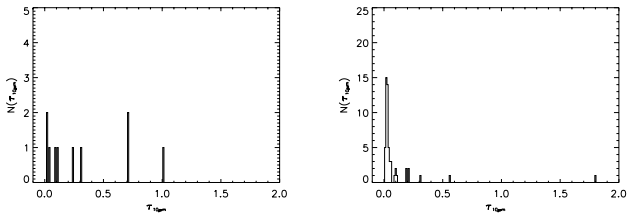

Figure 4. Optical depth distribution, left panel: supergiants and right panel: Miras + SRVs.

The pronounced peak present at a value below 0.05 does confirm the presence of a gap in the sequence of increasing optical depth in the IRAS two-colour diagram and its interpretation as a discontinuity in the mass loss rate distribution. The corresponding cutoff of the optical depth distribution at $\tau(10\ \mu{\rm m}) \sim 0.05$ is not likely due to selection effect since there is still some Miras with optical depths above this limit.

To estimate the dust mass loss rate corresponding to this cutoff, we consider a $1/{\rm r}^2$ dust density distribution (constant dust velocity and mass loss rate), in this case the optical depth $\tau(10\ \mu{\rm m})$ is given by:

$$\tau(10\ \mu{\rm m}) = Q_{\rm abs}(10\ \mu{\rm m})\pi a^2 n_{\rm d}(R_{\rm c})R_{\rm c} \qquad (1)$$

where $Q_{\rm abs}(10\ \mu{\rm m})$ is the absorption efficiency, a is the grain radius and $R_{\rm c}$ is the inner radius of the dust shell corresponding to the dust condensation, this parameter defined by $T(R_{\rm c})=T_{\rm c}$ depends on the luminosity.

And the dust mass loss rate is given by:

$$\dot{\rm M}_{\rm d} = 4\ \pi\ R_{\rm c}^2 \frac{4\ \pi\ a^3}{3}\ \rho_{\rm a} n_{\rm d}(R_{\rm c}) V_{\rm d} \qquad (2)$$

where $\rho_{\rm a}$ is the grain density and $V_{\rm d}$ is the dust velocity. We have adopted the following values: $\rho_{\rm a} = 3$ gcm^{-3}, $V_{\rm d} = 28$ km/s which is about twice a typical gaz asymptotic velocity (Tielens 1983), $Q_{\rm abs}(10\ \mu{\rm m}) = 0.04$ computed from the opacity $\kappa(10\ \mu{\rm m})$ of Ossenkopf et al. (1992) and a typical luminosity $L = 10^4\ {\rm L}_\odot$.

From equations (1) and (2), we obtain $\dot{\rm M}_{\rm d} = 9\ 10^{-9}\ {\rm M}_\odot\ {\rm y}^{-1}$ for $\tau(10\ \mu{\rm m}) = 0.05$.

The left panel of figure 4. shows the optical depth distribution for supergiants. The distribution seem more uniform in the full optical depth range spanned in this study. This suggests that other mechanism than the interplay of pulsation and radiation pressure is at the basis of mass loss in this case.

4. SUMMARY

The optical depth distribution of our sample has a minimum value of 0.01 which corresponds to the sensitivity limit im-

Table 1. A sample of a DUSTY fit parameters for 7 stars. Temperatures are in K, mass loss rates in 10^{-6} $M_{\odot}y^{-1}$, references are as follow: 1: Whitelock et al. (1994); 2: Le Bertre & Winters (1998); 3: Kahane & Jura (1994), 4: Jura & Kleinmann (1990)

IRAS designation	Name	T_*	T_c	$\tau(10\ \mu m)$	$\dot{M}$	Var.	ref.
IRAS 00193-4033	BE Phe	2667	750	1.8	9.1	M	2
IRAS 02351-2711	UU For	2667	500	0.18	1.8	M	1
IRAS 23412-1533	R Aqr	2500	750	0.09	0.17	M	2
IRAS 13114-0232	SW Vir	2890	500	0.02	0.4	SRb	3
IRAS 15492+4837	ST Her	3100	500	0.013	0.3	SRb	3
IRAS 22456+5453	U Lac	2500	750	0.15	2	SRc	4
IRAS 18050-2213	VX Sgr	1800	750	1	40	SRc	4

posed by the model fitting. The upper bound $\tau(10\ \mu m) = 1.8$ is found for the Mira BE Phe with a corresponding dust mass loss rate $\dot{M}_d$[1]=1.7 10^{-7} $M_{\odot}$ y^{-1}. Given this relatively high value, it is very likely that the Mira BE Phe fit the widely accepted description of mass loss process in AGB stars as a result of radiation-pressure driven wind.

Almost all the Miras and SRVs have optical depths at 10 μm below 0.05, whereas supergiants although located in the same regions in the IRAS two-colour diagram have an optical depth uniformly distributed in the full optical depth range. To assess this result, it is necessary to study a larger sample of supergiants located in the same regions of IRAS two-colour diagram.

This study constitutes the basis for future calculations of mass loss rates taking into account the accurate HIPPARCOS derived distances of these stars and a more complete treatment of individual dust composition and grain size properties.

ACKNOWLEDGEMENTS

I would like to thank Dr. A. Jorissen for a careful reading of the manuscript.

REFERENCES

Bessell M.S., Castelli F., Plez B., 1998, A&A 333, 231
de Graauw T., Haser L.N., Beintema D.A., et al., 1996, A&A 315, L49
Dorschner J., Begemann B., Henning Th., et al., 1995, A&A 300, 503
Draine B.T., Lee H.M., 1984, ApJ 285, 89
Fluks M.A., Plez B., The P.S., de Winter D., Westerlund B.E. 1994, A&AS 105, 311
Gail H.-P., Sedlmayr E., 1987, A&A 177, 186
Hron J., Aringer B., Kerschbaum F., 1997, A&A 322, 280
Ivezic Z., Elitzur M., 1995, ApJ 445, 415
Ivezic Z., Nenkova M., Elitzur M., 1997, User Manual for Dusty, Internal Report, University of Kentucky, accessible at http://www.pa.uky.edu/∼moshe/dusty
Jura M., Kleinmann S.G., 1990, ApJS 73, 769
Kahane C., Jura M., 1994, A&A 290, 183
Le Bertre T., Winters J.M., 1998, A&A 334, 173
Lloyd Evans T., Menzies M., 1973, in Fernie J.D., ed., Variable Stars in Globular Clusters and in Related Systems, Reidel, Dordrecht, p.151
Netzer N., Elitzur M., 1993, ApJ 410, 701
Ossenkopf V., Henning Th., Mathis J.S., 1992, A&A, 261, 567
Schaeidt S.G., Morris P.W., Salama A., 1996, et al., A&A, 315, L55
Schröder K.-P., Winters J.M., Sedlmayr E., 1999, A&A, 349, 898
Sedlmayr E., 1994., in Jorgenson U.G., ed., Molecules in the Stellar Environment, Springer-Verlag, Berlin, p.163
Smith B.J., Leisawitz D., Castelaz M.W., Luttermoser D., 2002, AJ, 123, 948
Tielens A.G.G.M., 1983, ApJ, 271, 702
van der Veen W.E.C.J., Habing H.J., 1988, A&A 194, 125
Whitelock P., Menzies J., Feast M., Marang F., Carter B., Roberts G., Catchpole R., Chapman J., 1994, MNRAS 267, 711

[1] this value is calculated from equation (1) and (2) with the same considerations as in section 3. (see also Table 1.)

CLASSIFICATION OF ISO SWS 01 SPECTRA OF PROTO-PLANETARY NEBULAE: A SEARCH FOR PRECURSORS OF PLANETARY NEBULAE WITH [WR] CENTRAL STARS

Ryszard Szczerba[1], Grażyna Stasińska[2], Natasza Siódmiak[1], and Sławomir K. Górny[1]

[1]N. Copernicus Astronomical Center, Rabiańska 8, 87-100 Toruń, Poland
[2]LUTH, Observatoire de Paris-Meudon, 5 place Jules Janssen, 92150 Meudon, France

ABSTRACT

We have analyzed ISO SWS 01 observations for 61 proto-planetary nebulae candidates and classified their spectra according to their dominant chemistry. On the basis of our classification and the more general classification of SWS 01 spectra by Kraemer et al. (2002) we discuss the connection between proto-planetary nebulae candidates and planetary nebulae, with emphasis on possible precursors of planetary nebulae with [WR] central stars.

Key words: ISO SWS01, proto–planetary nebulae, precursors of planetary nebulae with [WR] central stars.

1. INTRODUCTION

The proto-planetary nebula (PPN) phase, in the context of the late stages of low- and intermediate-mass star evolution, is a short lasting period (of the order of at most a few thousands of years) when stars evolve from Asymptotic Giant Branch (AGB) to planetary nebula (PN). The PPN phase is characterized by a rather small mass loss rate ($\sim 10^{-7}\,M_\odot yr^{-1}$), a decrease of the circumstellar shell optical depth due to expansion, and a decrease of the star radius and consequent increase of the effective temperature (typically from about 4000 K until the onset of ionization at about 25000 K) due to gradual consumption of stellar envelope, both by nuclear processing and by stellar wind.

PPNe, being immediate precursors of PNe, deserve special attention because they offer the possibility to identify the main physical and chemical processes which lead to diversity of shapes and chemical compositions in PNe and their central stars. One of the most intriguing class of PNe is the class of planetary nebulae with Wolf-Rayet type central stars (hereafter [WR]PNe – see e.g. Tylenda et al. 1993, Górny & Stasińska 1995, Tylenda 1996, Leuenhagen & Hamann 1998). Among about 1500 galactic PNe ∼50 are [WR]PNe (Górny & Tylenda 2000). Observations with the Infrared Space Observatory (ISO, Kessler et al. 1996) have shown that in [WR]PNe both forms of dust (C-rich: PAHs and O-rich: crystalline silicates) are present (Waters et al. 1998a, Cohen et al. 1999). For a discussion of scenarios put forward to explain this unexpected discovery see recent papers by Cohen et al. (2002), De Marco et al. (2002) and De Marco & Soker (2002).

In this paper we report on a search of the ISO Data Archive (IDA) for spectra of PPNe taken with the Short Wavelength Spectrometer (SWS 01, de Graauw et al. 1996) and present a classification of these spectra. We then briefly discuss the relation between PPNe and PNe based on the results of this classification and the one performed by Kraemer et al. (2002).

2. SAMPLE AND ISO DATA REDUCTION

Recently, Szczerba et al. (2001b) compiled from the literature a list of 220 PPNe candidates. We have searched the IDA for SWS 01 data within 1 arcmin around the IRAS position (or other position if the source has no IRAS name) for all PPNe candidates from the Szczerba's list. We have found 83 SWS 01 spectra for 61 objects.

The ISO SWS 01 data (offline processing - OLP version 10.1) analyzed in this work were all processed using ISAP (ISO Spectroscopic Analysis Package) version 2.1. The data analysis consisted of extensive bad data removal primarily to minimize the effect of cosmic rays. First, all detectors were compared to identify possible features. Then, the best detector was chosen to compare one by one with others. Finally, the spectra were averaged, using median clipping to discard points that lay more than 2.5σ from the median flux. Whenever memory effects or irregularities were present in the two scans of SWS 01 data, we averaged the two scans separately. Then the resulting two sub-spectra were used to check the reality of possible features. The spectra were averaged typically to a resolution of 300, 500, 800 and 1500 for SWS 01 data taken with speed 1, 2, 3 and 4, respectively. For the purpose of this paper the spectra were truncated at 27.5 μm since bands 3E and 4 have usually poor signal-to-noise ratio. In addition, the memory effects can influence our ability to recognize crystalline silicates, while cosmic rays could produce spurious features. Both these effects are difficult to take into account using the ISAP software only. This then almost precludes the recognition of the presence of crystalline silicates from the spectra we considered (see discussion below).

3. RESULTS

The main criterion applied during the classification of the SWS 01 spectra for the 61 PPNe candidates was based on the widely accepted CO paradigm (the chemistry depends on the C/O ratio in the ejected material). Some unexpected discoveries of mixed chemistry among late type stars are still rather more

Proceedings of the Symposium *"Exploiting the ISO Data Archive - Infrared Astronomy in the Internet Age"*, 24–27 June 2002, Sigüenza, Spain (C. Gry, S. B. Peschke, J. Matagne et al. eds., ESA SP-511)

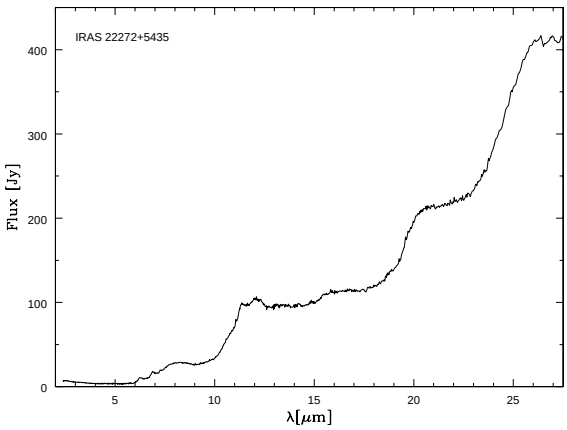

Figure 1. A representative SWS 01 spectrum (bands 1-3) of PPNe with 21 μm feature (class C 21).

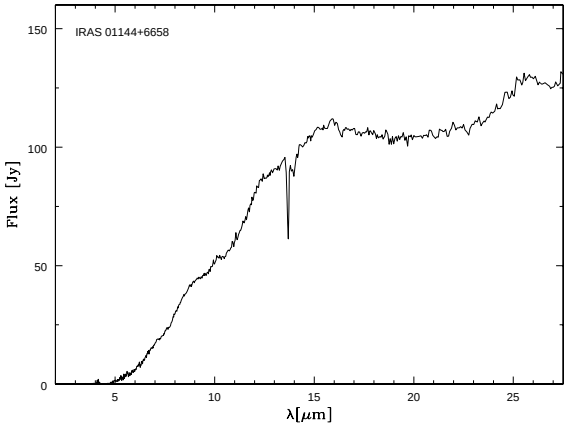

Figure 2. A representative SWS 01 spectrum (bands 1-3) of PPNe with C_2H_2 and HCN 13.8-14 μm features (class C mol).

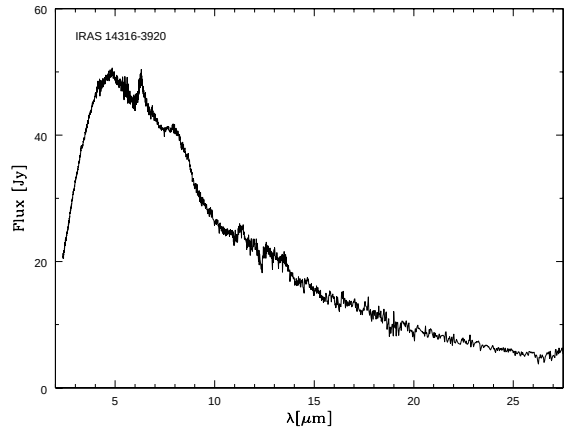

Figure 3. A representative SWS 01 spectrum (bands 1-3) of R CrB stars (class C RCrB.)

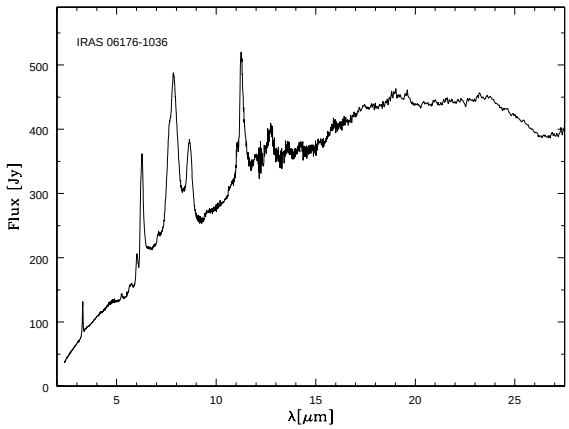

Figure 4. A representative SWS 01 spectrum (bands 1-3) of PPNe with PAH features (class C PAH).

exceptional than typical. The two main groups (C- and O-rich) are easily recognized from the analysis of dust and/or molecular features. Among sources dominated by C-based chemistry we have distinguished PPNe with the 21 μm feature (C 21 class), sources with C_2H_2 and HCN absorption features around 13.8-14 μm (C mol class), R CrB type sources with their characteristic maximum of emission around 6 μm (C RCrB class). Finally, all the sources *only* characterized by PAH features were grouped in a so-called C PAH class. A representative SWS 01 spectrum for each of these groups is shown in Figs. 1-4. Concerning O-rich sources, we simply distinguished between PPNe with the 9.7 μm feature in absorption (Si A class) or in emission (Si E class), and added a class of RV Tauri type sources where the emission feature around 10 μm has a peculiar shape (Si RVTau class). Representative SWS 01 spectra of O-rich PPNe are shown in Figs. 5-7. We were able to classify in such a way 47 sources out of 61 (the spectra of the remaining ones are too peculiar to determine what is their dominant chemistry). Table 1 shows the classes we assigned for these 47 sources, together with the KSPW class (Kraemer et al. 2002). Inside each of our classes, the sources are ordered by decreasing IRAS 25 and 12 μm flux ratio ($c21$=F_{25}/F_{12}). It can be seen that both classifications agree rather well. Since Kraemer et al. (2002) used *automatically* reduced data from the IDA, their classification is not always accurate. On the other hand, as mentioned in Sect. 2, our classification does not take into consideration the possible presence of crystalline silicate features.

4. DISCUSSION

From Table 1, the proportion of C-rich sources is 25/47 (53 %). However, because of source selection, the ISO sample is biased towards sources with the 21 μm feature, which amount to 9 objects in our sample. Therefore, the unbiased proportion of C-rich PPNe candidates is somewhere between 16/38 (42 %) and 53 %. Interestingly, the proportion of C-rich PNe is 35–40 % (Rola & Stasińska 1994, Kingsburgh & Barlow 1994).

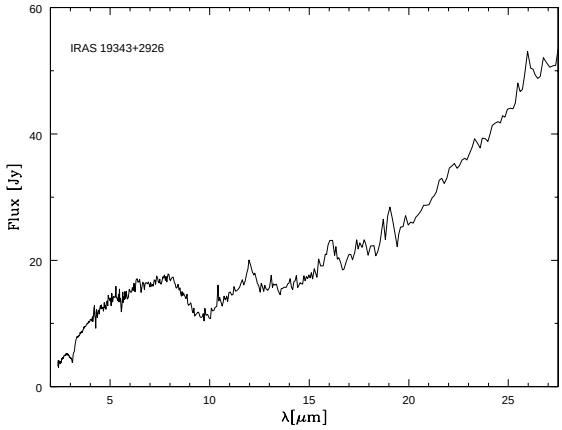

Figure 5. A representative SWS 01 spectrum (bands 1-3) of PPNe with 9.7 μm feature in absorption (class Si A).

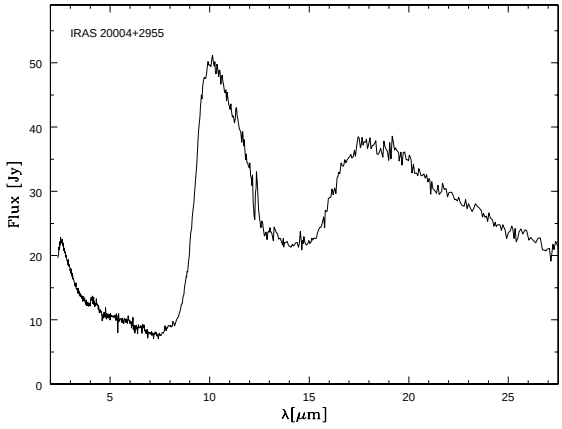

Figure 6. A representative SWS 01 spectrum (bands 1-3) of PPNe with 9.7 μm feature in emission (class Si E).

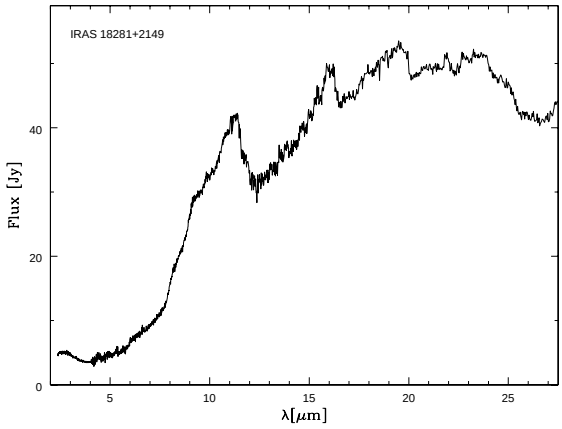

Figure 7. A representative SWS 01 spectrum (bands 1-3) of RV Tau star (class Si RVTau).

Table 1. Source classification

IRAS name	KSPW[1] class	*c21*	IRAS name	KSPW class	*c21*
C 21					
16594−4656	4.CT	7.72	20000+3239	4.CT	3.68
23304+6147	4.CT	7.13	Z02229+6208	4.CT	2.96
19500−1709	4.CT	5.18	22272+5435	4.CT	2.94
07134+1005	4.CT	5.14	05341+0852	4.PN	1.79
22574+6609	4.PUp:	4.09			
C mol					
RAFGL 2688[2]	4.CN	7.15	01144+6658	4.CR	1.79
23321+6545	4.CN:	4.69	19548+3035	4.CR	1.57
19480+2504	4.F	3.17			
C RCrB					
15465+2818	3.W	0.45	14316−3920	3.W	0.28
19132−3336	3.W	0.29			
C PAH					
13428−6232	4.Fu	15.1	13416−6243	4.CN:u	3.34
01005+7910	4.PUp	4.66	06176−1036	4.U/SC	1.24
17347−3139	4.UE	4.62	16235−4832	3.CR::	0.74
16279−4757	4.U/SC	3.82	10158−2844	2.U	0.21
Si A					
15553−5230	4.SA:	7.01	15452−5459	4.SAe	3.55
18276−1431	4.SA	6.45	17195−2710	4.SA	2.97
17150−3224	4.SA	6.43	19386+0155	4.SB	2.57
22036+5306	5.SA	5.49	19343+2926	5.SA	2.44
18596+0315	5.SA:	3.84	17516−2525	4.SAp	1.89
Si E					
12175−5338	4.SE:	7.98	11385−5517	5.SE:	1.49
18095+2704	4.SEC	2.79	20004+2955	2.SEc	3.55
18062+2410	4.SE:	2.59	17534+2603	3.SEp	0.46
19244+1115	4.SEC	1.71			
Si RVTau					
18281+2149	4.SEC	1.49	18448−0545	2.SEa:	0.45
22327−1731	4.SE::	1.30	12185−4856	7 R	0.35
20117+1634	4.SE::	0.56			

[1] –Kraemer et al. (2002);
[2] –RAFGL 2688 has not been observed by IRAS.

This suggests that most PPNe candidates from our sample will indeed become PNe (from now on we will drop the word "candidate" for simplicity).

We can now roughly estimate what number of PPNe from our classified ISO sample are expected to become [WR]PNe. Górny & Stasińska (1995) argued that the proportion of [WR]PNe relative to the total number of PNe is about 8 %. Then one expects the same proportion of [WR]PNe precursors among the sample of PPNe. This implies that 8 % of 47 PPNe, i.e $\sim$4 will become [WR]PNe.

As discussed recently by De Marco & Soker (2002) the most important characteristic of [WR]PNe seems to be dual dust chemistry. About 80 % of *late* [WR]PNe show the presence of silicates – mostly crystalline – while at the same time

all of them show PAH emission, see Szczerba et al. (2001a). Very likely the dual dust chemistry is a result of O-rich dust being formed when the star was O-rich and stored in some stable reservoir in the stellar vicinity, while the carbon chemistry occurs later when the [WR]PN progenitor is already C-rich. As concerns *early* [WR]PNe, crystalline silicates are seen in only one object (NGC 5315 – K. Volk, private communication) out of 6 with available ISO spectra. The reason for such a small proportion is not clear. Górny & Tylenda (2000) argued that there is an evolutionary link between late and early [WR]PNe, so a stable reservoir of crystalline silicates should be seen in later phases as well, unless a fast wind is able to destroy or remove the crystalline material from the star surroundings. Non-detection of crystalline silicates can also be due to a worse quality of ISO SWS data for early [WR]PNe. From the above considerations, it is natural to think that PPNe showing dual dust chemistry should evolve into [WR]PNe. In our sample, the famous Red Rectangle (IRAS 06176−1036) and IRAS 16279−4757 contain both C-rich dust and crystalline silicates (from the KSPW classification, see also Waters et al. 1998b and Molster et al. 1999) which makes them good candidates to be precursors of late [WR]PNe. Note that not all [WR]PNe are C-rich (Górny & Stasińska 1995, De Marco 2002), in consequence not all PPNe that will become [WR]PNe are necessarily C-rich. Therefore, further candidates for [WR] PNe precursors in our sample are then the O-rich sources AC Her (IRAS 18281+2149), IRAS 18095+2704 and IRAS 19244+1115.

If non-detection of dual dust chemistry in some [WR] PNe is not due to observational effects but is a sign of real absence of crystalline silicates, then it is possible that the precursors of these [WR]PNe may also not show crystalline silicate features. Recently, Hony et al. (2001) reported that some [WR]PNe show the 21 μm feature suggesting a possible link between them and PPNe with the 21 μm feature (our class C 21 or KSPW class CT). To our knowledge none of the C 21 source shows evidence of dual dust chemistry so they could be candidates for precursors of [WR]PNe without crystalline silicates. Demographic arguments show that this could be the case for only a small fraction of them. Indeed, there are at least 12 PPNe with the 21 μm feature (see e.g. Kwok et al. 2002) among 220 known PPNe, i.e. 5.5%. On the other hand only 20 % of late type [WR]PNe with analyzed ISO spectra do not have crystalline silicates. According to Górny & Tylenda (2000), 30 % of all [WR]PNe are of late type and, as mentioned above, [WR]PNe represent 8% of the total number of PNe. Thus, the proportion of *late* [WR]PNe without crystalline silicates is *at most* 20%× 30%× 8% = 0.5% of the total population of PNe. Therefore, most of 21 μm sources will not go through the *late* [WR]PN phase. One could still argue that they could evolve into PNe in which the [WR] phenomenon will appear only later. However, Górny & Tylenda (2000) have shown that most [WR]PNe do evolve from late to early type. Besides, among PNe, the 21 μm feature has been seen only in [WR]PNe, meaning that PPNe with the 21 μm feature cannot evolve to early [WR]PNe that have not gone through a late [WR] stage. Therefore, PPNe with the 21 μm feature cannot be considered, as a class, as precursors of [WR]PNe.

ACKNOWLEDGEMENTS

This work has been partly supported by grant 2.P03D.024.18p01 of the Polish State Committee for Scientific Research, by the Polonium program (contract No. 03242XJ) and by the Jumelage France-Pologne.

REFERENCES

Cohen, M., Barlow, M.J., Sylvester, R.J., et al., 1999, ApJ 513, L135
Cohen, M., Barlow, M.J., Liu, X.-W., Jones, A.F., 2002, MNRAS 332, 879
de Graauw, Th., Haser, L.N., Beintema, D.A., et al., 1996, A&A 315, L49
De Marco, 2002, in Planetary Nebulae, IAU Symp. 209, in press
De Marco, O., Barlow, M.J., Cohen, M., 2002, ApJ 574, L83
De Marco, O., Soker, N., 2002, PASP 114, 602
Górny, S.K., Stasińska, G., 1995, A&A 284, 949
Górny, S.K., Tylenda, R., 2000, A&A 362, 1008
Hony, S., Waters, L.B.F.M., Tielens, A.G.G.M., 2001, A&A 378, L41
Kessler, M.F., Steinz, J.A., Anderegg, M.E., et al., 1996, A&A 315, L27
Kingsburgh, R.L., Barlow, M.J., 1994, MNRAS 271, 257
Kraemer, K.E., Sloan, G.C, Price, S.D., Walker, H.J., 2002, ApJS 140, 389
Kwok, S., Volk, K., Hrivnak, B.J, 2002, ApJ 573, 720
Leuenhagen, U. & Hamann, W.–R., 1998, A&A 330, 265
Molster, F.J., Yamamura, I., Waters, L.B.F.M., et al., 1999, Nature 401, 563
Rola, C., Stasińska, G., 1994, A&A 282, 199
Szczerba, R., Górny, S.K., Stasińska, G., et al., 2001a, Ap&SS, 275, 113
Szczerba, R., Górny, S.K., Zalfresso–Jundziłło, M., 2001b, in ASSL Vol. 265, Post-AGB objects as a Phase of Stellar Evolution, eds. R. Szczerba & S.K. Górny, Kluwer Academic Publisher, Dordrecht/Boston/London, 13
Tylenda, R., Acker, A., Stenholm, B., 1993, A&AS 102, 595
Tylenda, R., 1996, in ASP Conf. Ser. 96, Hydrogen-Deficient Stars, eds. C.S. Jeffery & U. Heber (San Francisco), 101
Waters, L.B.F.M., Beintema, D.A., Zijlstra, A.A., et al., 1998a, A&A 331, L61
Waters, L.B.F.M., Waelkens, C., van Winckel, H., et al., 1998b, Nature 391, 868

THE EXTENDED ATMOSPHERE AND EVOLUTION OF THE RV TAURI STAR, R SCUTI

Issei Yamamura[1], Mikako Matsuura[2], Albert A. Zijlstra[2], and Timothy R. Bedding[3]

[1]Institute of Space and Astronautical Science (ISAS), Yoshino-dai 3-1-1, Sagamihara, Kanagawa, 229-8510, Japan
[2]Department of Physics, UMIST, P.O. Box 88, Manchester M60 1QD, UK
[3]School of Physics, University of Sydney 2006, Australia

ABSTRACT

We analyze ISO/SWS spectra of the RV Tau star, R Scuti. The data were obtained from the ISO data archive, and processed with OLP ver.10.1 and OSIA ver.2.0. We found that the infrared spectra of this star are dominated by emission bands of H_2O vapour. We also identify CO, SiO and CO_2 bands. Unlike the other RV Tau stars, the infrared spectra of R Sct are very similar to those of the oxygen-rich Mira variable, *o* Cet (Mira). However, 10 μm silicate band is very weak in R Sct. With these newly found properties of the star, we discuss structure and evolutionary stage of the star.

This study is an example that the uniform and high-quality data in the ISO Archive have a lot of potential to give an impact on stellar evolution.

Key words: stars: AGB and post-AGB – stars: atmospheres – stars: circumstellar matter – infrared: stars – stars: variables: general – stars: individual: R Sct

1. INTRODUCTION

RV Tau stars are pulsating variables showing alternating deep and shallow minima in their light curves. Their spectral type ranges from F to K supergiant, corresponding to the effective temperature ($T_{\rm eff}$) of 3000–6000 K. It has been suggested that these stars are in the post-AGB phase (Jura 1986). Abundance anomaly has been observed in some of the stars, which is interpreted by the metal depletion by the gas-dust separation in the circumbinary-discs (Waters et al. 1992; Van Winckel et al. 1999; Jura et al. 2000).

R Scuti is a bright RV Tauri star in optical to near-infrared wavelengths. Its primary period (period between deep minima) of variability is 147 days (Kholopov et al. 1988). $T_{\rm eff}$ varies in 4750–5250 K (Shenton et al. 1994) and the spectral type may become as late as M3 (Kholopov et al. 1988). CO radio observations by Bujarrabal et al. (1988) show that the star had experienced a heavy mass-loss phase in the past. The current mass-loss rate estimated from the IRAS data is smaller by two orders of magnitudes than that from CO observations (Alcolea & Bujarrabal 1991).

The ISO/SWS observations of R Sct were carried out in the program MOLBANDS (P.I. A. Heske). During systematic survey of molecular bands in the SWS spectra of evolved stars, we found that this object show interesting properties, as we describe in this paper. More detailed discussion of this star has been published in Matsuura et al. (2002b).

2. THE SWS SPECTRA OF R SCUTI

R Sct was observed with the SWS on March 10, 1996. The variability phase (defined as phase=0.0 at deep minimum) was 0.6. The observing mode is AOT01 and the corresponding spectral resolution is R =300–500.

Fig. 1 shows the spectra of R Sct in 2–16 μm. The spectra of the Mira variable, *o* Cet (Yamamura et al. 1999), is also shown for comparison. The spectra of R Sct are very similar to those of *o* Cet. H_2O, SiO, CO, and CO_2 features are identified. Especially the H_2O bands in R Sct are as prominent as those in *o* Cet, and dominate the infrared spectra. H_2O and CO_2 usually appear in stars with a spectral type later than M6. In other words, stars with an excitation temperature ($T_{\rm eff}$) lower than ∼3300 K. The detection of molecular bands in the spectra of R Sct is totally unexpected from its effective temperature (4750–5250 K).

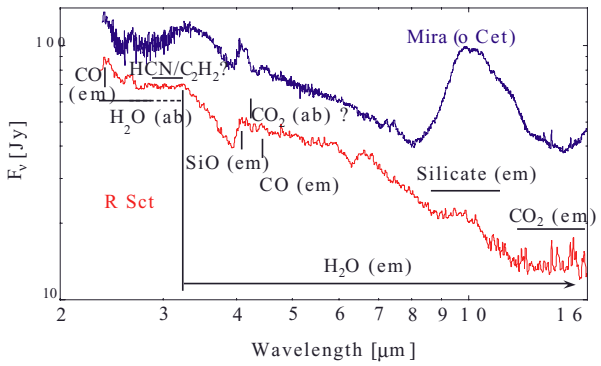

Figure 1. The ISO/SWS spectra of R Sct. The locations of the major molecular features are indicated. The spectra of the oxygen rich Mira variable, o Cet, are shown for comparison. The spectra of o Cet are scaled for convenience. Two stars show similar spectra below ∼5 μm.

Dust emission is also observed in the SWS spectra of R Sct. In Fig. 2, the spectra of R Sct around 10 μm are compared with those of two Mira variables, *o* Cet and T Cas. There is a tiny excess around 10 μm in R Sct, probably by amorphous silicate dust. This excess is significantly weaker than that in *o* Cet, which is in contrast to the similarity in the near-infrared spectra. T Cas shows typical spectra of an AGB star with moderate

Proceedings of the Symposium *"Exploiting the ISO Data Archive - Infrared Astronomy in the Internet Age"*, 24–27 June 2002, Sigüenza, Spain (C. Gry, S. B. Peschke, J. Matagne et al. eds., ESA SP-511)

mass-loss rate, with a weak silicate emission and the so called "13 μm" feature. This 13 μm feature is not found in R Sct. This feature is known to be prominent in the stars with relatively small pulsation amplitude and low mass-loss rate (Posch et al. 1999). The absence of the 13 μm feature in R Sct distinguishes this star from the "normal" AGB red-giants.

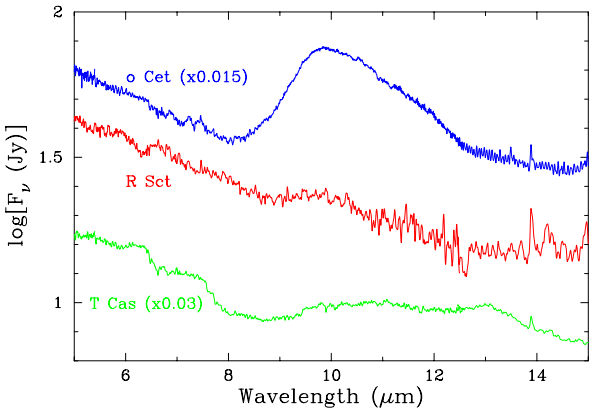

Figure 2. The spectra of R Sct around 10 μm are compared with those of two Mira variables, o Cet and T Cas. o Cet shows a prominent silicate band at $\sim$ 10 μm, while T Cas exhibits the 13 μm feature. In R Sct, only a weak silicate band is found.

The SWS spectra of R Sct seem to be peculiar even among those of the RV Tau stars. ISO/SWS observed five RV Tau stars, AC Her, HR Del, R Sge, SX Cen, and R Sct, in the AOT01 mode. The spectra of four out of these five stars are shown in Fig. 3. Except for R Sct, the spectra of other three stars are dominated by the dust emission peaked at 10–20 μm. In AC Her, crystalline silicate features are prominent. Meanwhile, the spectra of R Sct looks like a naked red-giant star with very little dust emission in the wavelength range.

3. MODELING THE SPECTRA

We model the molecular and dust features in the spectra of R Sct. We first fit the molecular bands up to 8 μm, then add the dust emission.

The synthesized molecular spectra are calculated using the *Slab* model (see, Yamamura et al. 1999). In this model, a molecular component is expressed by a plane-parallel layer, with a set of excitation temperature, column density, and relative size with respect to the central star. The emergent spectra are obtained by solving the radiative transfer through the multiple layers overlaid along the line of sight. The slab model approach is an approximation of the real molecular envelope in the star, and it does not assume or require that the molecules are really in such layers. The synthesized spectra give reasonably good fits to the observed spectra of red giants, and help to interpret the observed spectra (Matsuura et al. 2002a).

In the calculation, we assume that the molecules are in the Local-Thermodynamic Equilibrium (LTE). Solar isotopic ratio

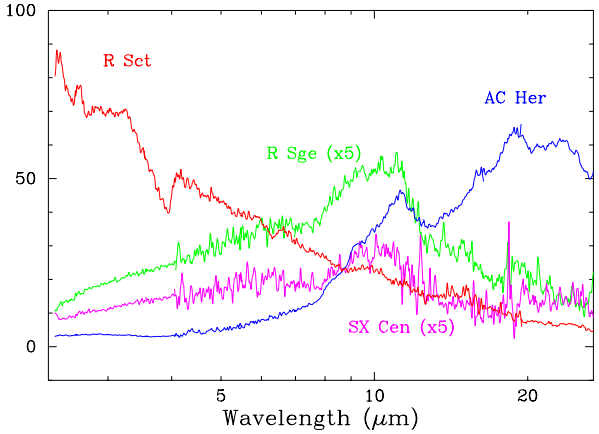

Figure 3. SWS spectra of four RV Tau stars. R Sct shows spectra similar to those of late M-type stars with the SED peaked in near-infrared or even shorter wavelength. Other three RV Tau stars show red SED. AC Her shows prominent crystalline silicate features. The spectral resolution is degraded to be R =200 in order to improve the signal to noise ratio.

is used for oxygen and silicon atoms, while ^{13}C:^{12}C= 1 : 9 is adopted (Bujarrabal et al. 1990) for carbon. The molecules and the line lists included in the calculation are as follows: H_2O: Partridge & Schwenke 1997; CO_2: HITRAN (Rothman et al. 1998); SiO: Langhoff et al. (1993); CO: HITEMP (Rothman et al. in preparation).

The best fit synthesized spectra are compared with the observed spectra in Fig. 4. The best fit parameters are summarized in Table 1. It is confirmed that following molecular bands are seen in emission in R Sct: H_2O bands at longer then $\sim$3.5 μm, SiO at 4.1 μm, CO at 4.6 μm, and CO_2 around 15 μm.

Table 1. The parameters used for fitting the R Sct SWS spectra. In the last column, 'A' and 'E' mean absorption and emission, respectively.

	T_{ex} [K]	N [cm^{-2}]	R [R*]	Appearance
CO	4000	1.2×10^{21}	1.8	E
H_2O-1	2050	1.4×10^{21}	3.5	E
SiO	=T(H_2O-1)	1.0×10^{21}	=R(H_2O-1)	E
H_2O-2	600	1.0×10^{19}	20	A (2.7 μm)
				E (6.2 μm)
CO_2	=T(H_2O-2)	5×10^{17}	=R(H_2O-2)	A (4.2 μm)
				E (13 μm)

The model fits the observed spectra well. The derived parameters are similar to those for the Mira variables except the larger numbers of layer sizes (e.g. Matsuura et al. 2002a). This is easily understood if one consider that the central star has higher $T_{\rm eff}$ and accordingly smaller radius, if the absolute luminosity is the same.

In the next step we add dust emission on the synthesized molecular spectra, to reproduce the excess in the 10 μm region. We use a spherical, optically thin dust shell model, with the density distribution being proportional to r^{-2}. The dust opacity

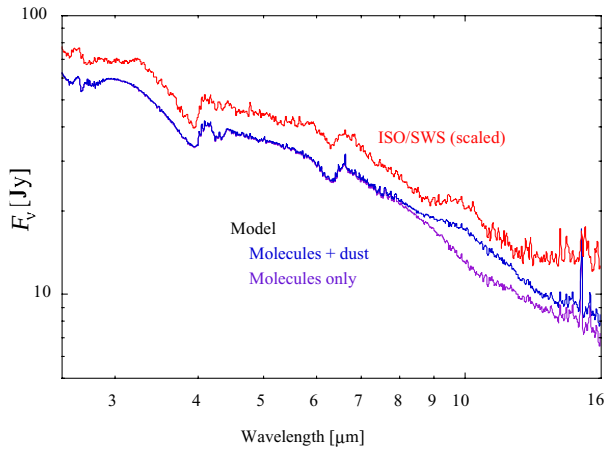

Figure 4. The synthesized model spectra are compared with the ISO/SWS spectra of R Sct (red line). The purple line shows the model spectra considering only molecules. Blue line represents the model taking dust emission into account.

table of "Case 1" in Ossenkopf et al. (1992) is adopted. In order to calculate the dust temperature, the central star is assumed to be a $T_\star = 7000$ K black body with a radius $R_\star = 3 \times 10^{12}$ cm ($L_\star = 4000$ L$_\odot$). In the calculation of the emergent spectra we use the molecular model spectra as the spectra of the central star.

Fig. 4 shows the fitting result. Inclusion of dust improves the fit. The dust mass-loss rate used for this calculation is 1.5×10^{-11} M$_\odot$ yr^{-1} at the expansion velocity of 10 km s^{-1} (Bujarrabal et al. 1988).

4. DISCUSSION

4.1. Disk or Extended Atmosphere?

The surprise in the SWS spectra of R Sct is that the spectra are dominated by the strong molecular bands, both in emission and absorption. Our analysis shows that several different bands of different molecules from different energy levels are detected in emission in the spectra of R Sct. This fact is most easily explained if the molecules are distributed beyond the size of the background continuum source (the star). Two configurations for distribution of the molecules are considered: a disc around the star, and an extended atmosphere. The presence of circumbinary-discs has been discussed in RV Tau stars (Van Winckel et al. 1999), while the atmosphere extended beyond the photosphere is though to be formed in the long-period pulsating variables of Mira or semi-regular types.

We argue that the molecular features appeared in the SWS spectra of R Sct are more likely explained by the extended atmosphere rather than the disc. There are three reasons for this conclusion. First, the temperature and column density of the molecular layers in R Sct are quite similar to those usually found in the extended atmospheres of AGB stars. Second, we found the H_2O absorption bands on top of its emission bands around 2.7 μm. It is interpreted that the cool H_2O layer, with a certain column density, is located in the line of sight of the warm H_2O layer. If molecules are in the disc, it is only possible if the disc is in edge-on. Simply the chance that we have the edge-on configuration is small. Finally, no clear evidence of disc around R Sct has been found (Van Winckel et al. 1999).

The variable amplitude of R Sct is 2–3 mag, which is smaller than Mira variables but comparable to those of semi-regular variables. It has been a long standing problem that how the extended atmosphere (or so called *warm molecular layer* (Tsuji et al. 1997)) is formed in these relatively weak pulsators. Further studies of the extended atmosphere in this star may give a clue to understand this problem.

4.2. Dust Formation and Mass loss

Our analysis shows that dust mass-loss rate derived from the excess in the 10 μm region is extremely small in contrast to the presence of well developed molecular layer. Generally the mass-loss activity and the development of extended atmosphere seem to correlate each other. The mass-loss rate of 10^{-8}–10^{-6} M$_\odot$ yr^{-1} are expected for the AGB stars with the spectra similar to R Sct (Fig. 2). However, if we assume the gas-dust mass ratio of 100, we obtain a gas mass-loss rate of only 1.5×10^{-9} M$_\odot$ yr^{-1}. This discrepancy implies that there must be some mechanism which currently prevent dust formation in the warm molecular gas of this star.

Heavy metal depletion has been reported in some RV Tau stars. Low abundance of metallic elements could results low dust formation efficiency and mass-loss rate. However, we think this is not the case for R Sct. The abundance analysis showed that this star is not extremely metal-poor (Giridhar et al. 2000). In addition, there are evidence that this star experienced large mass-loss rate phase in the past. Bujarrabal et al. (1988) observed CO radio lines and estimated the mass-loss rate of R Sct as 2×10^{-7} M$_\odot$ yr^{-1}. CO lines are sensitive to cool extended circumstellar envelope and they are often the measure of mass loss in the past. Alcolea & Bujarrabal (1991) fit the SED of R Sct with warm and cold dust components and derived dust mass-loss rate for cold dust as 2.4×10^{-9} M$_\odot$ yr^{-1}. If CO emission arises in the similar region with the cold dust, the two mass-loss rates are consistent with the *normal* gas-to-dust mass ratio of about 100. The mass loss in R Sct was "normal" in the past. The reason for low (dust) mass-loss rate in the current phase should be studied further.

4.3. The Evolutionary Stage of R Sct

Alcolea & Bujarrabal (1991) claimed that the large mass loss which produced the cold dust shell stopped about 2000 years ago. If we consider that R Sct is a post-AGB star, as generally believed for RV Tau stars, this decrease of mass-loss rate can be interpreted as that the star evolved from AGB to post-AGB phase. However, the discovery of warm molecules, probably in the extended atmosphere, discriminates R Sct from other RV Tau stars. Also the analysis of long-term pulsation period evolution over the 100 years does not fit with post-AGB scenario

(Matsuura et al. 2002b). We suggest that this star could be an AGB star in quiescent helium burning phase. The large mass-loss rate in the past may occur at the last thermal pulse.

One problem is that the $T_{\rm eff}$ of R Sct is about 5000 K, which is too high for AGB stars ($T_{\rm eff}$ $\sim$3300 K or even below). One possible explanation is that the star has just experienced a thermal pulse a few thousand years ago, and it is in the quiescent helium burning phase. (see e.g., Vassiliadis and Wood 1993).

5. POTENTIAL OF THE ISO ARCHIVE FOR STELLAR ASTROPHYSICS

This study is a good example of serendipitous discovery in a known object using the archived SWS data. Detailed analysis of the spectra and the follow-up studies will lead us to the better understanding of the nature of this particular object and the nature of RV Tau stars.

Several hundreds of stars were observed with the SWS and other ISO instruments. These data have a lot of potential for further studies of evolved stars. The advantage of the ISO data archive from the point of view of studies of evolved stars are:

- The SWS and LWS cover enormous broad wavelength range, in total from 2.3–200 μm. Analysis of the molecular and dust features are best done with complete coverage of different transitions in different wavelengths. Large fractions of the ISO's wavelength range will not be covered again in the near future.
- The large number of uniform sample allows us to consider the common nature in the stars (see, Cami 2002).
- Thanks to the ISO data archive, we can now combine the data of the same object taken in the different programmes, and study the time variation in the spectra. (e.g. Yamamura et al. 1999; Matsuura et al. 2002a; Onaka et al. 2002).

In order to treat these large data efficiently and extract important information effectively, systematic and automatic data reduction and analysis should be considered. The SWS stellar atlas by Kraemer et al. (2002) (also this issue) and the post-Helium survey atlas by Vandenbussche et al. (2002) (also this issue), with their systematic classification are the most appreciated works. Scientific activity motivated by these atlas are encouraged.

ACKNOWLEDGEMENTS

I.Y. is supported by the Grant-in-Aid for Encouragement of Young Scientists (No. 13740131) from Japan Society for the Promotion of Science.

REFERENCES

Alcolea J., Bujarrabal V., 1991, A&A, 245, 499
Bujarrabal V., Alcolea J., Bachiller R., 1990, A&A, 234, 355
Bujarrabal V., Bachiller R., Alcolea J., Martin-Pintado J., 1988, A&A 206, L17
Cami J., 2002, Ph.D. Thesis, University of Amsterdam
Giridhar S., Lambert D.L., Gonzalez G., 2000, ApJ 531, 521
Jura M., 1986, ApJ, 309, 732
Jura M., Chen C., Werner M.W., 2000, ApJ, 541, 264
Kholopov P.N., Samus N.N., Frolov M.S., et al., 1988, General Catalogue of Variable Stars, 4th ed. (Nauka Publishing House)
Kraemer K.E., Sloan G.C., Price S.D., Walker H.J., et al., 2002, ApJS 140, 389
Langhoff S.R., Bauschlicher Jr. C.W., 1993, Chem. Phys. Lett. 211, 305
Matsuura M., Yamamura I., Cami J., et al., 2002a, A&A 383, 972
Matsuura M., Yamamura I., Zijlstra A.A., Bedding T.R., 2002b, A&A 387, 1022
Onaka T., de Jong T., Yamamura I., 2002, A&A 388, 573
Ossenkopf V., Henning Th., Mathis J.S., 1992, A&A 261, 567
Partridge H., Schwenke D., 1997, J. Chem. Phys., 106, 4618
Posch T., Kerschbaum F., Mutschke H., et al., 1999, A&A 352, 609
Rothman L.S., et al., 1998, JQSRT 60, 665
Rothman L.S., et al., in preparation
Shenton M., Monier R., Evans A., 1994, A&A 287, 866
Tsuji T., Ohnaka K., Aoki W., Yamamura I., 1997, A&A 320, L1
Vandenbussche B., Beintema D., de Graauw T., et al., 2002, A&A 390, 1033
Van Winckel H., Wealkens C., Fernie J.D., & Waters L.B.F.M., 1999, A&A 343, 202
Vassiliadis, E.,& Wood, P.R., 1993, A&A 413, 641
Waters L.B.F.M., Trams N.R., Waelkens C., 1992, A&A 256, L15
Yamamura I., de Jong T., Onaka T., et al., 1999, A&A 341, L9